Loading and Release of Antibiotics from Cyclodextrin-modified Biomaterials

By Danny K. Malkowski, Department of Health Science and Technology
Master Thesis at Aalborg University

Department of Health Science and Technology

Fredrik Bajers Vej 7D

Telefon 94 40 75 73

Fax 98 15 40 08

http://www.hst.aau.dk

Title:

Loading and Release of Antibiotics from Cyclodextrin-modified Biomaterials

Project period:
September 8th 2008 – October 12th 2009

Written by:

_____
Danny K. Malkowski

Supervisors:
Peter Andreas Lund Jacobsen
Kim Lambertsen Larsen
Lars Arendt-Nielsen

SYNOPSIS

β-cyclodextrin modified Silica-gel and Hydroxyapatite matrices are investigated as potential candidates for bone implant applications that support tissue stabilisation and reparation, while simultaneously releasing antibiotics into the local area to protect the local tissue from possible post-surgical infections. A theoretical knowledge on biomaterials, bacterial infections, bone structure and function is acquired along with a general understanding of cyclodextrins and loading and release patterns for drugs when released from bioceramics. β-cyclodextrin was grafted to silica-gel and HA matrices and the amount of grafting was investigated with Thermogravimetric Analysis and a Phenol Assay Method. Changes in matrix structure was investigated with BET, elemental analysis and with a Scanning Electron Microscope setup with a Focused Ion Beam and an Energy Dispersive X-ray spectroscope. The presence of β-cyclodextrins was further presented by experiments conducted with a Confocal Laser Scanning Microscope. The loading of the two ligands Fusidic Acid and 1-Anilino Naphthalene 8-Sulfonic Acid within the modified and unmodified matrices was investigated by Absorption and Fluorescence Spectroscopy, respectively. Finally, a High Performance Liquid Chromatography release assay was prepared with Fusidic Acid as the ligand for modified and unmodified matrices of silica-gel and Hydroxyapatite.

Preface

This project has been composed in the period from the 8th of September 2008 to the 12th of October 2009 by Danny K. Malkowski at the 9th and 10th semester of the M.Sc. E. in Biomedical Engineering and Informatics with specialization in Drug and Tissue Technology at the Department of Health Science and Technology at Aalborg University. The project is addressed to students at my own level and others with an interest in cyclodextrins, silica-gel or hydroxyapatite for pharmaceutical use.

Book- and article sources are referred to in the text by [author, year of publication]. Websites are denoted by a number in square parenthesis, which refers to the source in the Bibliography. All sources of figures are mentioned under the figures or in the appropriate paragraph. When no source is mentioned, i have made the figures by myself.

The front page illustration was kindly created by Anne Krogh Mammen, 2D-designer at the Danish Youth Association of Science (UNF Danmark).

I would personally like to thank the following people who assisted me during the project period:

- Ph.d.-student Peter A. Lund Jacobsen, for suggesting ideas and thoughts for the project as well as for the essential sparring when interpreting the results

- Associate Professor Kim L. Larsen for his continuous support, sparring and thoughts

- René Holm at Lundbeck A/S, for providing CHN and XRPD results for the project

- And last, but not least, special thanks to my family and friends for all your support throughout the past 13 months

List of Abbrevations

1,8-ANS:	1-Anilino Naphthalene 8-Sulfonic Acid
BET:	Brunauer, Emmett, Teller - Gas absorption theory, named after its founders
CD:	Cyclodextrin
CGTase:	Cyclodextrin Glucosyltransferase
CHN:	Carbon, Hydrogen, and Nitrogen - Elemental Analysis method
CLSM:	Confocal Laser Scanning Microscopy
EDX:	Energy-dispersive X-ray spectroscope
FA:	Fusidic Acid
FIB:	Focused Ion Beam
FS:	Fluorescence Spectroscopy
HA:	Hydroxyapatite
HPLC:	High Performance Liquid Chromatography
SEM:	Scanning Electron Microscope
TGA:	Thermogravimetric Analysis
UV-Vis:	Ultraviolet-Visible
XRPD:	X-Ray Powder Diffraction

Contents

Introduction 1

Recently, inorganic materials have received a great deal of attention in the field of biomedical science [Vallet-Regi *et al.*, 2007]. The development of biomedical materials suitable for skeletal repair and reconstruction, often referred to as bioceramics, are one of the hottest topics in the scientific field of implants. The two main concerns are the preparation of the material so that it is suitable as a scaffold for the formation of new bone and the prevention of infections after a successful implantation of the application. While acquiring a proper biocompatibility is solely a matter of matrix design the prevention of post-surgical infections proves to be more complicated. The danish governments Serum Institute estimated a few years ago, that the yearly hospital expenses for treatment of post-surgical infections was approximately 950 million danish kroner. This corresponds to almost 2% of the overall hospital expenses for the year 2000 [1]. Thus, post-surgical infections are a very interesting field both for scientific and economic matters.

In order to treat bacterial infections, antibiotics can be used. The treatment dose has to be above the effective inhibitory dosis, and below the toxic dosis. Systemic antibiotic administration does not always allow for sufficient treatment of an infection, as a cause of poor blood flow in the target tissue. The development of biomaterials suitable as carriers for local drug administration at the implant site is therefore of great interest. Some bioceramics are capable of including pharmaceuticals into the porous bioceramic matrix. In this way it is believed to be possible to engage the primary function of the implant of tissue stabilisation and reparation, while simultaneously releasing antibiotics into the local area to protect it from possible infections. However, it has proven to be relatively difficult to maintain a controlled release of the drug from the matrix [Best *et al.*, 2008], [Vallet-Regi *et al.*, 2007].

Devices implementing cyclodextrins (CDs) into the biomaterial matrix of bioceramics, have been proposed as a possible solution for local drug administration, in order to maintain a continuous drug release and keep the drug concentration in the suitable range between the effective and toxic dosis [Ponchel *et al.*, 2004]. Because of their physical strength and chemical inertness, bioceramic materials such as silica-gel and hydroxyapatite (HA) have been proposed as inorganic oxide supports for functionalized drug delivery applications [Ponchel *et al.*, 2004], [Vallet-Regi *et al.*, 2007]. This leads us to the aim of this study.

Aim of Study

This thesis will focus on drug loading and release kinetics from the biomaterial matrices of silica-gel and HA that have been modified with CDs in order to investigate if the application has the potential for controlled local administration of antibiotics in bone tissue. In the following chapters, biomaterials are introduced in more detail followed by an explanation of the causes, tissue responses and current treatment methods of bacterial infections. Subsequently, further knowledge on the structure and function of bone tissue is acquired followed by the chemical and physical characteristics of silica-gel and HA. A general understanding of CDs is also given followed by the derivation and explanation of loading and release kinetic models. After sufficient knowledge on the mentioned matters has been acquired a series of experiments are conducted on CD modified silica-gel and HA wih two different ligand molecules. The choice of surface modification, ligand molecules as well as the type of experiments will be explained in more detail in chapter 8. The subsequent results will be compared and discussed with respect to the gained knowledge in chapters 1-7 and other papers.

Biomaterials

<div align="right">

2

</div>

The term biomaterials defines materials that are used for medical applications, intended to interact with a biological system. Many different shapes of biomaterials have been developed including powder, granules, tablets, coatings, and catheters. Many inorganic implants can be manufactured through the process of sintering, a method for making objects from powder, by heating the material in a sintering furnace below its melting point until its particles adhere to each other. By using a method involving a hot-press apparatus, consisting of a press machine and a furnace, it is possible to sinter the biomaterial under high pressure and high temperature at the same time and thus, sinter the biomaterial without decomposition [Aoki *et al.*, 1973]. Through the process of sintering it is possible to prepare structures for various applications. When designing both the biomaterial and the method of implantation the two most prominent issues are biocompatibility and subsequently infections after the implantation has occured. While the biocompatibility solely is a design issue of the biomaterial matrix, implant infections can be caused by many occurences. In fact, bacterial infections are a very serious issue with any type of biomaterial and type of implant. The reason herefore is mainly the surgical procedure itself, since the risk of contamination of the tissue is dramatically increased as soon as the protective barrier of the skin is penetrated. During surgery, the site of procedure is contaminated by bacteria spreading from the staff in the operating room, and also some amounts from the patient itself depending on the site of procedure. Most infections resulting from the implantation of biomaterial decvices are first detected after the surgery is completed, and can not always be treated sufficiently by the use of antibiotics without removing the implant again [2]. The following sections are an introduction to the most prominent biomaterials and their applications.

2.1 Percutaneous Devices

Since the 1950s various materials such as silicone rubber, alumina, titanium, and collagen have been used as materials for percutaneous devices that were utilized for the measurement of internal body information or the application of drops. The goal is to develop a percutaneous device that makes electrical input or output transportation and physical transportation possible long-term without any effects of inflammation or infection. A major issue is biocompatibility which occurs when the tissue around the device is unable to attach properly to it. One way to deal with the biocompatibility issue is by using materials that can bind sufficiently and directly to the tissue. Such materials are termed biomaterials and among the most prominent are silica-gel and HA. It is also possible to deploy biomaterials to the surface of otherwise incompatible materials that are in contact with the tissue. This will similarly prevent the tissue from rejecting the implant [Aoki, 1994]. The photograph in figure 2.1 illustrates the result of the surgical procedure using HA as material. The experiment was conducted by H. Aoki and colleagues [Aoki, 1994]. Small button-shaped percutaneous terminals were implanted into the forearms of the group members. It was reported that the terminals tightly adhered to the skin three days after implantation. Nine years after the operation had passed the subjects were still without any severe problems [Aoki, 1994].
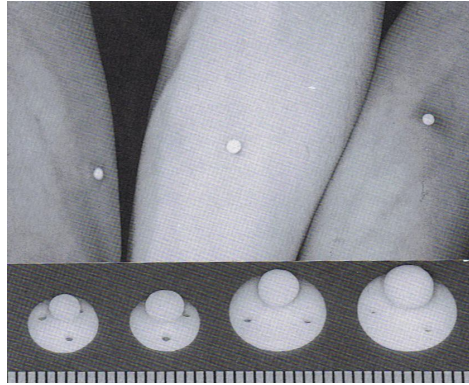
Figure 2.1: Photograph illustrating HA percutaneous terminals implanted into human forearms, taken five years after implantation. No infections or incompatibilities are observed [Aoki, 1994]

2.2 Artificial blood vessels

When a blood vessel is transplanted into a patient it is sometimes rejected by the tissue or begins to develop arteriosclerosis, especially when it is transplanted from one donor to another. It can also be problematic to transplant vessels from within the same patient because two surgeries are required for this method. Furthermore, many patients with circulation problems have no suitable vessels that can be transplanted [3].

Synthetic bioceramic tubes can be used as artificial blood vessels or as connectors for blood vessels to overcome those problems. The most successful artificial blood vessels in use today come from surgical techniques developed in the 1940s and 1950s. Figure 2.2 illustrates two artificial blood vessels made of HA and the operation view of a dog with newly implanted HA vessels. After three months there was no sign of inflammation, infections or tissue rejection [Aoki, 1994].
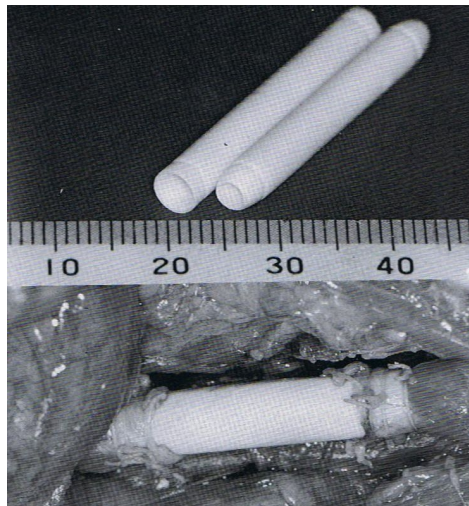
Figure 2.2: Photograph showing two HA artificial blood vessels and the surgical view of a dog with newly implanted HA artificial blood vessels. No signs of inflammation or tissue rejection are observed [Aoki, 1994]

However, many bioceramics are very brittle materials with extremely large elastic moduli and therefore their compliance is very different from that of an actual blood vessel. One solution is to create an artificial blood vessel with the biocompatibility of a bioceramic and the elastic

moduli of a flexible polymer. Such a material can be obtained through plasma jet coating of the bioceramic onto the polymeric surface [3].

2.3 Artificial Joints

When considering materials for artificial joints physicians are facing problems with corrosion and a phenomenon called the loosening effect, which can be observed when using implants made from metals and alloys. The loosening effect occurs when the surrounding tissue cannot bond to the implant surface, similar as with the percutaneous devices. Instead of bonding directly with the implant the body tends to produce a fibrous material around it in a similar way as if it was about to repair a wound or injury. The result is a thick connective tissue on the surface of the joint and the formation of gaps between the artificial implant and the tissue surface. If the implant does not integrate well with the surrounding bone, or is not held rigidly with a fastening device, the implant will be subjected to micromovement, and the surrounding bone will start to remodel. As the strength of bioceramics is mechanically weak, they can not be used for implants at high stress areas such as bone joints alone. Instead, implants consisting of stronger materials such as the bioinert material titanium or stainless steel are covered with the bioceramic by a sol-gel plasma spraying technique to prevent the loosening effect [Aoki, 1994], [Gupta *et al.*, 2008]. The difference can be seen in illustration 2.3.
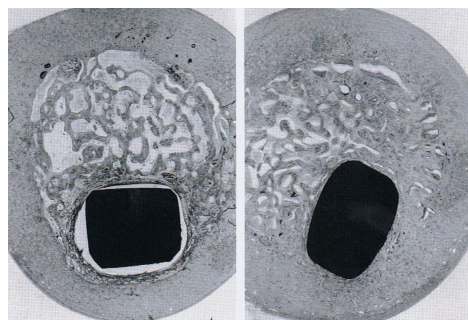
Figure 2.3: Image illustrating cross sections of artificial hip joints. To the left, a joint made of stainless steel and to the right, a joint made of the same stainless steel but coated with the bioceramic HA [Aoki, 1994]

2.4 Artificial bone

When bone defects occur due to tumors or accidents, bone grafts can be carried out. Grafting is a surgical procedure in which tissue is transplanted without a blood supply. The implanted tissue must acquire a blood supply from the new vascular bed that is formed after implantation, or die. In the field of bone grafting four methods are known; Autograft, Homograft, Heterograft, and Artificial graft.

- Autograft: To transplant tissue from one part of the body to another in the same organism.

- Homograft: The transplantation of an organ or tissue from one organism to another from the same species, but with a different genotype.

- Heterograft: Transplantation of organ or tissue in which the donor and acceptor organisms are from different species.

- Artificial bone graft: The organ or tissue that is implanted has been manufactured synthetically.

All organs have a parenchymal and stromal component. The parenchyma is the physiologically active part of the organ and the stroma is the scaffold that supports the organization of the parenchyma. In soft tissues that have lost most if not all of their parenchyma but still have the active stroma the structural and physiological functions of the tissue are usually able to fully regenerate with time. By providing a bone defect with a synthetic stromal substitute that contains a morphological environment suitable for osteoblasts and osteoclasts, such as a porous bioactive bioceramic scaffold, the regeneration of the bone has been observed to increase remarkably [Holmes, *et al.*, 2005].

Infections and Treatment

<div style="text-align: right">3</div>

A sufficiently large amount of foreign bacteria invading an eukaryotic host organism can give rise to an infectional state, causing cellular and tissue damage. Foreign microorganisms can release toxins that are harmful for the surrounding tissue and dying bacteria can release other harmful toxins as well. Regardless of bacterial type an infection will result in a counter-response from the host organism [Guldager, 2002]. These countermeasures, commonly known as the inflammatory response, are local reactive changes in the tissue after damage, irritation or infection. Factors apart from infections that can cause inflammation include physical damage to tissue or the presense of foreign bodies such as clinical implants or splinters.

3.1 Inflammation

Inflammation is the biological response of the organism to harmful stimuli. The symptoms include blushing, swelling, increased production of heat, and irritation of the nerve ends caused by release of cytokines and prostaglandins of the cells in close vicinity of the inflamed tissue. The joints that connect certain bone ends and the nervous system can also be affected by the effects of inflammation, resulting in decreased functionality [Guldager, 2002], [Martini, 2006]. If a patient is undergoing surgery he or she is also at an increased risk to get infected by bacteria or fungi from the air, as well as from the clothes and touches from the surgeons. Such infections can result in inflammation at the surgery site but also throughout various other parts of the body since the close contact with blood vessels during some surgeries may lead the bacteria or fungi to rapidly spread via. the bloodstream.

Inflammation is a local reactive change in the tissue after damage or irritation and various factors can cause inflammation. They include factors such as exposure to toxins, pathogens, sudden temperature changes that cause burns or frostbite, physical damage to the tissue or the presense of foreign bodies. The main purpose of inflammation is to stop the tissue destruction, degeneration and removal of the harmful substance, and removal of dead cells and foreign bodies to successfully start the healing process. Without inflammation the healing would never begin and progressive destruction would compromise the survival of the organism [Guldager, 2002].

Inflammation considers various biochemical reactions that take place in the local tissue. The process starts with a certain type of cells of the immune system, the mast cells. These cells are present in almost all types of organic tissue, particularly abundant in very exposed areas such as the nose, mouth and feet. They are also present along the inner mucous membranes of the body and blood vessels. The mast cells contain histamine which is located in granules in the cytosol. When stimulated by mechanical stress or chemical changes in the local environment degeneration of the granules in the mast cells occurs, which initiates the secretion of histamine into the injured tissue. This reaction is called degranulation. Histamine binds to the endothelial cells of the blood vessels which induces two reactions. The smooth muscle around the blood vessel starts to relax resulting in an increase of blood flow to the injured tissue, increasing the local oxygen and nutrient concentration and increases the number and activity of phagocytes and the removal of damaged cells and toxic chemicals. Simultaneously, the endothelial cells contract to increase the permeability of fluid and leukocytes through the capillary walls. These reactions are causing the characteristic visual features of inflammation, mainly the blushing and swelling of the tissue. Interaction with nerve endings in the region of injury often results in stimulations of the nervous system, which causes the physical characteristics commonly known as pain [Martini, 2006].

The first type of leukocytes that penetrate into the injured tissue are the granulocytes, which fight bacteria by releasing cytotoxic materials that are stored in granules in the cytosol, a reaction similar to the degranulation process in mast cells. The granulocytes also secrete chemical transmitters to attract the larger macrophages, which begin to engulf and digest pathogens and cells of the organism that have been killed or severally damaged upon the harmful influence [Martini, 2006], [Guldager, 2002]. If the harmful stimuli is not successfully removed from the affected area it can cause a more prolonged inflammation period which eventually leads to tissue damage. This chronic type of inflammation is differentiated from normal inflammation by prolonged duration. Chronic inflammation can be caused if physical objects are not removed from the necrotic space, or if the immune system is unable to remove and digest the harmful stimuli. It can also be caused by diseases such as tuberculosis, rheumatoid arthritis or pancreatitis [4].

When the granulocytes and macrophages have successfully removed all of the foreign substances from the tissue and eliminated dead cells and cellular debris, the healing process can begin. As tissue conditions returns to normal, fibroblasts enter the region and start to form a network of collagen known as scar tissue. The amount of cells in the damaged area is increasing with some cells migrating to the area, whereas others are created by division of mesenchymal stem cells. Over time, the initial injury will completely heal and the scar tissue will change conformation and gradually assemble a more normal appearance. However, the final steps of the healing process can take months or even years, relative to the extent of the injury. The healing process varies throughout the body. Each organ has a different ability to regenerate which can be directly linked to the composition and organization of tissue in the organ. Organs such as the skin usually regenerate completely over time, whereas cartilage, neural and muscle tissue regenerate very poorly. Although the connective tissues in muscle cells can be fairly well repaired, the majority of damaged muscle cells are replaced permanently by fibrous tissue produced by the fibroblasts, a process called fibrosis. If damage to the heart has occured, this results in a weakening of muscular strength and reduces the overall pumping effect of the heart. If a comprehensive damage has occured, the inability of regeneration could lead to heart failure [Martini, 2006].

3.2 Bacterial Infections

The cell envelope varies with the bacterial species which can be classified into two subdivisions; Gram-positive and gram-negative. The cell envelope of gram-positive bacteria consists of an inner plasma membrane which is enclosed by a thick peptidoglycan layer whereas the gram-negative bacterial envelope also includes an outer membrane of lipopolysaccharides and proteins [Holst *et al.*, 2002]. See figure 3.1 on the following page for a more detailed illustration of the distinct parts of the two bacterial cell wall types. When bacteria penetrate the hosts defenses and invade sterile tissues such as the liver, lungs, muscles or bones they multiply which results in an infection. The infection can occur in various forms, depending on the region of infection as well as the type of bacteria. In the simplest situation being the local infection, the bacteria enters one specific tissue and remains there giving rise to local boils or irritations.

A focal infection is the result of the infectious agent breaking loose from the local infection site and is carried into other tissues. Systemic infections are, as the name indicates, infections of the bloodstream. In this case, the cause of the infection remains at the local site of whereas the toxins that are produced are carried by the systemic circulation into other tissues. Examples include bacterial diseases such as syphilis or anthrax. Finally, the infection can actually be caused by a series of different bacteria leading to a more complicated disease where an initial primary infection is causing one or more secondary infections, either by the primary bacteria
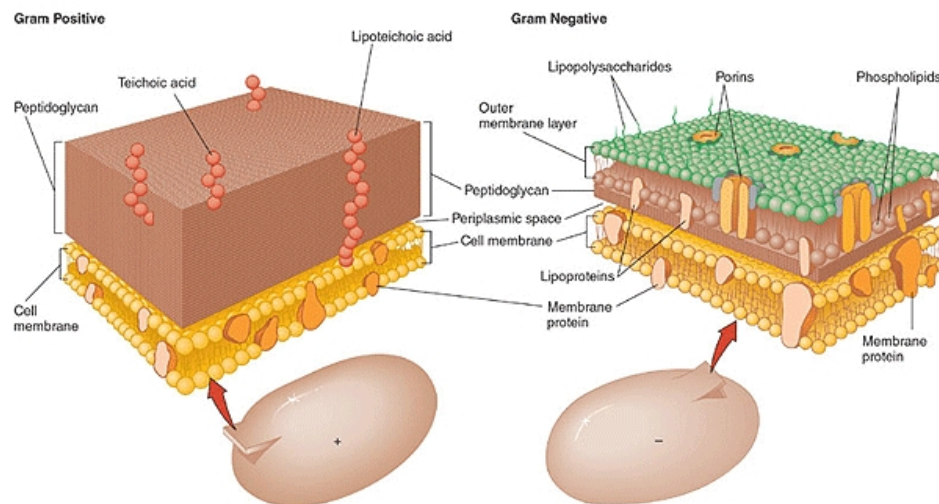
Figure 3.1: Illustration of the various structures of gram-positive and gram-negative bacteria, including the distinct features of the cell envelopes and walls. Modified from [Talaro, 2006].

attracting other types of bacteria or by weakening the defense mechanism that was initially holding back the secondary infection. It is important to notice that one is not initially infected by the disease but by the bacteria resulting in the disease. An infectious agent can be transmitted from host to host, a transmission process called communicable. A non-communicable infectious agent can be acquired either by the transmission from an internal area of the same host, e.g. if healthy tissue is invaded by the patients own microflora, or if the patient recently has been in accidental contact with a parasite or similar [Talaro, 2006].

Osteomyelitis is the clinical term defining the pathogenic infection of bone tissue as a result of surgery or trauma. The infection typically establishes itself focally in the spongy bone of the metaphysis from where it spreads to other areas of the bone. The infection leads to abscess formation which in turn results in necrosis and eventually breakage of the bone tissue because of degradation through virulence factors. Osteomyelitis is mostly observed in children and adolescents and also in patients with a penetrating trauma or who have been in surgery because of eg. fracture fixation, joint replacement, or tumor removal [5], [Talaro, 2006].

3.2.1 Nosocomial Infections

During hospital stays there is an increased risk for a patient to acquire an infectious disease. An infectious disease is defined as a clinically evident disease resulting from the presence of pathogenic microbial agents that are able to cause disease in animals and/or plants. When the disease is caused by the hospital stay, either directly or indirectly, such an infection is termed a nosocomial infection. Nosocomial infections are infections which are a result of treatment in a hospital or a healthcare service unit, but secondary to the patient's original condition. As hospitals undoubtedly are a natural place to look for high concentrations of patients with diseases and injuries it makes perfect sense that the concentration of pathogens is increased as well. It is thus not uncommon for a surgical patient's incision to become infected after the surgery. Furthermore, a weak immune system resulting from a primary disease makes it easier for other pathogens to establish an infection in the organism. Gram-negative bacteria coming from the intestinal flora of patients are resulting in more than half of the nosocomial infections whereas gram-positive bacteria from the surroundings such as body surfaces, clothes and surgery tools make up the remainder [Talaro, 2006].

Staphylococcus aureus is a very common inhabitant of the skin and mucous membranes in humans. It is a gram-positive bacteria and causes the most infections in hospitals. It is gradually becoming an increasing problem since it is able to develop resistance to antibacterial agents at a remarkable pace [6], [Talaro, 2006]. Upon infection an *S. aureus* bacterial colony is able to double within 20 minutes, which is why a small amount of bacteria can easily grow to several millions cells within a few hours. The optimal temperature for the growth of *S. aureus* is 37°C but it is able to grow at temperatures rangin from 6-46°C, which means it can grow in refrigerated food and medicines among others. It is able to survive at temperatures as high as 60°C for up to one hour. Furthermore, most of the bacterial strains are able to adapt to a wide range of concentrations of salt in solutes ranging from 0.1% to as high as 20% in NaCl concentration. The growth is enhanced by the presence of O_2 and CO_2 and they are able to digest various proteins, lipids and sugars. The carriage rate for normal healthy human adults typically varies between 20-60%, depending on the location of the group. Generally, the closer humans live together and are exposed to potential infections such as in jails or hospitals, the higher the carriage rate. All in all these specifications underline the difficulty of treating patients with a *S. aureus* infection [Talaro, 2006].

The pathogenesis of *S. aureus* is caused by a combination of virulence factors, which are produced by the bacteria. Virulence factors are molecules that cause a disease or influences the host to allow the pathogen to survive and grow. The major virulence factors produced by *S. aureus* in humans are blood cell toxins such as hemolysin and leukocidin, which damage the cell walls of red blood cells, leukocytes, skeletal and heart muscle, and renal tissue. Another important virulence factor of *S. aureus* is coagulase, an enzyme that coagulates blood and plasma. It is believed that coagulase causes fibrin to deploy around the bacteria, which in turn protects the bacteria from phagocytosis and promotes adherence to host tissues. Furthermore, *S. aureus* produces hyaluronidase, which digests hyaluronic acid, an important component in extracellular structures that binds connective tissues together and in articular cartilage. The multiple resistance of the majority of *S. aureus* strains is obtained through the production of enzymes that are able to inactivate many antibiotics such as penicillin [Talaro, 2006].

3.3 Antibiotics

The term 'antibiotic' is used to describe any substance that is antagonistic to the growth of microorganisms in high dilution. This original definition excludes naturally occurring substances, such as gastric juice and hydrogen peroxide (they kill microorganisms but are not produced by microorganisms), and also exclude synthetic compounds such as the sulfonamides (which are antimicrobial agents). Many antibiotics are relatively small molecules with a molecular weight less than 2000 Da.

Some antibiotics perform their effect by intercepting with the synthesis of the main components in the bacterial cell wall. The antibiotics act by inhibiting the enzymes that are responsible for the proteoglycan production in the cytoplasm. These enzymes, however, can only be inhibited for bacteria that are in the growth fase and synthesizing cell wall compounds. As a result, bacteria that are dividing produce a defective cell wall which eventually results in the destruction of the bacteria. If non-dividing cells are present they must be eliminated by the hosts own defence mechanisms [Ratledge *et al.*, 2001], [Perry *et al.*, 2002]. These include lysozyme which can degrade peptidoglycan in bacterial cell walls. As peptidoglycan is only found in bacteria, an antibiotic treatment will not harm the eukaryotic host cells, unless the host is prone to an allergic reaction caused by an overreaction of the immune system [Perry *et al.*, 2002].

Osseous Tissue

<div style="text-align: right">4</div>

Bones are part of the skeletal system, which functions as structural support and protection for soft tissues and organs in the entire body. Many soft tissues and organs are attached to the skeletal system and skeletal elements such as the ribs and skull protect vital organs such as the heart, the lungs and the brain. The shaft, or diaphysis, of each bone consists of a layer of compact bone which is relatively solid. It forms a protective layer around a central space called the marrow cavity [Martini, 2006]. Red and white blood cells as well as other blood elements are differentiated from mesenchymal stem cells which reside inside the marrow cavity. Furthermore, bones function as a mineral reserve that maintains normal concentrations of calcium and phosphate ions in body fluids. These minerals participate in various physiological processes, and several are important as enzyme co-factors [Junqueira *et al.*, 2005], [Martini, 2006].

4.1   Development, Growth and Healing Mechanisms

Osseous tissue, like any other connective tissue, origins from the mesenchyme, an embryonic tissue formed by elongated cells, the mesenchymal cells. The mesenchyme develops mainly from the middle layer of the embryo, the mesoderm. Mesodermal cells migrate from their site of origin and in turn end up surrounding and penetrating developing organs. Furthermore, the mesenchymal cells develop into other types of structures such as endothelial cells, muscle cells, adipose cells, and blood cells. Thus, the different connective tissues are essentially responsible for providing and maintaining form. They provide a matrix that connects and binds the cells and organs and gives support to the body [Junqueira *et al.*, 2005]. Bone is formed during fetal development in two ways; either by replacing existing cartilage with bone by deposition of bone matrix and subsequent degradation of the cartilage, called endochondral ossification, or by mineralization of bone matrix secreted by osteoblasts and hereby developing bone directly from the mesenchyme or fibrous connective tissue, a process called intramembranous ossification [Martini, 2006].

Intramembranous Ossification   takes place within condensations of mesenchymal or fibrous connective tissue and is the source of most of the flat bones such as the frontal and parietal bones of the skull or the lower jaw. The process begins when groups of cells differentiate into osteoblasts which produce the bone matrix. The following calcification results in the incapsulation of some of the osteoblasts which in turn become osteocytes. The mechanism of calcification is yet not fully understood, but it is known that calcification begins by the deposition of calcium salts on collagen fibrils, which is a process induced by proteoglycans and high-affinity calcium binding glycoproteins [Junqueira *et al.*, 2005]. The apparent calcified islands of developing bone continue to grow until they fuse together, giving the bone a spongy structure. The remaining connective tissue is subsequently penetrated by blood vessels and undifferentiated mesenchymal cells, giving rise to the bone marrow cells. After subsequent remodeling, the spongy bone in turn becomes the more compact bone [Martini, 2006].

Endochondral Ossification   is the development of bone from a hyaline cartilage model. During fetal development, most bones originate as hyaline cartilage miniature models of the corresponding adult bone. The process of endochondral ossification is further illustrated in figure 4.1. Endochondral ossification is also an essential process during the rudimentary formation of long bones, the growth of the length of long bones, and the healing of bone

fractures. The process begins with the formation of a hyaline cartilage model during the first six weeks of fetal development. The cartilage is mainly composed of an extracellular matrix of fibers and ground substance. The extracellular matrix is synthesized by chondrocytes. The cartilage model continues to grow by expansion of the cartilage matrix and production of new cartilage on the outer surface. When the enlarging process begins, chondrocytes at the very center of the hyaline cartilage model will begin to increase greatly in size and the matrix is reduced to thin strands of fibers which begin to calcify through the process of intramembranous ossification. The enlarged chondrocytes become surrounded by calcified cartilage and die and disintegrate because diffusion of nutrients cannot occur through the layer [Martini, 2006].
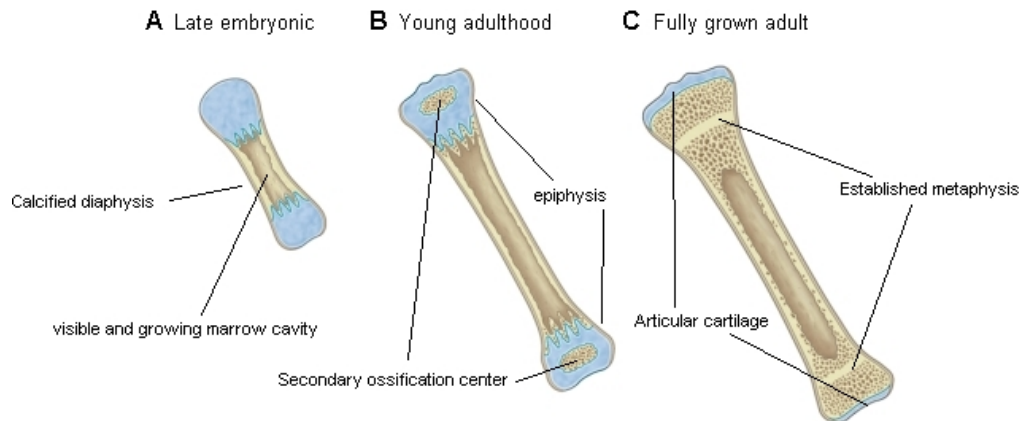

Figure 4.1: Illustration showing the main steps of endochondral ossification. A: Late embryonic bone with ossified diaphysis and the formation of the marrow cavity. B: Bone from young adulthood showing secondary ossification centers and the growing epiphyseal cartilage. C: Fully grown adult bone with no epiphyseal cartilage. Illustration modified from [7]

Blood vessels now begin to grow into the perichondrium, which is the protective outer layer of the hyaline cartilage. The perichondrium consists of two layers; the outer fibrous layer which provides mechanical support and attaches to other tissue whereas the inner, cellular layer is important to the growth and maintenance of the cartilage. These cells now differentiate into osteoblasts which begin to produce a thin layer of bone on the inside of the perichondrium. The perichondrium has now become a periosteum because it now technically covers bone instead of cartilage. Capillaries and fibroblasts now start to migrate into the central cavities of the cartilage, due to the increased blood supply from the blood vessels, and the fibroblasts begin to differentiate into osteoblasts that replace the calcified cartilage with spongy bone, forming the diaphysis. In this way the primary ossification center is produced, where bone development begins. After a while, as the bone enlarges in length and diameter, osteoclasts emerge and begin to disintegrate the center of the newly formed bone creating the marrow cavity. As the bone matrix is being added to the outer surface of the growing bone, osteoclasts are removing bone matrix from the inside at a slower rate, which gradually increases the marrow cavity as the bone grows larger in diameter [Martini, 2006].

The next step in bone formation is the migration of osteoblasts and capillaries into the two ends of the cartilage model, creating two secondary ossification centers and the epiphyses of the bone. The appearance of secondary ossification centers usually occurs right before or after birth in most bones. With time, the secondary ossification centers become filled with spongy bone. A thin cap of articular cartilage remains exposed at the joint cavity, providing support and reducing friction. Another layer of cartilage, the epiphyseal cartilage, remains between the epiphyses and diaphysis. This cartilage continues to grow at the epiphysis side whereas it is gradually turned into bone from the diaphysis side by continuously invading osteoblasts. Essentially, the bone is hereby able to grow throughout early adulthood. During puberty

the rising levels of sex and growth hormones induces the osteoblasts to migrate and produce bone faster in the epiphysial cartilage until it ultimately disappears and bone growth is halted [Martini, 2006].

4.1.1 Bone Remodeling

Bone remodeling is the process of partial resorption of bone tissue followed by subsequent laying down of new bone tissue. It goes on throughout life as part of normal bone maintenance. Remodeling can replace the matrix without changing the shape or it may change the mineral content distribution and internal architecture of the bone. The remodeling process involves an interplay between osteocytes, osteoblasts, and osteoclasts. During early adulthood the osteoblasts are very active in building new bone tissue whereas osteoclasts remove bone tissue at a slower pace. With the development of the adult skeleton structure the two turnover rates become more balanced, but they still remain active after the epiphysial cartilages have been closed [Martini, 2006]. In the first year of life almost 100% of the skeleton is replaced, whereas in adults remodeling proceeds at about 10% per year [8].

The skeleton contains almost all of the bodys calcium reserves in the form of calcium and phosphate ions. Through the continuous interchange of calcium ions between the blood and the bone the remodeling process maintains a steady concentration of calcium ions in the blood and other tissues. The calcium blood level is maintained by parathyroid hormone and calcitonin, which are released from the parathyroid and thyroid glands, respectively. Osteoclasts have receptors for calcitonin, which has an inhibitory effect on osteoclast activity, while no receptor sites are present for parathyroid hormone. Parathyroid hormone in turn promotes osteoclastic resorption by stimulating osteoblasts that in turn begin the secretion of a cytokine, called *osteoclast-stimulating factor* [Junqueira *et al.*, 2005], [Martini, 2006]. Because bones are so adaptable, their shapes and structural integrity reflect the forces applied to them over time. During prolonged heavy exercise bones will grow thicker and stronger, whereas bones that are not subjected to ordinary stresses due to inactivity become thin and brittle. Degenerative changes in the bones occur after relatively brief periods of inactivity. For example, if stress is reduced on an injured leg while a cast is worn the bone will lose up to one third of its mass. However, the bone rebuilds just as quickly when normal weight loading is resumed [Martini, 2006].

As part of the normal aging process bones gradually become thinner and weaker. This reduction in bone mass begins between ages 30 and 40. During this period osteoblast activity gradually declines while osteoclast activity remains almost the same, resulting in inadequate ossification; a physiological term called osteopenia. Once the reduction process begins men lose about 3% of their skeletal mass every decade while women lose about 8%. When the reduction of bone mass becomes evident and visible as the fragile bones are likely to break when exposed to stresses considered normal for younger individuals the condition is known as osteoporosis. Since the sex hormones are important in maintaining the normal rates of bone deposition and resorption the condition usually accelerates after the menopause in women as the circulating concentrations of estrogens are decreasing. Since men continue to produce testosteron severe osteoporosis is less common in men below the age of 60 [Martini, 2006].

4.1.2 Bone Healing

When a bone is broken the bone matrix is destroyed, many blood vessels are broken, and the bone cells in the local area of the fracture will die due to lack of nutrients from the blood supply. The damaged blood vessels will produce a blood clot that closes off the injured area. The periosteum around the fracture will respond with rapid cycles of cell division with cells migrating into the fracture zone. In the centre of the fracture the cells differentiate into chon-

drocytes and start producing blocks of hyaline cartilage that form an enlarged collar around the fracture. At the ends of the fracture the periosteal cells differentiate into osteoblasts that will begin to build a bony bridge from the bone fragments on either side of the fracture. As the bridge-building process continues osteoblasts start to replace the hyaline cartilage at the centre of the fracture with spongy bone through a combination of endochondral and intramembranous ossification while the macrophages remove dead cells and bone debris. Osteoblasts and osteoclasts will continue to remodel the fracture region for up to a year and once completed the fracture site is usually thicker and stronger than normal. Unlike other connective tissues, bone can regenerate without the formation of scar tissue, which means there will be no remaining indications of an occured fracture once the repair is completed [Junqueira *et al.*, 2005], [Martini, 2006].

4.2   Bone Components

Bone tissue, or osseous tissue, is the major structural and supportive connective tissue of the body. It consists of several specialized cells and a matrix of extracellular protein fibers and a ground substance. About 2/3 of the matrix consists of a mixture of mostly calcium phosphate with lesser amounts of calcium carbonate. The ground substance volume in bone is very small and surrounds insoluble crystals of the calcium salts. The rest of the matrix is composed of collagen fibers. The combination of fibers and calcium salts gives bone remarkable properties. The structural components of compact bone are illustrated further in figure 4.2.
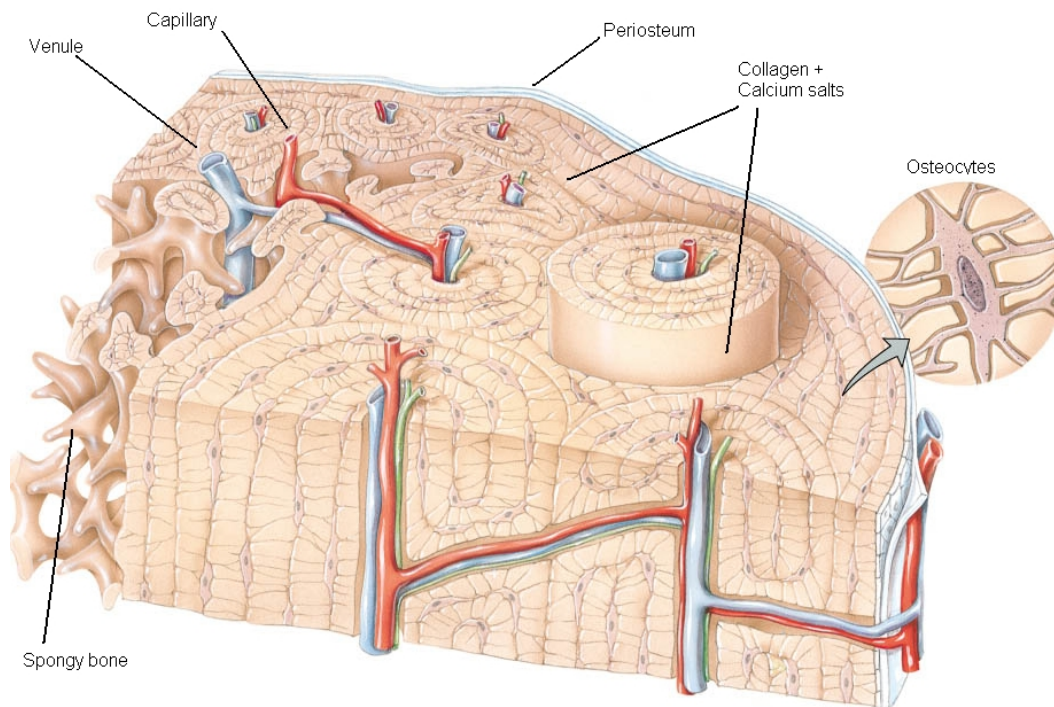

Figure 4.2: Illustration showing the organization of the various structures of compact bone. Illustration modified from [9]

Calcium salts are very hard but brittle, whereas collagen fibers are very strong but relatively flexible. By combining the distinct properties a very strong flexible combination is obtained, which is highly resistant to impact and stress. The combination results in a structure that can compete with the best steel-reinforced concrete [Martini, 2006]. The following three sections describe the bone components collagen fibers, calcium salts and cartilage in more detail.

Collagen Fibers   are formed by proteins that polymerize into elongated structures and are thus classified as fibrous connective tissue. Each collagen fiber consists of a bundle of fibrous protein subunits that are wound together like a rope, giving the fiber its long, straight, and unbranched shape. Collagen is the most abundant protein in the human body, representing 30% of its dry weight. The collagens of vertebrates comprise a family of more than 25 members where collagen type I is the most abundant as it has a widespread distribution in structures such as bones, dentin, tendons, organ capsules, and dermis. Collagen type I is composed of three peptide chains, called fibrils, with a molecular mass of approximately 100kDa forming a right-handed helix which is held together by hydrogen bonds and hydrophobic interactions between the protein subunits. The length and width of each fibril is 280nm and 1.5nm, respectively. In tissues such as bone the collagen fibers are organized in parallel to each other, forming collagen bundles, where the subunits overlap each other in a stepwise fashion. This arrangement results in a structure that varies between dark and light bands as a series of ridges with a 64nm periodicity when observed in the electron microscope [Junqueira *et al.*, 2005].

Calcium salts   are responsible for the hardness of the bone matrix and account for almost 2/3 of its weight. Calcium and phosphorus are epecially abundant and present in the form of Calcium phosphate and calcium carbonate, as briefly mentioned in the introduction of this section. More specifically, calcium phosphate interacts with calcium hydroxide to form crystals of HA while simultaneously incorporating other salts such as calcium carbonate, and ions such as potassium, sodium, magnesium, and fluoride into the crystal structure [Martini, 2006]. HA crystals can form on the framework provided by the collagen fibers. The HA crystals of bone appear as plates that lie alongside the collagen fibrils when observed through an electron micrograph [Junqueira *et al.*, 2005]. Furthermore, the surface ions of the HA crystals are hydrated allowing the formation of a socalled hydration shell of water and ions around the crystals, which facilitate the ion exchange between the body fluids and the crystal. HA crystals have been thoroughly examined in X-ray diffraction studies which concluded the chemical composition to be $Ca_{10}(PO_4)_6(OH)_2$. However, human HA crystals show imperfections and are not identical with the synthetical variants nor the types usually found in rock minerals [Junqueira *et al.*, 2005]. For a more thorough description of HA, see section 5.2.

Cartilage   is the second supporting connective tissue, responsible for providing a strong framework together with bone, which supports the rest of the body. Cartilage is a special form of connective tissue that facilitates bone movement and acts as a sliding area for joints, supports soft tissues and bears mechanical stresses without permanent distortion. It is surrounded by the perichondrium, which acts as a barrier between the cartilage and the surrounding tissue. The perichondrium contains of an outer layer being a fibrous region of dense irregular connective tissue, and an inner cellular layer. The outer layer provides mechanical support and protection for the cartilage and attaches it to other structures while the inner layer is important to the growth and maintenance of the cartilage. The cartilage matrix is extracellular and enriched with collagen, hyaluronic acid, proteoglycans and glycosaminoglycans. The only cells present in the matrix are chondrocytes, which are responsible for the synthesis and secretion of these extracellular compounds [Martini, 2006].
Three types of cartilage exist, all varying in composition of matrix components. The most common form is hyaline cartilage, which provides stiff but somewhat flexible support while reducing friction between bony surfaces. Bone development in the embryo occurs from a hyaline cartilage model as described in section 4.1. Elastic cartilage is extremely flexible and resilient and is present in elastic tissues including the flap of the outer ear, and the epiglottis attached to the very root of the tongue. Fibrocartilage, the last major cartilage type, is extremely durable and tough caused by densely interwoven collagen fibers. Fibrocartilagi-

nous pads are present within or around joints such as the meniscus of the knee, between the spinal vertebrae, and between the pubic bones of the pelvis. Their main function is to resist compression and absorb schocks while preventing damage from direct bone-to-bone contact [Junqueira *et al.*, 2005], [Martini, 2006].

Damaged cartilage regenerates very poorly and often incompletely. The regeneration occurs by the invasion of cells from the perichondrium which generate new cartilage. However, in more extensively damaged areas the perichondrium produces a scar of dense connective tissue instead of new cartilage which can interfere with normal movements in joints such as the knee [Martini, 2006].

4.3 Bone Cells

Four general types of cells are responsible for the formation, remodeling and maintenance of the various bone components, not including cartilage. Cartilage is formed and maintained by chondrocytes which, although they are essential in the embryonic formation of the hyaline cartilage model of bones, will not be covered in more detail in this work. The four types of bone cells are osteocytes, osteoblasts, osteoclasts, and osteoprogenitor cells. Hormones control the activity and concentration of bone cells throughout the whole human life span. This is especially noticed during puberty and when becoming of old age. When humans reach puberty, bone growth accelerates due to the increased levels of sex hormones while bones become gradually weaker and more brittle around the age of 40 as a result of declining osteoblast activity while osteoclast activity continues at previous levels [Martini, 2006]. In the following three sections the four types of bone cells will be explained in more detail.

Osteoprogenitor Cells and Osteoblasts are closely related. Osteoprogenitor cells are stem cells of the mesenchyme which divide to produce daughter cells that differentiate into osteoblasts, hereby maintaining the population of osteoblasts and subsequently being very important in the repair of fractures. Osteoprogenitor cells are located in an inner cellular layer that lines the marrow cavities and in the lining of passageways that penetrate the bone matrix [Martini, 2006]. Osteoblasts are responsible for the production and release of proteins and other organic components such as proteoglycans and collagen, forming new bone matrix. When the osteoblasts are active, the various matrix components are secreted at the surface of the osteoblast that is in contact with older bone matrix which produces a new uncalcified matrix, called osteoid. Soon after the osteoid production the osteoblasts also assist in the deployment of calcium phosphates and salts in the osteoid organic matrix [Junqueira *et al.*, 2005], [Martini, 2006]. Osteoblasts are only located at the surfaces of bone tissue in a way that resembles the structures of simple epithelium, having a cuboidal shape and basophilic cytoplasm when they actively produce new bone matrix. When this activity declines, they become gradually more flat in shape and their cytoplasmic basophilia declines as well. They can, however, easily revert to the cuboidal shape if necessary [Junqueira *et al.*, 2005].

Osteocytes are derived from osteoblasts. During osteogenesis some osteoblasts become completely surrounded by bone matrix, whereafter they convert into osteocytes. The incapsuled osteocyte forms a tiny pocket called a lacuna between the layers of matrix and each lacuna is only occupied by one osteocyte. The many lacunae are connected with each other and to the central canal through a network of small passageways called canaliculi. Each osteocyte extends into the canaliculi and forms gap junctions when making contact with other osteocytes, which enables them to exchange nutrients, minerals, hormones, ions, and certain chemicals [Martini, 2006]. Osteocytes are the most abundant type of bone cell and are responsible for the maintenance of the protein and mineral content of the surrounding matrix. They

are long-living cells and distinct themselves from osteoblasts by being more flat and almond-shaped than osteoblasts while having a significantly reduced rough endoplasmic reticulum and Golgi complex [Junqueira *et al.*, 2005]. They are, however, still able to participate in bone repair. If they are released from their lacunae because of an injury to the surrounding bone matrix they are able to convert into osteoblasts or osteoprogenitor cells again which enables them to produce new bone matrix and support the healing process of the fracture [Martini, 2006].

Osteoclasts remove and recycle bone matrix, effectively removing the calcium salts by decomposing the collagen, proteoglycan and glycoprotein structures of the organic matrix. A microenvironment is created between the osteoclast and the surface of the bone matrix close to it, in where the osteoclast secretes acids and proteolytic enzymes such as collagenase that dissolve the organic matrix and release the deposited minerals [Junqueira *et al.*, 2005]. The balance between osteoclast and osteoblast activity is essential in the maintenance of calcium and phosphate concentrations in other tissue parts of the body such as blood and muscle, as described in the previous section on bone remodeling.
Osteoclasts have a distinct histology from osteocytes and osteoblasts as they are derived from the fusion of many bone marrow-derived mononucleated cells, related to the hematopoietic stem cells that divide into monocytes and macrophages. They are large cells and can contain from 5 and up to 50 or more nuclei, relative to the smaller osteocytes and osteoclasts that only consist of one single nuclei [Junqueira *et al.*, 2005]. Figure 4.3 illustrates the differentiation pathways of osteoblasts, osteocytes, and osteoclasts.
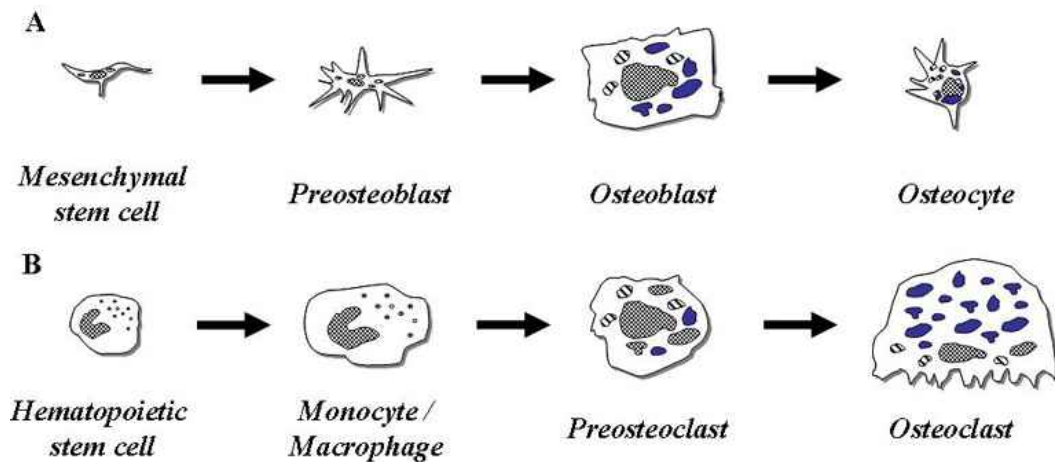

Figure 4.3: Illustration showing the differentiation of A: osteoblasts and osteocytes, and B: osteoclasts. The illustration is modified from [Marquis *et al.*, 2009]

Bioceramics

<div style="text-align: right; font-size: 3em;">5</div>

Bioceramics can be categorised as either bioinert or bioactive, depending on the type of bioceramic and the host interaction. The term bioinert for the purpose of biomedical implants is defined as a minimal response from the body in which the implant becomes covered by a thin fibrous non-adherent layer. A bioactive material is defined as a material that elicits a specific response at the interface of the material, which results in the formation of a direct bond between the tissue and that material [Brendel *et al.*, 1992]. The bioactive ceramics can be either resorbable or non-resorbable, meaning they are decomposed and used as building blocks for the creation of new cell tissue or, they are not decomposed but act as a scaffold for new cell tissue forming around the ceramic, respectively [Ginebra *et al.*, 2006]. The macroporosity of the bioceramic implant is a key factor to successfully stimulate and support capillary growth and oxygen supply. In the following two sections the bioactive bioceramics of Silica-gel and HA will be explained in more detail.

5.1 Silica-gel

Silica-based materials have recently been extensively reported as possible candidates for drug delivery ceramics, as they show capabilities to perform as controlled drug release systems for drugs of a wide range. They are characterized by narrow pore size distributions and ordered pore systems, as well as large specific surface areas. Since they are bioactive and non-resorbable they are capable of promoting bone tissue regeneration, but will not be decomposed by the body as new bone tissue forms [Vallet-Regi *et al.*, 2007]. The silica-based materials are able to do so because of the formation of an apatite layer on their surfaces when the materials are placed in the body. In fact, the more specific bioactive glasses have a higher binding strength than titanium, which is currently the most common type of implant for bone prostheses [Li *et al.*, 1994]. The apatite formation is caused by the development of a negatively charged silica surface after implantation and the high density of silanol groups on the surface. The silanol groups are flexible enough to supply the correct atomic distance and can provide the sites for apatite nucleation that is required by the crystal structure of HA, the main bone apatite in higher vertebrates and humans as described in section 5.2. In this nucleation process CaO and P_2O_5 is accumulated at the sites from the body fluids near the silanol groups [Li *et al.*, 1994], [Soga *et al.*, 1992].

Silica-gels are commonly used as beads packed in a semi-permeable plastic for the use as desiccants to control local humidity in order to avoid spoilage or degradation of medicine and food. The most common daily day application where silica-gel beads can be found are in the small white bags that have been placed inside newly manufactured shoes and clothings. It is the high surface area of around 6-800m^2/g that allows silica-gel to absorb relatively large amounts of water, making it very useful as a drying agent. Furthermore, silica-gels are used as a stationary phase in chromatography. Because of silica-gels polarity, due to the representation of many silanol groups on the surface, non-polar components elute before polar ones. However, if hydrophobic groups, such as C_{18} groups, are attached to the silanol groups the polar components elute first, as the long non-polar side chain now wins over the hydrogen bonding silanol group [10]. Silanol groups can be modified almost in the same way as alcohol groups. Among other reactions, they can form ester compounds and undergo nucleophilic substitution reactions if they are activated first. The lone pairs of electrons on the oxygen of the hydroxyl group also makes silanols nucleophiles. The OH group is not a good leaving group in nucleophilic substitution reactions, so neutral silanols do not react in such reactions.

However, if the oxygen is first protonated to give R-OH$_2^+$, the leaving group now being water is much more stable, and the nucleophilic substitution can take place [Dewick, 2006].

The representation of many silanol groups on the surface of silica based materials is very useful regarding drug delivery techniques as they can be altered chemically in order to modify and enhance the adsorption, confinement and release of the appropriate drug. Drug molecules adsorb relatively easy to the surface of the inner silica pore walls. The ratio between the pore size and diameter and the size and chemical nature of the drug is therefore the most important factor besides pore wall modification, considering both drug loading and the subsequent controlled release to the desired environment [Horcajada, *et al.*, 2004].

Preparation and Synthesis

Silica-gels can be formed by acidification of aqueous solutions of sodium silicate, Na$_2$SiO$_3$. Sodium Silicate is stable in neutral or alkaline solutions, whereas the silicate ion readily reacts with hydrogen ions in acidic conditions, forming silicic acid. After acidification, the gelatinous precipitate of silicic acid is washed free of electrolytes and dehydrated by heating or spray drying which in turn forms the silica-gel structures [Greenwood *et al.*, 1984].

Another way to prepare pure silica-gel is through the hydrolysis of tetraethoxysilane in an aqueous solution of polyethylene glycol as described by Li and colleagues [Li *et al.*, 1994]. The remaining organic phase after hydrolysis is washed out with an ethanol/water solution and dried whereafter it is heated at 400°C for 2 hours. The resulting silica-gel was characterized as having both micrometer- and nanometer-range interconnected pores [Li *et al.*, 1994].

5.2   Hydroxyapatite

Among bioceramics, HA is probably the most promising one because of its biocompatibility with osseous and soft tissues and bone ingrowth and ongrowth capability [Correia *et al.*, 1996]. HA is a bioactive, bioresorbable ceramic. It is osteoconductive, and osteoblasts can actively use the HA in a potential bioceramic implant in order to regenerate bone tissue [Best *et al.*, 2008], [Ginebra *et al.*, 2006]. It is thus widely used as occular implants, bone substitutes for filling bone defects, as coating agent for various metallic implants, and as scaffold matrix for tissue engineering [Murugan *et al.*, 2005]. Since HA was first synthesized and sintered in 1972, many different biomaterials have been developed with HA including bone cements, bone formation promoters, artificial blood vessels, and drug delivery carriers [Aoki, 1994].

HA provides a storage for control of calcium uptake and release and exists as bone mineral, counting for approximately 5% of the body weight. Almost 70% of bone tissue is made of HA [Ginebra *et al.*, 2006]. HA is soluble in acidic solutions, but not in alkaline solutions. It is slightly soluble in distilled water and the solubility increases when electrolytes are added. Furthermore, the solubility changes in various ways when amino acids, enzymes, proteins, and other organic compounds are present. The solubility changes are closely related to the tissue biocompatibility. Chemically considered as a basic calcium phosphate and having a Ca/P ratio of 1.67, HA can be represented by the following chemical formula as seen in formula 5.1 [Murugan *et al.*, 2005], [Aoki, 1994].

$$Ca_{10}(PO_4)_6(OH)_2 \hspace{4cm} (5.1)$$

The crystal structure of synthetic HA is hexagonal bipyramidal and has lattice constants of a=9.423Å and c=6.875Å, respectively. Biological HA is called dahllite and contains small amounts of carbonate. Dahllite does not grow to large sizes but rather forms an aggregation of small crystals. The space group of dahllite is P6 without a center of symmetry, while the

space group for synthetic HA is $P6_3/m$. Furthermore, bone as well as dahllite experiences piezoelectricity while synthetic HA does not. Piezoelectricity is the ability of a material to generate an electric potential in response to applied mechanical stress. In the case of bone it is thought to act as a biological force sensor.

Figure 5.1 on the following page illustrates the crystal structure of synthetic HA along the c- and a-axes. The Phosphorus atom is surrounded by four Oxygen atoms forming a tetrahedron, thus the five atoms form a PO_4 group. Calcium atoms are represented in two independent sites in the crystal structure. The first site is surrounded by six Oxygen atoms from PO_4 groups in an octahedral formation. The second site forms a triangle with two other Calcium atoms. The triangles are stacked on top of each other, normal to the c-axis, and rotated 60°. Each triangle encloses an OH-group, which is slightly shifted above or below the center of the plane in the triangle. In total, the Calcium atoms present at the second site are surrounded by six Oxygen atoms belonging to five PO_4 groups and the enclosed OH group [Aoki, 1994].

Preparation and Synthesis

HA is the biological apatite of bones and teeth in most vertebrates. In order to process the biological apatites into HA the bone is first prepared through crushing and treatment with proteases and enzymes. Hereafter the material is washed clean with distilled water and all non-precipitated material is removed. The material is then dried and pulverized, resulting in useful biological HA powder [Aoki, 1994]. Up to the present there are four methods that are mainly used for producing HA synthetically; Wet and dry synthesis, the use of hydrothermal processes, and through various forms of sol-gel formations. The wet method is ideal for mass production of small crystalline or non-crystalline HA, while the dry method is used for the preparation of well crystallized HA powder. In order to prepare single crystals of HA, a hydrothermal proces is widely used while thin membranes of polycrystalline HA structures are synthesized mainly through sol-gel processes [Correia *et al.*, 1996], [Gupta *et al.*, 2008]. In the following two sections the wet, and the dry method is described.

The Wet Method

HA can be synthesized through various aqueous reactions. The most preferred process involves a neutral reaction between alkaline and acid solutions at room temperature, as seen in reaction 5.2.

$$10Ca(OH)_2 + 6H_3PO_4 \rightarrow Ca_{10}(PO_4)_6(OH)_2 + 18H_2O \qquad (5.2)$$
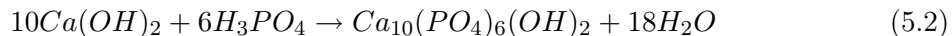
The acid H_3PO_4 is slowly titrated into the solution containing $Ca(OH)_2$. The result of this reaction is HA microcrystals with a crystal size of less than 0.1μm. When suspended in solution the crystals usually aggregate to particles with sizes between 5μm to 30μm. The specific surface areas of the dried HA powder are less than 80 m^2/g. However, when the HA microcrystals are synthesized using an ultrasonic homogenizer the aggregate sizes are less than 10μm and the surface areas are larger than 100m^2/g [Aoki, 1994]. HA can also be synthesized by reactions between Ca-salts and P-salts such as between $CaCl_2$ and Na_2PO_4. Furthermore, a process in which $(NH_4)_2HPO_4$ and $Ca(NO_3)_2$ is used as reactants also work well for HA synthesis in aqueous solutions [Correia *et al.*, 1996].

The Dry Method

By heating the starting compounds at high temperatures app. between 900-1400°C a solid-state reaction is employed, which forms HA, CO_2, and water as seen in reaction 5.3.
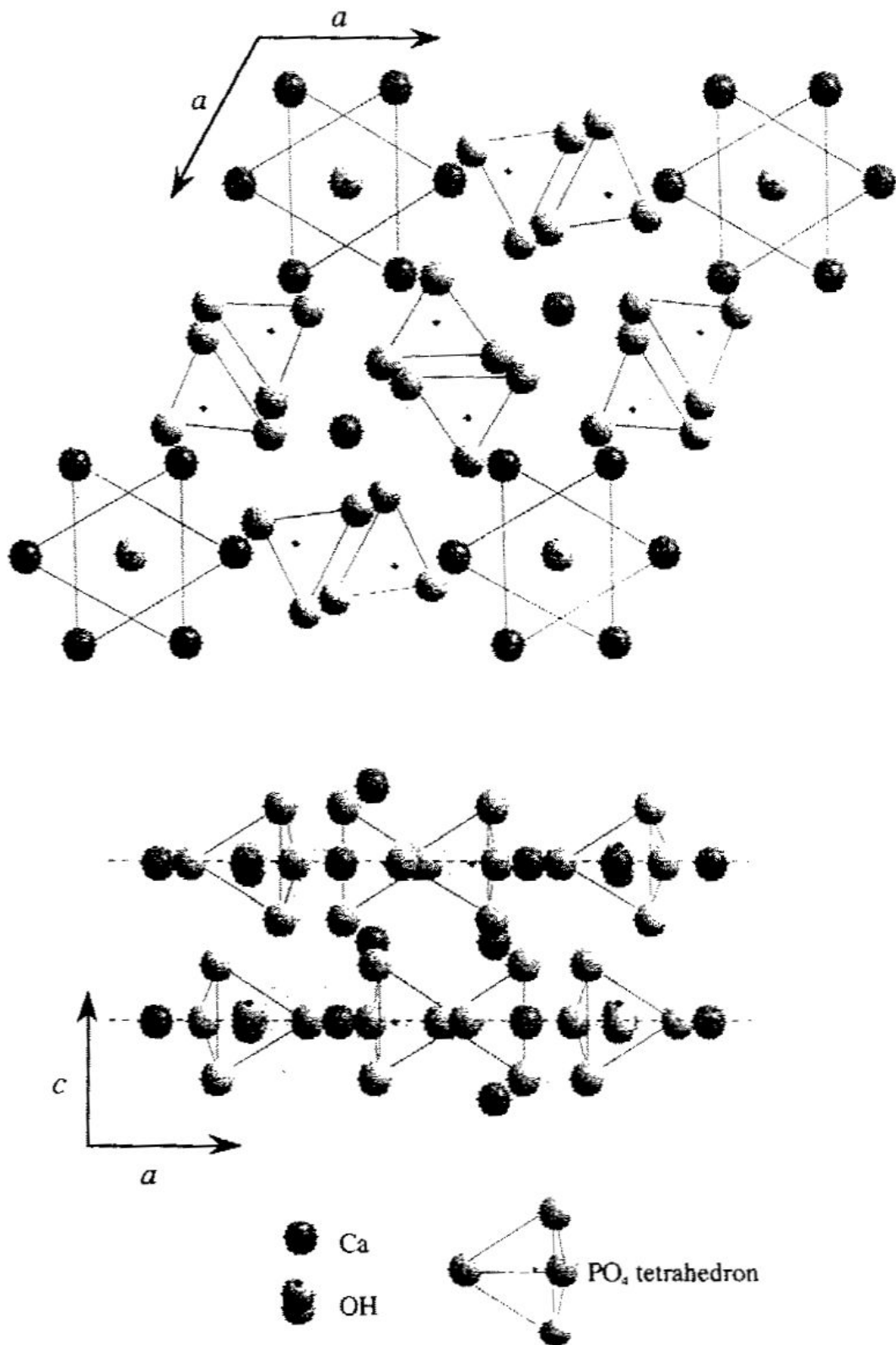
$$6CaHPO_4 \cdot 2H_2O + 4CaCO_3 \xrightarrow{900-1400°C} Ca_{10}(PO_4)_6(OH)_2 + 4CO_2 + 14H_2O \qquad (5.3)$$

Figure 5.1: Illustration of the crystal structure of synthetic HA, with space group P6$_3$/m and with lattice constants a=9.423Å and c=6.785Å.

The end product of HA by the dry method is very clean and with a far better crystallinity than can be accomplished with the wet method [Aoki, 1994].

5.3 Bioceramics as Drug Delivery Systems

Drug release from the matrix of bioceramics has been investigated thoroughly in the past [Higuchi, 1963], [Ginebra *et al.*, 2006]. Biomaterials are very promising agents for new bioactive and bioresorbable drug delivery systems. They are very porous materials and as a result have a relatively large surface area. Moreover, they have a unique ability to adsorb various chemical species on their surfaces, which makes them great potentials as a drug carrier. Furthermore, Silica and HA bioceramics are suitable for surface modifications as they present OH-groups on their surfaces, like many other bioceramics [Ginebra *et al.*, 2006].

Drug delivery systems made of HA can either be manufactured as microparticles, porous scaffolds, or as implant coating. The most important factor independent of the shape when considering controlled release of a certain drug is to be able to control the pore size of the matrix. The pore size has to be tailored from the beginning in order to control the confined drug and the release kinetics once implanted [Vallet-Regi *et al.*, 2007]. In general, larger pore sizes will lead to a higher drug load within the pore channels, as it allows a closer packing of the guest molecules on the pore surface.

B. Martel and colleagues investigated the possibility to functionalise vascular polyester prostheses with CDs in order to establish their cytocompatibility and to examine the potential of an improved and prolonged antimicrobial effect of the graft in biological medium when loaded with ciprofloxacin [Martel *et al.*, 2007]. The obtained results from this study showed significantly increased amounts of ciprofloxacin attached to the CD modified graft relative to the virgin graft. The modified graft could absorb more than four times the amount of ciprofloxacin than the virgin graft, resulting in a higher initial-burst effect. Furthermore, Martel and colleagues observed a shorter drug release time when applied to solutions that were mimicking the composition of human blood plasma, relative to the drug release profile into pure water. They concluded that the reduced release time was due to the difference in ionic strength and to the presence of proteins in the blood plasma medium. Thus, the salts and proteins in the medium played the role of a competitor to ciprofloxacin resulting in the shorter release time.

F. Chai and colleagues studied the effects of drug release from bone-grafts that were modified with hydroxy-propyl-β-CD polymers [Chai *et al.*, 2009]. The aim was to determine if a controllable and sustained local drug delivery for systemic antibiotic treatments was achievable for bone tissue implants. A grafting yield of roughly 1.6wt% was obtained for the hydroxy-propyl-β-CD polymers and the kinetic release studies of antibiotic loaded CD-modified HA showed a prolonged release profile of up to 96 hours for the drug and also a significantly increased initial-burst effect, similar to as what was observed by Martel and colleagues.

Introduction to Cyclodextrins

<div align="right">

6

</div>

When starch or amylose is exposed to enzymatic degradation by e.g. α-amylase, the product consists of small linear polysaccharides. However, if it is exposed to Cyclodextrin Glucosyltransferase (CGTase) the primary products are CDs, a family of ring structures consisting of D-glucopyranosyl units connected by α(1-4)-glycosidic linkages [Szejtli, 1996]. CGTase is common to many bacteria, but is not known to be produced in any other species. CDs containing 6, 7 or 8 glucopyranosyl units are the most common products of the CGTase transglycosylation and are named α-, β-, and γ-CD, respectively [Loftsson *et al.*, 1996]. CDs with less than 6 glucopyranosyl units can not be produced by enzymatic degradation due to steric hindrance, but can be synthesized chemically. Molecules with more than 8 glucopyranosyl units are also uncommon, but have been reported [Larsen, 2002]. The D-glucopyranose monomer and a 7-membered CD can be seen in figure 6.1.
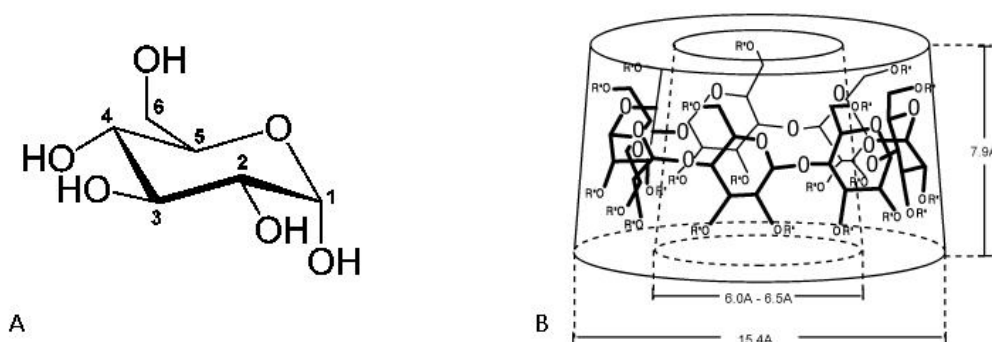
Figure 6.1: A: The monomeric structure of α-D-glucopyranose. CGTase is able to synthesize CDs with pyranosyl units as building blocks. B: Illustration of a CD consisting of 7 glucopyranosyl units, commonly known as β-CD [11].

The structure of CDs is of toroidal shape with the primary and secondary hydroxyl groups of the glucopyranosyl units exposed to the solvent. Because of this structure the interior part of CDs is not hydrophobic, but considerably less hydrophilic than the exterior part. This makes the interior part a much more favourable environment for hydrophobic molecules than the aqueous solution, which is why CDs are widely used in various industrial fields such as the nutrition, analytical chemistry, textile, and pharmaceutical industries [Szejtli, 1996], [Ponchel *et al.*, 2004]. In the nutritional industry, CDs are employed for the preparation of cholesterol free products. The hydrophobic cholesterol molecule is easily trapped inside CD rings that are removed by precipitation. Other food applications further include the ability to stabilize volatile compounds and the reduction of unwanted tastes and odour [11]. However, CDs have also gained considerable attention in the areas of pharmaceutics and drug delivery as their unique structure improves the solubility and stability of otherwise poorly insoluble drugs, due to the partial or full inclusion of the drug molecule into the interior hydrophobic cavity, hereby shielding the guest molecule from the aqueous solution. In addition, CDs can also be used to reduce gastrointestinal irritation when administering drugs orally, and to prevent drug-drug and drug-excipient interactions [Loftsson *et al.*, 1996].

When a more or less poorly water-soluble solute is dissolved in an aqueous solution with CDs a significant increase in solubility of the solute can be observed. The reactivity of the included "guest molecule" is also modified. In general the reactivity decreases, but in some cases the inclusion also results in a modification of the reaction pathway that increases

reactivity. The spectral properties of the guest also changes due to the transfer from polar to apolar surroundings. These changes are commonly observed as shifts in UV maxima of several nanometres and improved fluorescence abilities as most compounds which are strongly fluorescent in organic solvents only show negligible fluorescence in aqueous solutions. If CDs are added to the solution, a significant enhancement of the fluorescence will occur as the CD cavity behaves similarly to the organic solvent [Szejtli, 1996].

6.1 Guest Complexation

The inclusion of a molecule into the CD cavity is not fully understood. However, according to J. Stejtli, the driving force seems to be a combination of various effects depending on the specific guest and type of CD. Since CDs are uncharged, ionic bonds can be precluded as a dependent driving force. Also, no covalent bonds are established between CDs and the guest molecules, which leaves us with possible contributions from van der Waals forces, hydrogen bonds, and hydrophobic interactions. Furthermore, water molecules present in the CD cavity cannot maintain a tetrahedral structure like bulk water, which results in an enhanced enthalpy of the molecules. The role of water substitution has been proven to be one of the universal driving forces for molecular inclusion. By applying small amounts of relatively apolar solvents to CDs in an aqueous solution, the solubility of the CD was slightly improved [Szejtli, 1996]. Hydrogen bonds and van der Waals forces are simply too weak by themselves in order to contribute to a stable CD inclusion complex, which is why several simultaneous weak bonding interactions are needed to form a potentially stable complex. As a result, the inclusion complex is only formed when the CD structure supports a close proximity between the hydrogens of the CD cavity and the guest molecule.

As briefly mentioned, no covalent bonds are formed or broken when the guest complexation takes place. The inclusion of a guest molecule is basically a substitution of water from inside of the cavity with a more favourable guest molecule, driven by enthalpy and entropy contributions. The complexation is reversible and an equilibrium is established in the solution once the lowest state of energy has been reached. The equilibrium is defined as in eq. 6.1.

$$a[Guest] + b[CD] \leftrightarrow [Guest_a CD_b] \tag{6.1}$$
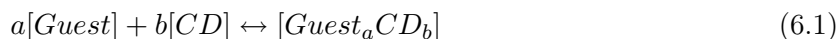
Where a and b are the number of moles of guest and CD, respectively. The equilibrium constant, K, can then be defined as in eq. 6.2.

$$K = \frac{[Guest_a CD_b]}{[Guest]^a [CD]^b} \tag{6.2}$$

Ionization and size of the guest molecule plays an important role in the complexation procedure and strongly affects the equilibrium constant. In general, the larger the guest molecule the slower the formation and decomposition of the inclusion complex will occur. The fitting is primarily determined by geometric and steric factors. The central cavity diameter of the three most common CDs, are 5.0Å, 6.3Å, and 7.8Å, for α-, β-, and γ-CD, respectively. The importance of a proper fitting into their cavities has been illustrated by several observations [Szejtli, 1996], [Loftsson *et al.*, 1996]. For example, toluene fits very well into the cavities of α-CD and β-CD while only loosely bound to the inside of γ-CD. Naphthalene however, does not fit into the cavity of α-CD while it is well suited for inclusion into the β-CD and γ-CD toroids. Anthracene only forms an inclusion complex with the γ-CD, simply being too bulky for the smaller interiors of α-CD and β-CD [Szente, 1996]. The three aromatic substances are illustrated in figure 6.2.
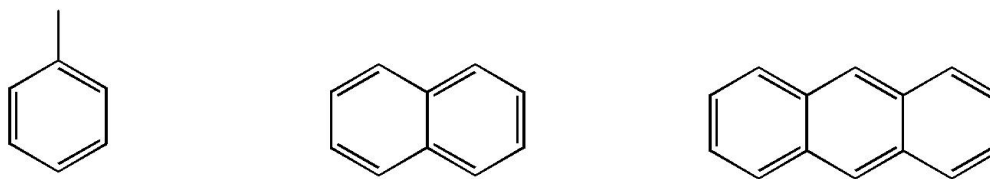
Figure 6.2: From left to right: The molecular structures of toluene, naphthalene, and anthracene, respectively.

Furthermore, there is a positive correlation between the hydrophilic structure of the guest molecule and the stability of the inclusion complex. Generally speaking, the presence of hydrophobic side chains such as methyl- or ethyl-groups increases the stability of the complex, while hydroxy-groups decrease the stability. Whether carboxy-groups affect the stability seems to depend on their ionized forms. Since water molecules bind more strongly to the ionized form than the neutral form of the carboxy-groups the guest-CD complex stability is more likely to decrease with increasing ionization of the guest molecule [Szente, 1996].

Manipulating with the medium in which the inclusion complex formation takes place, can also have an influence on the stability and structure of the guest-CD complex. This can be done by adding cosolvents such as alcohols, alkanols, and surfactants to the aqueous solution. Changes like this are most often considered as disturbing factors in the inclusion process, however, some of them may actually be beneficial. Ethanol is e.g. one of the most frequently used cosolvents, when considering preparation of CD-complexes with drugs or flavours [Szente, 1996].

6.2 Cyclodextrin Derivatives

Although CDs are relatively hydrophilic on the exterior surface their solubility in aqueous solutions is rather limited, that being especially the case for β-CD [Szejtli, 1996]. It is suggested that the low solubility is caused by relatively high crystal lattice energy. Creating CD derivatives by substituting one or more of the primary or secondary hydroxy-groups on the D-glucopyranosyl units can remarkably increase the solubility. Chemical modification of CDs is fairly unspecific compared to enzymatic modification and various products of CD derivates are created in the process. By randomly substituting hydroxy-groups, the crystal lattice energy is greatly reduced as the derivates order themselves in amorphous crystal structures [Loftsson et al., 1996].

By specific chemical synthesis or enzymatic reactions, branched CDs can be created. Branched CDs are native CDs with a side chain of saccharides attached to the parent CD by a α(1-6)-glycosidic linkage. Branches can be obtained by chemical synthesis but are usually prepared by enzymatic reactions. The branches can be homogeneous with units composed only of glucose or of malto-oligosaccharides or heterogeneous in which one or more units of galactose or mannose are incorporated in the polysaccharide branch as well. Homogeneous branched CDs are usually prepared in order to increase the molecular solubility, whereas heterogeneous branched CDs have mainly been created for the purpose of drug delivery, as animal cells have specific recognition sites for galactose, mannose and other specific carbohydrates [Jicsinszky et al., 1996].

7

Loading & Release Models

In order to be able to understand and explain the absorption and release patterns of a drug from a delivery matrix a theoretical approach is needed. Binding isotherms are models that allows one to describe the connection between the free amount of drug in solution with the amount of drug bound to a material. In order to describe this relationship, experiments are conducted where the material to be investigated is applied to solutions with varying known drug concentrations. After equilibration, the concentration of free drug remaining in the solution (F) is measured and the amount of bound drug, (B), can be calculated as B = I - F, where I denotes the initial amount of drug in the solution. The binding isotherm can then be studied by plotting F against B. The binding isotherms can be categorized into two main types, the homogeneous and heterogeneous isotherms. Homogeneous isotherms assume that there exist a finite number of binding sites on the material, all having the same affinity and specificity for the incorporated drug whereas heterogeneous isotherms assume a varying system of binding sites where the affinity and specifity for the drug are not necessarily the same values for the binding sites [Larsen, 2006].

7.1 Ligand Binding

If we imagine a system with finite drug molecules and delivery matrix binding sites, one can investigate the relations between drug and delivery matrix. We begin by defining the drug or ligand as L, and the matrix or substrate as S. Let the value m define the maximum number of binding sites on L for S and h being the number of occupied sites so that $h = 1, 2, 3, ..., m$. m is thus the maximum amount of binding sites that each matrix site can bind to on the drug. Similarly, we let the value n define the maximum number of binding sites on S for L and i being the number of occupied sites so that $i = 1, 2, 3, ..., n$. n is thus the maximum amount of binding sites for a drug molecule on a matrix site. We can now define expressions for S and L for what is called the mass balance. S_t and [S] define the total and unbound substrate concentrations whereas L_t and [L] define the total and unbound ligand concentrations [Connors, 1987]. We note that [L] is identical to the free drug concentration F, but for obvious reasons of simplification [L] is chosen to define the free drug or ligand concentration in the following theoretical expressions. The expressions are defined as follows:

$$S_t = [S] + \sum_{\substack{h=1 \\ i=1}}^{m,n} h[S_h L_i]$$

$$L_t = [L] + \sum_{\substack{h=1 \\ i=1}}^{m,n} i[S_h L_i] \tag{7.1}$$

As an example, we will set $m = 1$ and $n = 2$. In this case, The substrate or matrix, S, will have two binding sites for the ligand or drug L, which in turn can only bind to one matrix molecule. From the above equations this gives us $S_t = [S] + [SL] + [SL_2]$ and $L_t = [L] + [SL] + 2[SL_2]$. The example is illustrated in figure 7.1 for further understanding. As a measure of extent of binding the average number of drug molecules bound to the matrix, B, is defined as below:
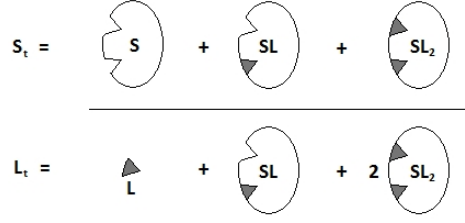
$$B = \frac{L_t - [L]}{S_t} \tag{7.2}$$

Figure 7.1: Figure illustrating the concentrations in the case where m = 1 and n = 2.

Combining equation 7.1 with 7.2 gives a general interpretation of B. We define $m = 1$ to limit the interpretation to suit the appropriate model. Thus, $m = 1$ is reasonable for our model with one macromolecular drug delivery matrix and n drug molecules, but the limitation is also very reasonable for many other equilibria including protonations or metal ion complexation. With $m = 1$, B becomes:

$$B = \frac{\sum_{i=1}^{n} i[SL_i]}{S_t} \tag{7.3}$$

In order to proceed in defining a general binding model, we need to eliminate all complex concentrations from the above stated formula. This can be achieved by substituting the stability constant expression in terms of the overall constants:

$$\beta_{hi} = \frac{[S_h L_i]}{[S]^h [L]^i} \tag{7.4}$$

This is possible since multiplying the stepwise binding constants, K_{1i}, will give the overall stability constant β_{1i}. The statement is illustrated below for the case of $i = 2$:

$$K_{11} = \frac{[SL]}{[S][L]}$$

$$K_{12} = \frac{[SL_2]}{[SL][L]}$$

$$K_{11}K_{12} = \frac{[SL]}{[S][L]}\frac{[SL_2]}{[SL][L]} = \frac{[SL_2]}{[S][L^2]} = \beta_{12}$$

If we now substitute S_t, and then β_{1i}, into equation 7.3, we get:

$$B = \frac{\sum_{i=1}^{n} i[SL_i]}{[S] + \sum_{i=1}^{n}[SL_i]}$$

$$= \frac{\sum_{i=1}^{n} i\beta_{1i}[S][L]^i}{[S] + \sum_{i=1}^{n} \beta_{1i}[S][L]^i}$$

Dividing with [S] on both sides of the fraction gives us the final definition of the average number of drug molecules bound to the matrix, B:

$$B = \frac{\sum_{i=1}^{n} i\beta_{1i}[L]^i}{1 + \sum_{i=1}^{n} \beta_{1i}[L]^i} \tag{7.5}$$

The simplest mathematical binding model is the Langmuir isotherm which considers one single substrate entity, $m = 1$. The isotherm is based on the assumptions that binding of drug only occurs in a monolayer on the material surface, that the model is homogeneous with n distinguishable sites, and that the drug binding to one site on the surface is independent of the occupation at other binding sites. The binding of drug occurs within an equilibrium with the rate k_a for adsorption and k_d for desorption, the overall binding constant hereby becoming $K = \frac{k_a}{k_d}$. The number of occupied binding sites, B, relative to the total amount of binding sites, n, is defined as $\theta = \frac{B}{n}$. Hence, θ can be considered as a parameter that describes the fractional binding at the surface. The model is often used to interpret the adsorption to a solid surface from a gas or liquid phase. In order to derive the theoretical binding isotherm, it is necessary to consider the various isomeric complexes that can be formed with the different ways i drug molecules can be distributed among n binding sites:

$$\frac{n!}{(n-i)!i!}$$

The microscopic binding constant, k, is identical for all n binding sites as the model presumes that drug binding to one site is independent of drug binding to another site. It is thus, the stepwise binding constants K_{1i} that describes the binding of the ith molecule to the matrix. Apart from k, K_{1i} is therefore dependent on the ratio between the occupied and unoccupied sites on the matrix. That is, K_{1i} is dependent on the number of unoccupied sites on SL_{i-1} or $n - (i - 1)$, which favors association, and the number of occupied sites on SL_i or simply i, which favors dissociation. This gives us the following equation:

$$K_{1i} = \frac{n - (i - 1)}{i} k$$

$$= \frac{n - i + 1}{i} k \tag{7.6}$$

From [Connors, 1987], we are given the standard derivation of the binding isotherm 7.6. The overall binding constant, β_{1i}, is thus given as:

$$\beta_{1i} = \prod_{j=1}^{i} K_{1j} = k^i \prod_{j=1}^{i} \frac{n - j + 1}{j}$$

The above product is seen to be equivalent to the binomial coefficient, $\binom{n}{k}$, or:

$$\prod_{j=1}^{i} \frac{n - j + 1}{j} = \frac{n(n-1)\dots(n-i+1)}{1 \cdot 2 \cdot 3 \dots i} = \frac{n!}{i!(n-i)!}$$

And thus, β_{1i} can be written as:

$$\beta_{1i} = \frac{n!}{i!(n-i)!} k^i$$

If we now insert the overall binding constant into the average number of drug molecules bound to the matrix, 7.5, we end up with:

$$B = \frac{\sum_{i=1}^{n} i \frac{n!}{i!(n-i)!} k^i [L]^i}{1 + \sum_{i=1}^{n} \frac{n!}{i!(n-i)!} k^i [L]^i}$$

$$= \frac{\sum_{i=1}^{n} i \frac{n!}{i!(n-i)!} k [L]^i}{1 + \sum_{i=1}^{n} \frac{n!}{i!(n-i)!} k [L]^i} \tag{7.7}$$

The denominator is observed to be the binomial expansion of $(1+k[L])^n$, or:

$$(1 + k[L])^n = 1 + \sum_{i=1}^{n} \frac{n!}{i!(n-i)!} k[L]^i \tag{7.8}$$

Differentiating 7.8 with respect to x = k[L] and rearranging by multiplying with x on both sides results in the following form of the expression:

$$nk[L](1 + k[L])^{n-1} = \sum_{i=1}^{n} i \frac{n!}{i!(n-i)!} k[L]^i \tag{7.9}$$

Substituting 7.8 and 7.9 into 7.7 results in the final form of the binding isotherm:

$$B = \frac{nk[L](1 + k[L])^{n-1}}{(1 + k[L])^n}$$

$$= \frac{nk[L]}{1 + k[L]} \tag{7.10}$$

We now define the rates of change in binding site occupation in the terms of adsorption and desorption for the Langmuir Isotherm approach. They are stated as follows:

$$v_a = \frac{d\theta}{dt} = k_a[L](n - B) = k_a[L]n(1 - \theta)$$

$$v_d = \frac{d\theta}{dt} = k_d B = k_d n\theta$$

When equilibrium occurs, the adsorption and desorption rates will be equal and the socalled Langmuir isotherm can be derived:

$$k_a[L]n(1 - \theta) = k_d n\theta$$

$$\frac{k_a}{k_d}[L]n(1 - \theta) = n\theta$$

$$K[L] = \frac{\theta}{1 - \theta} \tag{7.11}$$

The correctness of the adsorption and desorption rates for the Langmuir Isotherm model is proven by substituting $\theta = \frac{B}{n}$ into 7.11. We thus observe that equation 7.10 is indeed a theoretical definition of the Langmuir isotherm, defined as:

$$B = \frac{nk[L]}{1 + k[L]}$$

$$= \frac{nkF}{1 + kF} \tag{7.12}$$

Plotting F against B/F gives a straight line if the drug binding to the delivery matrix can be described as a langmuir isotherm. An example of this socalled *Scatchard plot* can be seen in figure 7.2. An approximated version of the Langmuir isotherm, which is based on the assumption that the material has two types of binding sites, one with high affinity and one with low affinity for the respective drug. The approximated model is still homogeneous but now considers two sets of parameters, hence the name Bi-Langmuir isotherm. When plotting F against B/F in the Scatchard plot for the Bi-Langmuir isotherm, the data often form a curve instead of a straight line. The resulting two straight lines of the Bi-Langmuir isotherm describe the high and low affinity binding sites [Larsen, 2006].
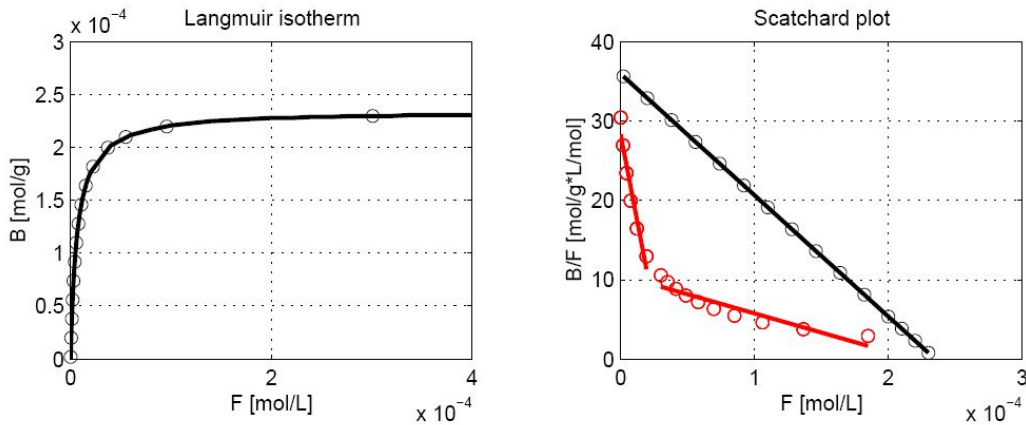
Figure 7.2: The left illustration shows the typical distribution of datapoints in a Langmuir isotherm. To the right, an example of the Scatchard plot, showing data points for both Langmuir and Bi-Langmuir isotherms [Larsen, 2006].

Langmuir-Freundlich Isotherm

In order to take eventual interactions between occupied binding sites into consideration the Freundlich isotherm is useful. It is a simple heterogeneous binding model and is based on the assumption, that the binding energy changes logarithmically as a function of drug concentration. The isotherm considers two parameters, a and m, and assumes that there are an infinite number of binding sites [Larsen, 2006]. The isotherm is expressed as stated in the equation below:

$$B = aF^m \tag{7.13}$$

The parameter a defines the total amount of binding sites and their average binding constant. Parameter m is the heterogeneity index and ranges between 0 to 1, where 1 determines

complete homogenity. As the parameter approaches 0 the material gradually becomes more and more heterogeneous. The Freundlich isotherm can only be applied by its own when the concentrations are well below the saturation limit for the material as it is known that the material becomes saturated if the concentration of drug is high enough [Larsen, 2006]. An equilibrium has been established and it becomes increasingly less energetic favourable to bind any substantial amount of drug above this point. B will therefore approach the total number of binding sites asymptotically as in the Langmuir isotherm, which can be expressed with the following equation:

$$B = n\frac{aF^m}{1 + aF^m} \tag{7.14}$$

The modified isotherm is called the Langmuir-Freundlich isotherm. If the free drug concentrations F are small, the equation will reduce to a Freundlich isotherm with a finite number of binding sites, n. If the concentrations are very large the asymptotical approach of B towards n is seen, as with the Langmuir isotherm [Larsen, 2006]. If the data are applied to a double logarithmic plot as seen in figure 7.3, it can be studied if the material follows the Freundlich or Langmuir-Freundlich isotherm.

It is important to notice that it is not possible to accurately calculate the value of parameters in the previous described isotherm models for drug adsorption, when considering combined interacting materials as with the β-CD modified HA. Instead, the acquired data from the experiments are plotted in the supportive scatchard and double logarithmic plots in order to determine and discuss the drug binding pattern of each sample material.
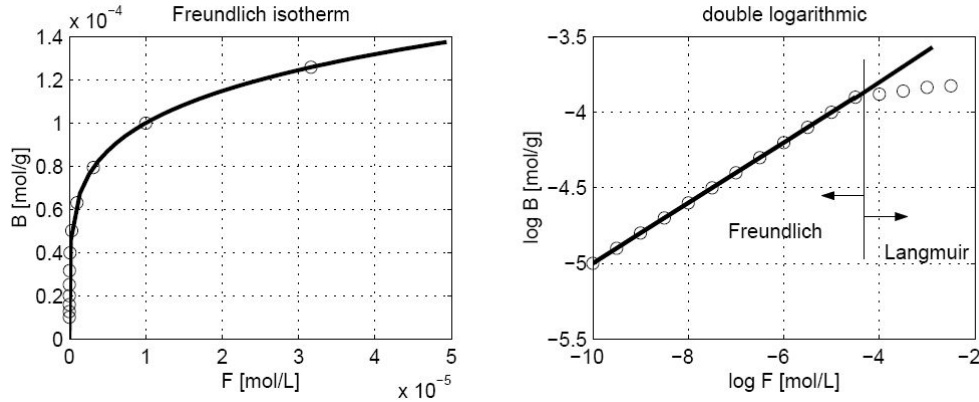

Figure 7.3: The left illustration shows the typical distribution of datapoints in a Freundlich isotherm. To the right, an example of the double logarithmic plot, showing data points for a Langmuir-Freundlich isotherm [Larsen, 2006].

7.2   Ligand Release

Drug release from the matrix of hydroxyapatite has been investigated thoroughly by Ginebra and colleagues, using a modified version of Higuchis law [Ginebra *et al.*, 2006], [Higuchi, 1963]. The expression of Higuchis law can be seen in equation 7.15.

$$M_t = AM_0[\frac{D'\epsilon}{\tau}C_S(2C_0 - \epsilon C_S)t]^{1/2} \tag{7.15}$$

M_t is the amount of drug released at the time t, A is the surface area of the amount of material, and M_0 is the total amount of drug that is present within the material matrix [Ginebra *et al.*, 2006]. ϵ is the porosity, which is a term that can be considered as the void spaces in a material. Porosity is defined as the ratio between the volume of void space inside of the material and the total bulk volume of the material. It is usually measured as a fraction ranging between 0-1. D' is the diffusion coefficient, which is the rate at which the drug will move from the inside and out of the matrix. It is a theoretical value and can eventually be calculated if all other parameters are known. τ is the tortuosity, an estimated value, which considers the average amount as well as the steepness of turns inside the material matrix. The range of the parameter goes from 1 for a straight line to infinite which is the tortuosity for a perfect circle [12].
C_S and C_0 are constants defining the drug solubility within the matrix, and the initial drug concentration, respectively. The drug solubility within the matrix will be higher if the drug is more hydrophobic and the solubility is lower if the drug is more hydrophilic whereby it may dissolve more readily in the solvent [Ginebra *et al.*, 2006].
The way changes in the above described parameters affects the drug release is illustrated for the convenience of the reader in figure 7.4.
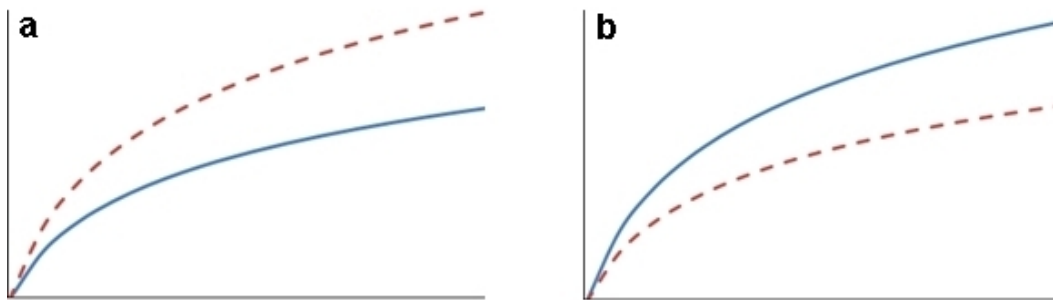

Figure 7.4: The solid line in both images illustrates the initial theoretical release pattern of a drug. If one or more of the variables considering the surface area, porosity and rate of diffusion are increased or the tortuosity is decreased the amount of drug released with time, t, tends to increase. This is illustrated in figure a. The opposite changes in one or more of the parameters results in lower amounts of drug released, illustrated in figure b.

The surface area of the matrix is proportional to drug release. If the surface area decreases the amount of drug that can pass the surface per time unit will decrease as well and vice versa. Similarly, the relative amount of drug released is also proportional with the rate of diffusion as well as with the porosity of the matrix. If the tortuosity of the matrix is high, however, the amount of released drug with time is relatively low since the drug is facing a more difficult and complex pathway from within the matrix before reaching the surface.

Course of Action

8

The previous chapters have given a broad introduction into the various aspects that have to be considered when it comes to understand the structure and function of biomaterials, the risk of post-surgical infections, and how they can be treated or prevented. This chapter summarizes and connects the gained information and describes how the chosen biomaterials are to be modified and subsequently investigated to determine their potential for controlled local administration of antibiotics in bone tissue.

The goal of developing a suitable drug administration route is to acquire a concentration of the active drug at the target of action, which is above the minimum effective dose and below the minimum toxic dose. In order to achieve this concentration the interaction between drug solubility and the membrane permeability of the drug is normally of crucial importance. In general, an effective drug must be water soluble to some degree in order to be rendered active but must also possess lipophilic characteristics in order to permeate biological membranes. The most potent drugs will have a high solubility and high permeability, relative to the amount of applied drug and type of formulation [Loftsson *et al.*, 2007], [Wang *et al.*, 2005]. In the case of the implant being the drug delivery agent, however, many of these obstacles are avoided. Since the site of infection is the same as the implantation site itself, the most important factor becomes the solubility of the drug in the body fluids surrounding the implant. This is to prevent bacteria from multiplying as soon as the implant comes into contact with the tissue of the implantation site and for a short period of time after the surgery has been completed. The permeability of cellular membranes of the drug becomes of little importance as the function of the application is to prevent an infection to occur locally, and not to treat an already existing infection that has spread into the surrounding tissue.

The routes of administration can roughly be divided into three main groups; topical, enteral, and parenteral. Delivery methods using a topical route are administering the drug locally where the effect of the drug is desired, whereas enteral and parenteral administration routes have a systemic effect, the difference being that enteral routes are applied through the digestive tract and the parenteral routes are not [Wang *et al.*, 2005], [13]. Thus, a topical administration route will be designed that is able to release the desired antibiotic drug into the local surroundings of the implant in a controlled way to prevent nosocomial infections. As described in chapter 6, CDs represent primary and secondary hydroxy-groups at the ends of the CD toroid, which can be utilized and modified in order to immobilize and hereby attach them covalently to the respective bioceramic surface. In the following two sections the cyclodextrin immobilization method and the chosen antibiotic ligand, Fusidic Acid, will be introduced. Finally, the various methods that will be used for the investigation of the CD attachment to the bioceramic as well as the drug loading and release kinetics will be introduced.

8.1 Cyclodextrin Immobilization

Immobilization is defined as a restriction of movement. Many different kinds of immobilization methods are available, the most widely used methods being cross linking, entrapmment, and carrier binding. This work focuses on the latter immobilization method. The carrier binding technique concerns binding of the CD to a carrier directly or by a linker. The carrier can be a surface or a stable structure in a solution. The chemical and mechanical properties of the carrier are significant factors when choosing immobilizing procedure [Drevon, 2002].

Immobilization of β-CD on Surface OH-groups

In order to modify silica-gel and HA with CDs, a slightly altered version of the method presented by Ponchel and co-workers has been used, in which they used the 7-membered β-CD molecule as surface modification for silica-gel [Ponchel *et al.*, 2004]. The β-CD is immobilized by preliminary modification of the hydroxy-groups by 3-glycidyl oxypropyl trimethoxysilane, functioning as a spacer arm between β-CD and the bioceramic matrix. The method results in the formation of an ether linkage between the surface and the β-CD molecule, involving a chemical reaction between a primary hydroxyl group on the β-CD and the highly reactive epoxy-group of the spacer arm.

The immobilization procedure takes place in two steps. First, the hydroxy-groups of the bioceramic are activated and set to react with the trimethoxysilane spacer. As the spacer is highly reactive towards oxygen, the activation step is prepared accordingly and conducted in a nitrogen atmosphere. Hereafter, β-CD is mixed with sodium hydride in order to form reactive alcoholates from the primary hydroxy-groups. The resulting mixture is added to the spacer arm modified bioceramic, which finalizes the immobilization procedure. It is assumed that the β-CDs will immobilize on the bioceramic in a monolayer, due to steric hindrance. The method is illustrated in figure 8.1.
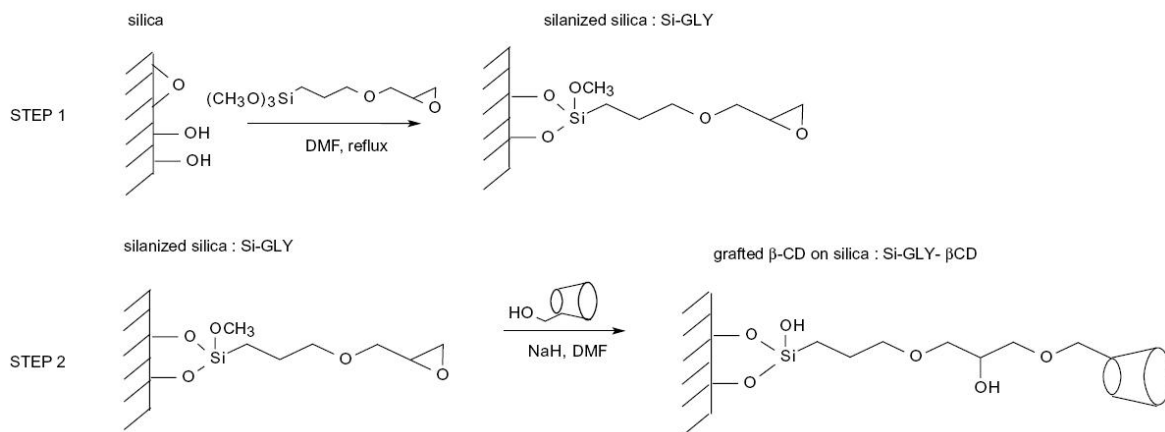
Figure 8.1: Immobilization of β-CD to OH-groups on a bioceramic surface, using a trimethoxysilane spacer arm. the method involves a chemical reaction between a primary hydroxyl-group on the β-CD and the highly reactive epoxy-group of the spacer. Modified from [Ponchel *et al.*, 2004].

8.2   Fusidic Acid

Fusidic Acid (FA) has been chosen as drug model in this work because of its effect against multiple-resistant *S. aureus*, one of the main causes of nosocomial infections as described in chapter 3. FA has been effectively used for more than three decades in clinics against severe gram-positive infections. It is furthermore an active agent against staphylococci that is resistant to other classes of antibiotics [Fantin *et al.*, 1993]. The average MIC_{50} for *S. aureus* lies between 0.059 - 0.066 μg/mL, or approximately $1.28 \cdot 10^{-7}$mol/L, with an observed maximum MIC_{50} at 0.16μg/mL $3.09 \cdot 10^{-7}$mol/L [Andersen, 2001]. FA is often used topically, but may also be given systemically as tablets or injections [14]. When given systemically the antibiotic spreads widely throughout various parts of the body including bones and joint fluid. The molar mass of FA is 516.709g/mol and the pKa value of FA is at 5.35. The water solubility has been determined to 1.16mg/mL at pH levels of 7.5, simulating the conditions of body fluids (pH 7.2-7.5). Furthermore, the binding constant of FA towards free β-CDs has

been determined to be 382±36 M^{-1} [Andersen, 2001]. The molecular structure of FA can be seen in figure 8.2.
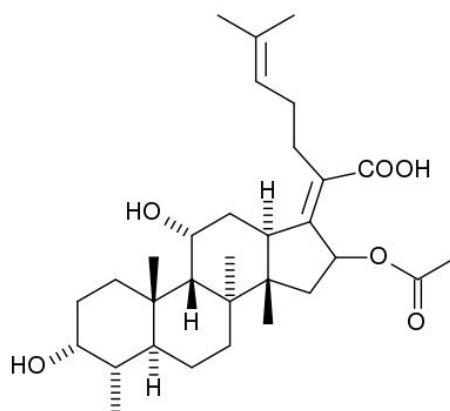

Figure 8.2: Illustration of the molecular structure of fusidic acid [14].

FA is termed 'bacteriostatic' since it inhibits bacterial replication without killing the bacteria, but may be bactericidal at high concentrations [Howden, *et al.*, 2006]. It is active against *S. aureus*, most coagulase-negative staphylococci, Corynebacterium species, and most clostridium species. However, it has no useful activity against streptococci, enterococci or most gram-negative bacteria (except *Neisseria*, *Moraxella*, *Legionella pneumophila* and *Bacteroides fragilis*) [14].

One of the most crucial steps in bacterial protein synthesis is the elongation phase, in which the protein polypeptide strain grows as the ribosome moves along the mRNA in a stepwise fashion. The process involved in moving the ribosome onto the next RNA codon is called translocation and requires energy. The two elongation factors EF-Tu and EF-G are vital in this proces, where EF-G is particularly involved in the translation step and responsible for the hydrolysis of GTP to GDP, which provides the translocation with the necessary energy [Besier *et al.*, 2003]. FA works by binding to the EF-G on the ribosome and prevents the release of the GDP complex from it, thus inhibiting the next stage in protein translation [Howden, *et al.*, 2006].

FA monotherapy has been strongly associated with the emergence of FA resistance among various *S. aureus*-type infections. The key causes for resistance are mutations in the fusA gene, which encodes for EF-G. A single mutation in the fusA gene resulting in an amino-acid exchange in EF-G can reduce FA binding affinity to the elongation factor, and thus significantly reduce inhibition of bacterial protein synthesis. However, FA in combination with other agents such as rifampicin has proven effective for otherwise difficult to treat infections such as skin and joint infections due to multiple-resistant *S. aureus* [14].

8.3 Experimental Methods

When investigating the potential of the modified bioceramics as an application for local drug delivery it is first of all necessary to understand the structure of the bioceramic matrix before and after β-CD attachment. Subsequently, the loading and release kinetics can be investigated by analyzing the complexation between drug and bioceramic matrix with and without β-CD. In the following, the methods that have been chosen for the investigation of the surface modification and loading and release kinetics of the drug in this work will be introduced.

8.3.1 Investigating CD Attachment and Changes in Surface Structure

The amount of attached β-CD to the matrix surface will be investigated with three distinct methods; Thermogravimetric Analysis (TGA) and the Phenol Sugar Assay method. Furthermore, it is expected that the attachment of both the 3-glycidyl oxypropyl trimethoxysilane spacer arm and, subsequently, β-CDs will significantly alter the structure of the bioceramic surfaces. Changes of the structure from modified and unmodified matrices is investigated with BET, CHN analysis, and X-Ray Powder Diffraction (XRPD).

Thermogravimetric Analysis TGA can be described as a very fine balance placed inside a furnace. It presents several possibilities for investigating the mass or changes of mass as a function of temperature and/or time by means of controlling heating rate or temperature programs with intervals of controlled heating rates and isothermal steps. Changes of mass stem from chemical reactions, magnetic, or electrical transformations of the material and during sublimation, evaporation, and decomposition. The difference in temperature for decomposition (and the resulting loss of mass) results in multistep losses of mass which is utilized when investigating the different surface modifications of the used bioceramic matrices [Ehrenstein et al., 2004]. When using TGA a known amount of matrix with and without modifications is heated to 800°C with a heating rate of 10K/minute. As temperature increases, organic compounds will begin to pyrolyse and carried away from the system by a constant flow of Argon gas. The reduction in weight of each sample is measured inside the TGA apparatus with intervals of 1°C whereafter the data of the various matrices and modifications are compared with each other.

Phenol Sugar Assay The Phenol Sugar Assay method is used to obtain a colorimetric quantitative determination based on the reaction between carbohydrates with concentrated sulphuric acid and phenol. When mixing CDs with concentrated sulphuric acid the glucosidic bonds of the CDs are first hydrolyzed, whereafter the resulting glucopyranose molecules are dehydrated into 5-hydroxymethyl furfural [Robyt, 1999]. A scheme that shows the reaction steps from glucopyranose to 5-hydroxymethyl furfural is illustrated in figure 8.3.
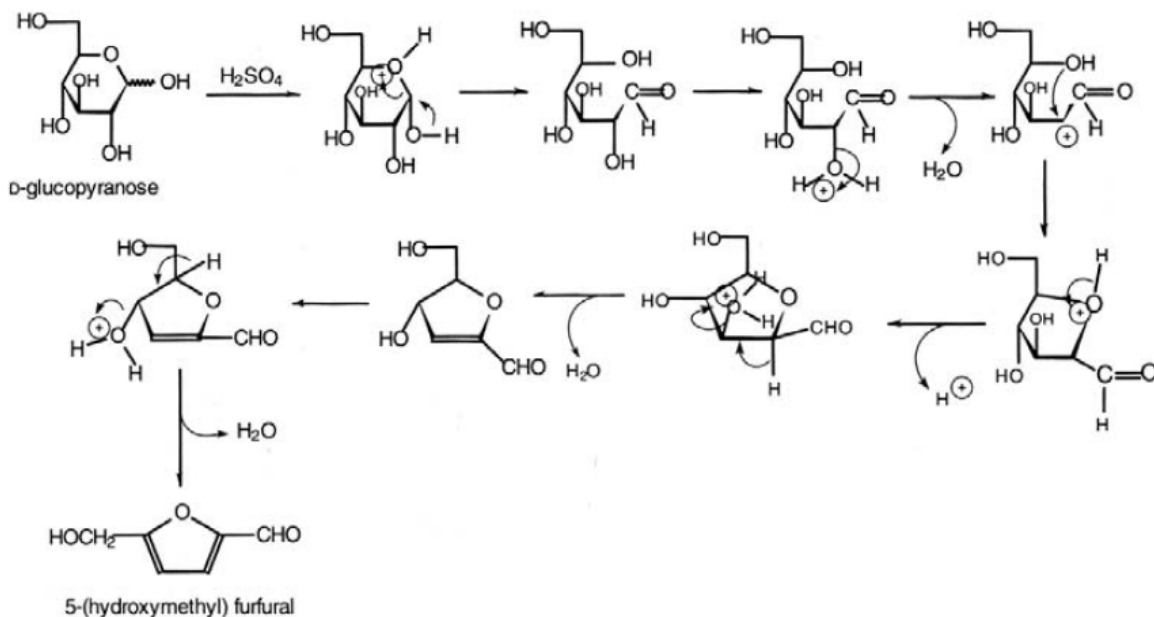

Figure 8.3: Illustration of the dehydration of glucopyranose by concentrated sulphuric acid [Robyt, 1999].

When subsequently mixed with phenol, the monosaccharide derivate condenses with phenol to form a coloured product that is suitable for spectrometric measurements with absorbance at wavelengths between 470-490nm [Robyt, 1999].

BET BET is a theory used by scientists to describe adsorption of gas molecules onto solid surfaces. The BET method is widely used in surface science for the calculation of surface areas of solids by physical adsorption of gas molecules. Derived by Brunauer, Emmett and Teller, it is basically an extension of the Langmuir equation which accounts for the existence of multilayers in the adsorption process [Brunauer *et al.*, 1938]. It is still the most frequently used model even though it has been greatly criticised. The theory uses the assumptions of the Langmuir theory, primarily the postulate that the rate of adsorption onto surface sites is equal to the rate of evaporation from occupied sites. It is also assumed that the energy of adsorption for the second and subsequent layers of adsorbed material is equal to that of liquefaction, and the total number of molecules adsorbed is the sum of all the adsorbed layers [15]. The method is used to determine the surface area of the examined bioceramics as well as the total pore volume.

CHN Analysis Elemental Analysis is a process where a sample of some material is analyzed for its elemental and sometimes isotopic composition. The most common form of elemental analysis, CHN analysis, is accomplished by combustion analysis. In this technique, a sample is burned in an excess of oxygen, and various traps collect the combustion products carbon dioxide, water, and nitric oxide. The weights of these combustion products can be used to calculate the composition of the unknown sample. The analysis is used to examine the elemental composition of carbon, hydrogen and nitrogen within silica-gel and β-CD modified silica-gel specimen.

X-Ray Powder Diffraction XRPD is a technique that uses X-ray Diffraction on powder samples for structural characterization of materials. In an ideal situation a powdered sample represents every possible crystalline orientation equally. When the scattered radiation from a powder diffractometer is collected on a flat plate detector the rotational averaging leads to more smooth diffraction rings around the beam axis rather than the very distinct spots that are observed for single crystal diffraction. The angle between the beam axis and the ring is called the scattering angle and in X-ray crystallography always denoted as 2θ. In accordance with Bragg's law, each ring corresponds to a particular reciprocal lattice vector G in the sample crystal [Kittel, 2005], [16]. This leads to the definition of the scattering vector as:

$$G = q = 2k \cdot \sin(\theta) = \frac{4\pi \cdot \sin(\theta)}{\lambda} \tag{8.1}$$

Powder diffraction data are usually presented as a diffractogram in which the diffracted intensity I is shown as function either of the scattering angle 2θ or as a function of the scattering vector q. The latter variable has the advantage that the diffractogram no longer depends on the value of the wavelength λ [16]. The purpose of the XRPD experiments in this work is to determine the structural conformation of the bioceramic surfaces of silica-gel and β-CD modified silica-gel.

FIB-SEM The scanning electron microscope (SEM) is a type of electron microscope that images the sample surface by scanning it with a high-energy beam of electrons. The electrons interact with the atoms that make up the sample producing signals that contain information about the samples surface topography, composition and other properties such as electrical

conductivity. The signals result from interactions of the electron beam with atoms at or near the surface of the sample. In the most common mode of detection, secondary electron imaging, the SEM can produce very high-resolution images of a sample surface, revealing details about less than 10 nm in size. In order to be able to investigate a specimen all water must be removed from the sample because the water would vaporize in the vacuum that is created in the SEM chamber. Furthermore, the sample must be electrically conductive at the surface and electrically grounded to prevent the accumulation of electrostatic charge at the surface. The charging will result in scanning faults and other image artifacts. Thus, metal objects require special preparation for the procedure. Non-conductive specimens have to be coated with a thin coating of electrically conducting material, commonly gold, since the samples will otherwise charge when scanned by the electron beam. The thin conductive layer is usually deposited on the sample either by low vacuum sputter coating or by high vacuum evaporation [Waser, 2003], [17].

A Focused Ion Beam setup, or FIB, is similar to the SEM except that a focused beam of gallium ions is used instead of a focused beam of electrons. The ion beam can be operated at low beam currents for imaging or high beam currents for site specific removal of material by sputtering, allowing precision milling of the specimen down to a sub micron scale. Until recently, the overwhelming usage of FIB has been in the semiconductor industry [Stevie et al., 2005]. In this project, however, a FIB-SEM system is used to investigate the surface and matrix composition of virgin and modified silica-gel. Since the specimens are non-conductive they are covered with a thin layer of gold as explained above. Furthermore, the specimen stage has to be tilted to an angle of 54° as the FIB beam is located in this position of the apparatus and has to be in a vertical position above the specimen. The setup is illustrated in figure 8.4.
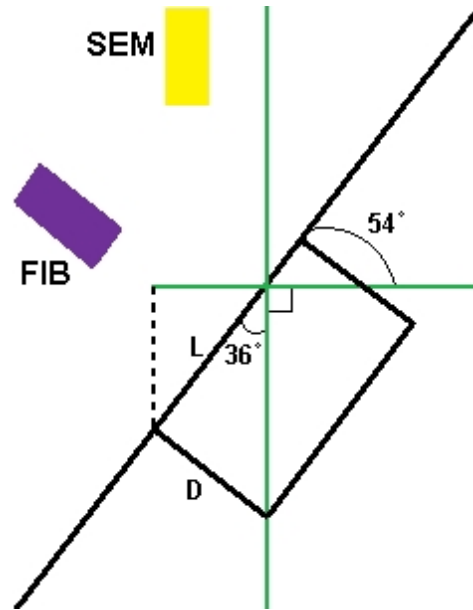

Figure 8.4: Illustration of the FIB-SEM setup, including the known angles and lengths from any SEM scan of a specimen when the plane is tilted to an angle of 54°.

When measuring into a tilted specimen with the SEM the acquisition software automatically corrects the scale of the image to resemble the scanning angle of the FIB. Thus, when scanning with the SEM the correct scale of the surface of the sample specimen is shown. We are, however, interested in the depth of the milled region of interest and not the width of length. The depth, D, can be calculated from the projection of it to the surface giving the length, L, and the angle 180° - 90° - 54° = 36°. Thus, the depth can be calculated with the equation:

$$D = tan(36°) \cdot L \qquad (8.2)$$

After placing the specimen into the setup, a small cavity is milled with the FIB system into the surface of each matrix sample whereafter the elemental composition throughout the crust of the specimen is investigated with an energy-dispersive X-ray spectroscope (EDX). The EDX system analyzes x-rays emitted by the matter in response to being hit with charged particles. At rest, an atom within the sample contains ground state electrons in discrete electron shells bound to the nucleus. To stimulate the emission of characteristic X-rays from a specimen, a high energy beam of X-rays is focused into the sample being studied. The incident beam may excite an electron in an inner shell, ejecting it from the shell while creating an electron hole where the electron was. An electron from an outer, higher-energy shell then fills the hole, and the difference in energy between the higher-energy shell and the lower energy shell may be released in the form of another X-ray. The number and energy of the X-rays emitted from a specimen can be measured by an energy dispersive spectrometer. As the energy of the X-rays are characteristic of the difference in energy between the two shells, and of the atomic structure of the element from which they were emitted, this allows the elemental composition of the specimen to be measured. Elements with atomic numbers ranging from that of beryllium to uranium can be detected. The minimum detection limits vary from approximately 0.1 to a few atom percent, depending on the element and the sample matrix [18].

8.3.2 Methods for the Analysis of Ligand Loading and Release

When it comes to investigate quantitative ligand loading and release kinetics of the modified and unmodified matrices the principles of light absorption and Fluorescence Spectroscopy (FS) was chosen. Release kinetics of Fusidic Acid are investigated with High Performance Liquid Chromatography (HPLC). Furthermore, experiments with Confocal Laser Scanning Microscopy (CLSM) are conducted to qualitatively determine matrix binding of a secondary fluorescent ligand, 1-Anilino Naphthalene 8-Sulfonic Acid (1,8-ANS). This secondary ligand is chosen for both FS and CLSM experiments since Fusidic Acid is unable to emit any sorts of light that can be detected.

Absorption Spectroscopy Fusidic Acid, the antibiotic ligand, is capable of absorbing light at wavelengths below 250nm, and concentrations can thus be determined quantitatively in a UV-Vis spectrophotometer, where light is emitted onto a cuvette containing the sample while a detector behind the cuvette measures the intensity of the light that passes through the cuvette and the sample. The difference in intensity of the light before and after it passes through the cuvette is absorbed by the molecules in the sample and can be used to determine concentrations of light absorbing molecules. Various concentrations of FA are prepared and mixed with modified and unmodified silica-gel and HA matrices in order to determine the amounts of free and bound drug molecules according to the loading isotherm models described in chapter 7. Thus, all samples contain the same amount of matrix.

Confocal Scanning Laser Microscopy The CLSM apparatus is used to qualitatively investigate fluorescence emissions from modified and unmodified HA and Silica-gel matrices with 1,8-ANS as a ligand. 1,8-ANS is a very effective way to identify the presence of β-CDs sinse the fluorescence intensity is boosted multiple times when the molecule becomes prone to less hydrophilic environments such as the cavity of a CD. A setup of the CLSM apparatus can be seen in illustration 8.5.
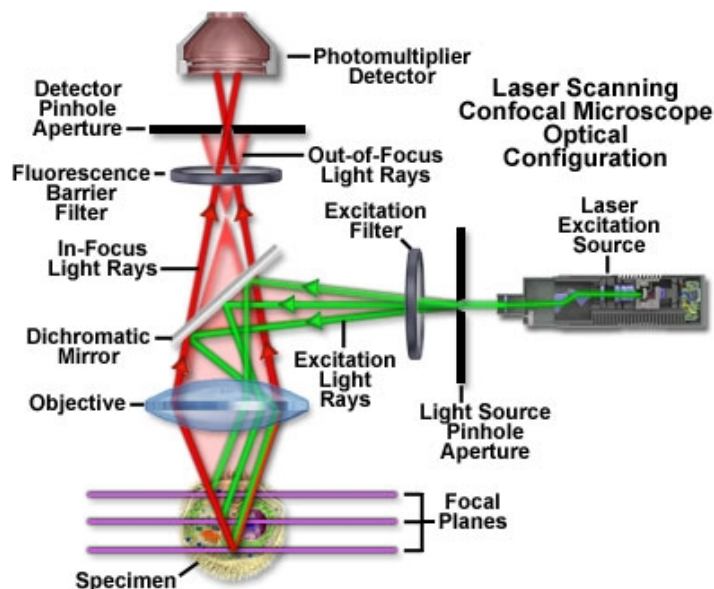
Figure 8.5: Illustration of the CLSM setup. Modified from [19]

In CLSM, a laser beam passes through a light source aperture that is situated in a conjugate plane with a scanning point on the specimen and a second pinhole aperture positioned in front of the detector. The laser beam is then focused by an objective lens into a small focal volume within or on the surface of the specimen. In biological applications especially, the specimen may be fluorescent. Scattered and reflected laser light as well as any fluorescent light from the illuminated spot is then re-collected by the objective lens [19]. The significant amount of fluorescence emission that occurs at points above and below the objective focal plane is not confocal with the pinhole and forms extended foggy disks in the aperture plane. Because only a small fraction of the out-of-focus fluorescence emission is delivered through the pinhole aperture, most of this extraneous light is not detected by the photomultiplier and does not contribute to the resulting image. Refocusing the objective in a confocal microscope shifts the excitation and emission points on a specimen to a new plane that becomes confocal with the pinhole apertures of the light source and detector. This permits one to obtain images of planes at various depths within the sample specimen [Pawley, 2006].

Fluorescence Spectroscopy The free and bound 1,8-ANS molecules are quantitatively investigated in a Fluorescence Spectrophotometer. The FS apparatus emits light at a distinct wavelength onto the sample molecules which are excitated to a higher state of energy. The FS apparatus measures the emitted light from the sample in a 90° angle and the acquired data can then be used to determine quantitative concentrations of 1,8-ANS of each sample. Just as with FA, various concentrations of 1,8-ANS are prepared and mixed with modified and unmodified bioceramic matrices. Both absorption and emission of energy are unique characteristics of a particular molecular structure. If a material has a direct bandgap in the range of visible light, the light shining on it is absorbed, causing electrons to become excited to a higher energy state. In order to return to the electronic ground state again the molecule can emit a photon, thus losing its energy. Another method would be the loss of heat energy. When the emitted photon has less energy than the absorbed photon, this energy difference is called Stokes shift. When the relaxation occurs both non-radiatively and radiatively, the result is molecular movement and the emission of light with lower energy and thus a higher wavelength [Lakowitz, 1999]. The excitation and relaxation of a potential fluorescent molecule

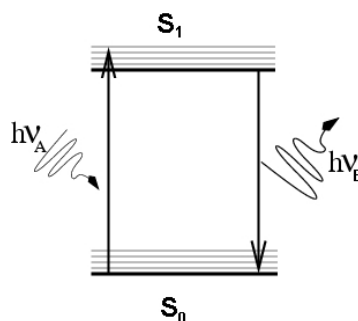is illustrated in the jablonski diagram found in figure 8.6.

Figure 8.6: Jablonski diagram illustrating the excitation and subsequent emission of light from a fluorescent molecule. Incoming excitating light is illustrated as $h\nu_A$ whereas the emitted light is is illustrated as $h\nu_E$. The energy lines in the top and bottom of the diagram symbolize energetic non-radiative relaxation levels of molecular vibration and movement.

High Performance Liquid Chromatography   HPLC is used to determine concentrations of released FA from modified and unmodified Silica-gel and HA matrices. First, all examined matrices are loaded with FA by mixing a fixed amount of matrix with a highly concentrated solution of FA in a buffer that resembles the composition of human body fluids. Hereafter the matrix sample is filtered and dried whereafter it is placed in a column. A solution consisting of buffer only is now sampled through the column and the FA concentrations within each sample is examined.

HPLC is a form of column chromatography used in biochemistry and analytical chemistry to separate, identify, and quantify compounds. HPLC consists of a column that holds chromatographic packing material, also called the stationary phase, a pump that moves the mobile phases and the liquid sample through the column, and a UV detector that shows the retention times of the respective molecules of the sample. The retention time varies depending on the interactions between the stationary phase, the molecules being analyzed, and the combination of solvents that are used in the mobile phase. A separation in which the mobile phase composition remains constant throughout the whole procedure is termed isocratic. The mobile phase composition does, however, not have to remain constant. A separation in which the mobile phase composition is changed during the separation process is described as a gradient elution [Harris, 2007]. The components of the mobile phase are typically termed 'A', 'B', 'C', etc.. The components that change in concentration during the gradient are typically a weak solvent which allows the solute to elute only slowly, and a strong solvent which rapidly elutes the solutes from the column. The weak solvent is often water, while the strong one is an organic solvent miscible with water, such as acetonitrile, methanol, THF, or isopropanol [20].

Materials and Methods

Synthesis of β-CD modified Silica-gel and HA

4g silica-gel (CAS: 7631-86-9) or HA (CAS: 12167-74-7) is dried and mixed with 200ml N,N-Dimethylformamide (CAS: 68-12-2) in a large roundbottom flask in a nitrogen atmosphere. The solution is heated to 90°C for 15 minutes. Hereafter 4ml 3-glycidyloxypropyl trimethoxsilane (CAS: 2530-83-8) is added to the solution, which is left for reaction for 24 hours whereafter the heating is turned off. When the solution has reached room temperature it is washed three times with N,N-Dimethylformamide. The precipitate is now moved to a new roundbottom flask where it is heated to 90°C in a nitrogen atmosphere.
Simultaneously, 1.3g β-CD (CAS: 7585-39-9) is added to 200ml N,N-Dimethylformamide and mixed. 1g Sodium hydride (CAS: 7646-69-7) is washed with n-hexane (CAS: 110-54-3) for 10 minutes whereafter it is filtered and added to the β-CD solution together with 0.5ml tert-pentanol (CAS: 75-85-4). The solution is left for reaction for 6 hours whereafter the filtrate is added to the silica-gel or HA solution and left for 48 hours at 90°C in a nitrogen atmosphere. Hereafter the solution is filtered twice in N,N-Dimethylformamide, twice in millipore water and twice in demineralized water. The pellet is placed in a soxhlet extractor with water for three days at 140°C. Finally, the powder is removed and dried in a vacuum heating chamber at 50°C overnight.

CD Quantification

Thermogravimetric Analysis

Thermogravimetric Analysis is conducted with a Netzsch STA 449C Jupiter thermo-micro balance TG-DSC, a Netzsch TASC 414/4 controller, and a Julabo F25 Refrigerated Circulator. Approximately 25mg of each sample is weighted in an Al_2O_3 crucible and the exact mass of the sample is set to 100% in the acquisition software. Three samples are conducted for each bioceramic; one with matrix only, one with matrix and attached 3-glycidyl oxypropyl trimethoxysilane spacer arm, and one with β-CD attached to the matrix via. the 3-glycidyl oxypropyl trimethoxysilane spacer arms. The protective gas was Ar at a flow rate of 18ml/min while the purge gas also being Ar with a flow rate of 40ml/min. The Thermogravimetric Analysis was conducted at a temperature range from 50-800°C with a heating rate of 10K/min. Initial heating from room temperature and up to 50°C before measurement began was at a heating rate of 15K/min.

Phenol Sugar Assay

10ml solutions of a 0.1mg/ml β-CD standard solution in demineralized water are prepared as seen in table 9.1. 0.6ml of each standard solution is put in four pyrex glass tubes. Three tubes are samples, one tube is a blind reference. 2.5ml concentrated sulphuric acid (CAS: 7664-93-9) is now added to all tubes and left for three hours in a water bath at 50°C.
When analyzing the bioceramic and β-CD modified bioceramic, 6 pyrex glass tubes are prepared with 20 mg sample with 0.6ml water before 2.5ml concentrated sulfuric acid is added to all tubes. These samples are also placed in a water bath at 50°C for three hours. When the reaction time has elapsed, 75μl 90% w/v phenol (CAS: 108-95-2) is added to three of the samples, the remaining three being blinds. The phenol solution is prepared by weighting 9.4g phenol and mixing it with 1.1ml demineralized water. The samples are left for one hour at

Concentration μg/ml	0.1mg/ml standard [ml]
0	0
2.5	0.25
5	0.5
10	1.0
15	1.5
20	2.0
30	3.0

Table 9.1: Preparation of concentrations for the phenol assay standard. The final volume is 10 ml.

room temperature to develop yellowish color. The light absorption of each sample is measured with a UV-VIS spectrophotometer at 487nm.

Investigating Matrix Changes Upon CD Immobilization

CHN Analysis

The elemental composition of virgin and β-CD modified silica-gel with and without FA as ligand was evaluated by elemental analysis. Silica-gel and β-CD modified silica-gel are each applied to 50ml $2.32 \cdot 10^{-3}$M (1.2g/L) FA stock concentration. The samples were left for equilibrium alignment for twentyfour hours and subsequently filtered and dried in a vacuum heating chamber at 50°C overnight. The analysis was performed with the Flash EA1112 (Thermo Fisher, Milan, Italy). Helium was used as the carrier gas. An amount of approximately 2.0-2.5 mg sample was weighed into a pure tin microvial using a microanalysis scale. After directly injecting a defined amount of oxygen, the sample was combusted at a temperature of 950°C. This generated the gases CO_2, H_2O, NO_x, and SO_2. The gas components were introduced in a chamber with active copper which reduced NO_x to N_2. The three gases N_2, CO_2, and H_2O were separated on a gas chromatographic column. The gas was detected by a thermal conductivity detector. A corresponding calibration curve, based upon calibration towards standards supplied by the manufacturer: atropine, nicotinamide, and acetanilide, was made before analysis. Considering the amount of the weighed sample, the percentage of each gas was calculated.

X-Ray Powder Diffraction

The crystalline state of virgin and β-CD modified silica-gel with and without FA as ligand was evaluated by X-ray powder diffraction. Silica-gel and β-CD modified silica-gel are each applied to 50ml $2.32 \cdot 10^{-3}$M (1.2g/L) FA stock concentration. The samples were left for equilibrium alignment for twentyfour hours and subsequently filtered and dried in a vacuum heating chamber at 50°C overnight. Diffraction patterns were obtained on a PANalytical X'Pert PRO X-Ray Diffractometer (Panalytical, Almelo, The Netherlands) in α-1 configuration equipped with an X-celerator detector. Cu (=1.5406Å) was used as anode material and the crystal graphite monochromator operated at a voltage of 40 kV and a current of 45 mA. The samples were analyzed in the 2Θ angle range of 5° to 40° and the process parameters were set as follows: step size of 0.045° (2Θ), scan step time of 0.5 seconds, and time of acquisition of 2 hours.

Investigating Silica-gel with the FIB-SEM setup

Four specimen are prepared, consisting of two virgin and two β-CD modified silica-gel samples. Each sample was attached to the surface of a SEM specimen using silver glue. One sample from each group has previously been prepared with a $2.32 \cdot 10^{-3}$M (1.2g/L) FA solution for 24 hours, whereafter they were filtered and dried at 50°C in a vacuum chamber overnight. Hereafter the specimen were coated with a thin layer of gold with a sputter coater and placed inside the vacuum chamber. The specimen stage was tilted to an angle of 54° as the FIB beam is located in this position of the apparatus and has to be in a vertical position above the specimen. A suitable area for measurement is found with SEM, a suitable area being a very planar surface area on a medium to large particle since the SEM beam is now in a 54° angle to the vertical plane of the sample. Thus, a rough surface site could result in detection problems since the sides of the particles would block any signal that comes from the region prepared by the FIB beam.

After a suitable region has been found, the site is prepared with a thin layer of platinum to protect the region from Gallium ion implantation and damage. Subsequently, the FIB milling procedure can now be started. The milling begins a few μm in front of the platinum-covered site of interest and goes approximately 1-2μm into the site of interest, in order to make room for the SEM beam which is still placed in an angle of 54° towards the specimen stage. When a sufficient depth has been reached (usually 5-15μm), the EDX system and software is used to acquire and analyze the elemental composition of the side of the newly milled hole in the specimen particle.

Loading Isotherms of HA and Silica-gel with FA as Ligand

Method 1

A 0.02g/L stock solution of fusidic acid (CAS: 6990-06-3) is prepared in PBS buffer at pH 7.4. 33 10ml standard solutions with fusidic acid concentrations of 0, 2, 4, 6, 8, 10, 12, 14, 16, 18, and 20mg/L, with three solutions of each concentration, are prepared for the standard curve. Light absorption was measured at 215nm with a UV-VIS Spectrophotometer. Before measurement each sample was injected into the cuvette through a single-use filter to treat the standard samples in the same way as intended for the experimental samples.

Method 2

A 0.2g/L stock solution of fusidic acid is prepared in PBS buffer at pH 7.4. Hereafter it is placed in a water bath at 45°C for 8 hours. The stock solution is treated with ultrasound for 5 minutes every 30 minutes. 33 10ml standard solutions with fusidic acid concentrations of 0, 2, 4, 6, 8, 10, 12, 14, 16, 18, and 20mg/L, with three solutions of each concentration, are prepared for the standard curve. 5ml 0.12g/L fusidic acid is now added to silica-gel and β-CD modified silica-gel samples with 2.5, 5, 10, 15, 20, 25, 30, 35, 40, and 100mg matrix. The measurements are determined with four distinct samples for each concentration. The samples are left for equilibrium alignment for twentyfour hours. Hereafter all samples are centrifuged at room temperature for five minutes at 3000rcf. 3ml supernatant is extracted from each sample and light absorption is measured at 215nm with a UV-VIS Spectrophotometer. The fusidic acid concentrations are plotted with respect to the standard curve.

Final Examination Method for Loading Isotherms

A 1.2g/L ($2.32 \cdot 10^{-3}$M) stock solution of fusidic acid is prepared in 25mM phosphate buffer at pH 9.5. Subsequently, the pH of the stock solution is lowered to pH 7.4 with a few drops of 0.5M HCl. 18 10ml standard solutions with fusidic acid concentrations of 0, 20, 40, 60, 120, and 240mg/L, with three solutions of each concentration, are prepared for the standard curve. 40mg of either virgin silica-gel or HA or β-CD modified silica-gel or HA is applied to samples of 10ml fusidic acid solutions as seen in table 9.2.

Concentration μg/ml	Concentration mol/L	1.2g/L standard [ml]
5	$9.68 \cdot 10^{-6}$	0.042
10	$1.94 \cdot 10^{-5}$	0.083
20	$3.87 \cdot 10^{-5}$	0.166
30	$5.81 \cdot 10^{-5}$	0.250
40	$7.74 \cdot 10^{-5}$	0.333
80	$1.55 \cdot 10^{-4}$	0.666
120	$2.32 \cdot 10^{-4}$	1.000
180	$3.48 \cdot 10^{-4}$	1.500
240	$4.64 \cdot 10^{-4}$	2.000

Table 9.2: Preparation of fusidic acid solutions for sample addition. The final volume is 10 ml.

The measurements are determined with four distinct samples for each concentration. The samples are left for equilibrium alignment for twentyfour hours. Hereafter all samples are centrifuged at room temperature for five minutes at 3000rcf. 3ml supernatant is extracted from each sample and light absorption is measured at 240nm with a Varian Cary 50 Bio UV-Visible Spectrophotometer. The fusidic acid concentrations are plotted with respect to the standard curve.

CLSM of HA and Silica-gel with 1,8-ANS as Ligand

Two stock solutions of $1 \cdot 10^{-3}$ and $1 \cdot 10^{-4}$ of 1,8-ANS (CAS: 28836-03-5) are prepared in milli-Q water. Ten matrix samples with varying 1,8-ANS concentrations, modifications and FA complexation are prepared. Four of the samples, one with and one without β-CD modification of both silica-gel and HA, are prepared and 10ml of the $1 \cdot 10^{-3}$ 1,8-ANS stock concentration is added. Two samples with virgin and β-CD modified silica-gel are prepared with 10ml of the $1 \cdot 10^{-4}$ 1,8-ANS concentration. Finally, four samples of silica-gel, two with and two without β-CD modification, are prepared with 10ml $2.32 \cdot 10^{-3}$M (1.2g/L) FA as ligand and left for 24 hours to equilibrate. Hereafter, the samples were filtered and dried overnight at 50∘C in a vacuum chamber. Subsequently one sample with and without β-CD modification is prepared with 10ml of $1 \cdot 10^{-4}$ 1,8-ANS. The amount of all matrix samples is 40mg and the final volume was always 10ml. All samples are left for equilibrium alignment for 24 hours whereafter a matrix sample is removed from each of them and placed on a specimen plate. Finally, the samples are investigated with a Zeiss Axiovert 100M Confocal Laser Scanning Microscope. The images were taken at the following settings: resolution 230μm x 230μm, Scaling 0.22μm x 0.22μm, Objective: Neofluar 40x/0.75, excitation at 351nm, and emission range at 452nm to 485nm.

Loading Isotherms of Silica-gel Matrices with 1,8-ANS as Ligand

A $5 \cdot 10^{-3}$ stock solution of 1,8-ANS (CAS: 28836-03-5) is prepared in milli-Q water. 1ml of the stock solution is diluted to a concentration of $5 \cdot 10^{-4}$ whereafter 5 10ml standard solutions with 1,8-ANS concentrations are prepared for the standard curve as seen in table 9.3.

Concentration [M]	$5 \cdot 10^{-4}$ standard [ml]
$5 \cdot 10^{-5}$	1.0
$2.5 \cdot 10^{-5}$	0.5
$1 \cdot 10^{-5}$	0.2
$5 \cdot 10^{-6}$	0.1
$2.5 \cdot 10^{-6}$	0.05

Table 9.3: Preparation of 1,8-ANS solutions for standard curve. The final volume is 10 ml.

40mg of either virgin silica-gel or β-CD modified silica-gel is applied to samples of 10ml 1,8-ANS solutions as seen in table 9.4. The experiments with 1,8-ANS are also conducted on virgin and modified silica-gel matrices that were previously loaded with FA where the Silica-gel and β-CD modified silica-gel are each applied to 50ml $2.32 \cdot 10^{-3}$M (1.2g/L) FA stock concentration. Subsequently, samples were left for equilibrium alignment for twentyfour hours and filtered and dried in a vacuum heating chamber at 50°C overnight. The samples are left for equilibrium alignment for twentyfour hours. Hereafter all samples are centrifuged at room temperature for five minutes at 3000rcf. 3ml supernatant is extracted from each sample that lie within the concentration range of the standard curve. Samples with higher initial concentrations are diluted accordingly. Fluorescence peak emissions are examined with an excitation wavelength of 311nm and an emission spectrum between 450-600nm. Measurements were acquired with a Varian Cary Eclipse Fluorescence Spectrophotometer. The 1,8-ANS concentrations are plotted with respect to the standard curve.

Concentration [M]	$5 \cdot 10^{-3}$ standard [ml]
$2.5 \cdot 10^{-3}$	5.0
$1 \cdot 10^{-3}$	2.0
$7.5 \cdot 10^{-4}$	1.5
$5 \cdot 10^{-4}$	1.0
$2.5 \cdot 10^{-4}$	0.5
$1 \cdot 10^{-4}$	0.2
$7.5 \cdot 10^{-5}$	0.15
Concentration [M]	$5 \cdot 10^{-4}$ standard [ml]
$5 \cdot 10^{-5}$	1.0
$2.5 \cdot 10^{-5}$	0.5
$1 \cdot 10^{-5}$	0.2
$5 \cdot 10^{-6}$	0.1
$2.5 \cdot 10^{-6}$	0.05

Table 9.4: Preparation of 1,8-ANS solutions for sample addition. The final volume is 10 ml.

Examination of FA Release from Silica-gel and HA Matrices

Standard solutions with FA concentrations of 0, 10, 20, 40, 60, 120, and 240μg/ml, with two solutions of each concentration, are prepared for the standard curve. 0.4g of either virgin

or β-CD modified HA or silica-gel are each applied to 50ml 1.2g/L ($2.32 \cdot 10^{-3}$M) FA stock concentration. The samples were left to equilibrate for twentyfour hours and subsequently filtered and dried in a vacuum heating chamber at 50°C overnight.

After drying, each sample was added to a column. A reservoir of 25mM phosphate buffer at pH 7.4 was placed above the column in order to control the amount of buffer added and to maintain the same amount of buffer volume in the column at any time. When the experiment begins sampling occurs directly into a series of vials that are placed on top of a balance, which is used to determine the amount of acquired volume within each vial at a conversion rate of 1g/ml. Each time a vial is filled with 1g of buffer the balance is slightly rotated and the next vial hereby starts to fill with buffer solution from the column. As such each vial contains 1ml of liquid buffer from the column.

After sampling all vials were placed in a HPLC apparatus, with an autosampler and a UV-Vis detector. Data acquisition occcured at a wavelength of 240nm. The starting eluent was set to 60% Methanol, 20% Acetonitrile and 20% 0.01M Phosphoric acid. A gradient was set to start after 1 minute and end after 15 minutes of total sampling time whereby the eluent concentrations slowly changed to 75% Methanol, 20% Acetonitrile and 5% 0.01M Phosphoric acid. The gradient was modified from [Brown *et al.*, 1997]. The retention time of fusidic acid was measured to be 8.291 minutes.

Results 10

This chapter presents data from β-CD quantification on silica-gel and HA investigated with TGA and the Phenol Sugar Assay method. Subsequently, data from the BET, CHN analysis, and XRPD experiments before and after β-CD immobilization are represented. Hereafter results from the silica-gel investigations with the FIB-SEM setup are illustrated. These are followed by data from the steps of optimization and final UV-Vis, CLSM, and FS experiments describing ligand loading and, finally, HPLC experiments describing the FA release from Silica-gel and β-CD modified silica-gel matrices.

10.1 CD Quantification

TGA These results describe the β-CD coverage of silica-gel and HA after immobilization, and were conducted with TGA and the Phenol Sugar Assay method. TGA data for Silica-gel are illustrated in figure 10.1.
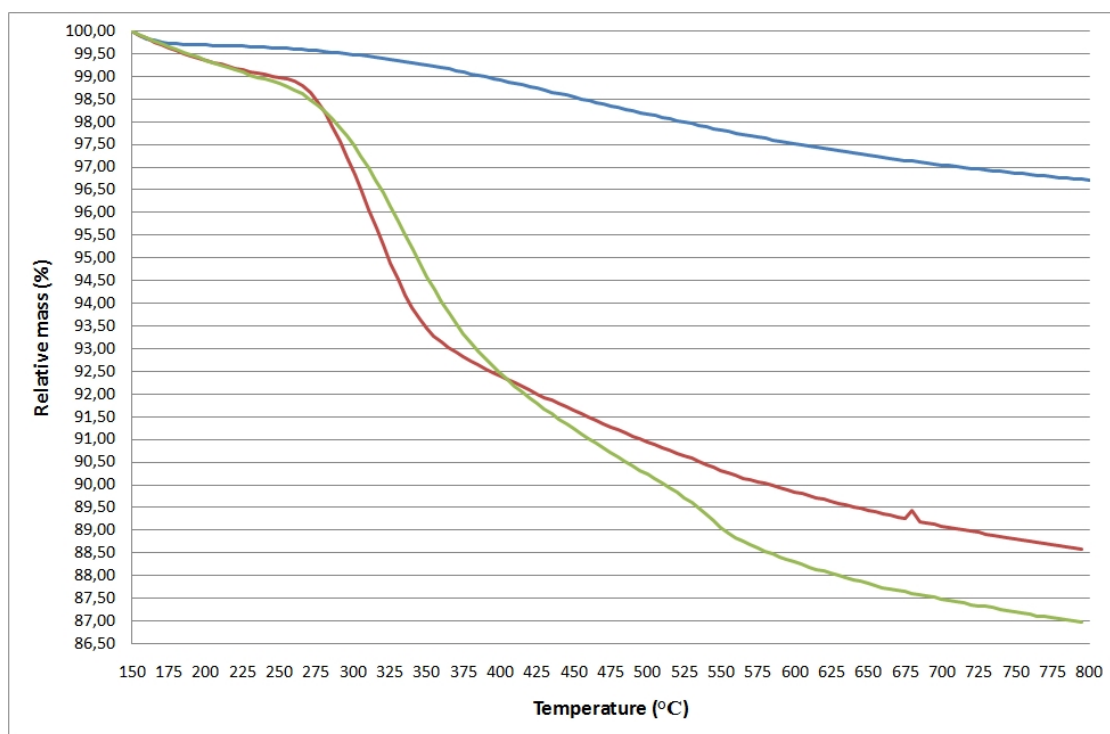
Figure 10.1: Thermogravimetric Analysis showing the relationship in weight percentage between blue: pure silica-gel; red: silica-gel with silane-spacer arm; green: silica-gel with spacer arm and β-CD.

From 600-800°C the percentual decrease in mass is approximately the same in all three samples. Pure silica-gel loses 3.3% of its initial weight, while silica-gel with silane-spacer attached loses 11.4%, and silica-gel with silane-spacer $+ \beta$-CD loses 13.0%. This shows that there is at least 1.6wt% β-CD attached to the silica-gel surface.

TGA data for HA are illustrated in figure 10.2. Pure HA loses 0.32% of its initial weight, while HA with silane-spacer loses 0.27%, and HA with silane-spacer $+ \beta$-CD loses 0.21%. Thus, the results show that pure HA is losing slightly more mass than the modified samples.
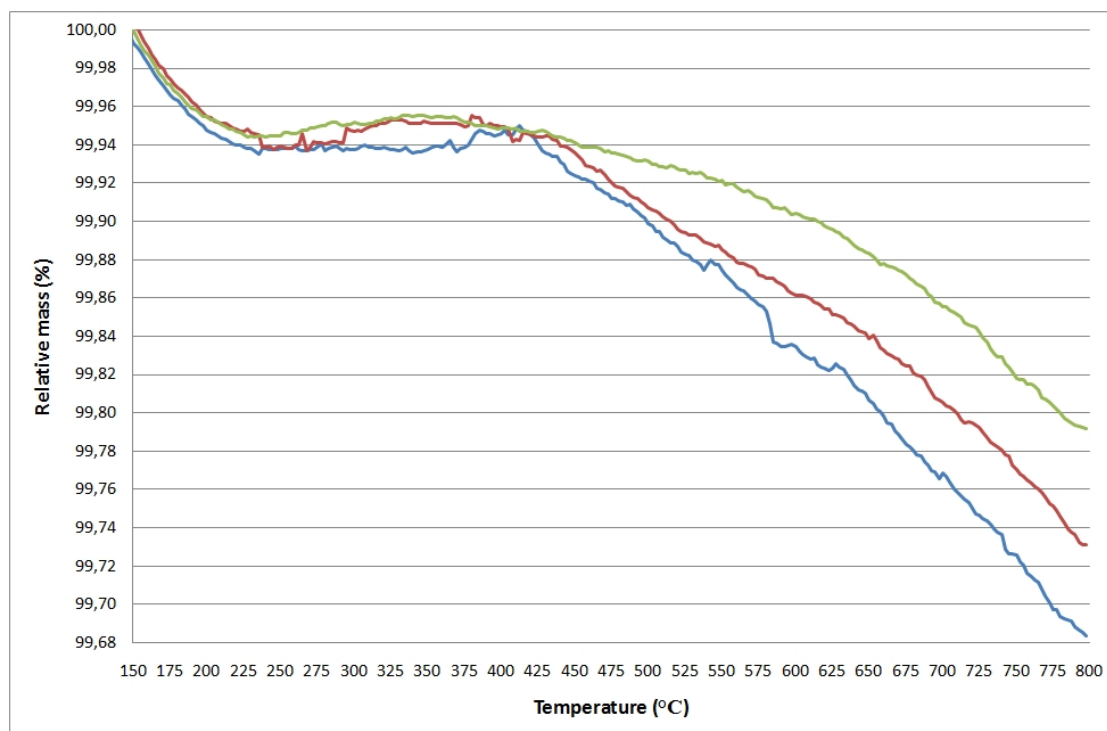
Figure 10.2: Thermogravimetric Analysis showing the relationship in weight percentage between pure HA, HA with silane-spacer arm, and HA with spacer-arm and β-CD.

Phenol Sugar Assay Method   The experiment was conducted in order to determine the amount of β-CD attached to the respective matrix. The data acquired from the Phenol Sugar Assay method can be seen in table 10.1.

Matrix type	μmol β-CD/g matrix	wt% β-CD/g matrix
silica-gel	38.1 $\pm$7.4	4.3 $\pm$0.8
HA	2.7 $\pm$0.9	0.3 $\pm$0.1

Table 10.1: β-CD coverage of silica-gel and HA after β-CD immobilization

The above data show that approximately 4.3wt% β-CDs have been immobilized on the silica-gel samples, and 0.3wt% on the HA samples. Here it is important to notice the relatively significant variations in the experimental outcomes, which are 19.4% and 32.3% for silica-gel and HA, respectively.

10.2 Investigating Matrix Changes Upon CD Modification

BET The following BET results were provided by the Chemical Section of Aalborg University in Esbjerg. The experiment was conducted in order to investigate the surface area and total pore volume of silica-gel before and after β-CD modification. The data in table 10.2 show the surface area and total pore volume for silica-gel before and after β-CD modification.

Data	Before β-CD attachment	After β-CD attachment
Surface Area	470.40 m^2/g	322.27 m^2/g
Total Pore Volume	0.709 cm^3/g	0.484 cm^3/g

Table 10.2: BET-data showing the surface area and total pore volume for silica-gel before and after β-CD modification.

It can be seen that the surface area and total pore volume is reduced after β-CD modification. This is most likely a result of a combination of factors, such as the presence of attached silane spacer arms with β-CDs but also of silane spacer arms only that are not attached to any β-CDs, both resulting in an altered surface structure. Furthermore, physical stress from grinding by the stirring during the synthesis is also likely to have an affect on the relative surface area.

CHN Analysis The results were conducted in order to determine the elemental composition of carbon, hydrogen, and nitrogen before and after β-CD attachment to silica-gel, with and without FA. Table 10.3 shows the amount of Carbon, Hydrogen, and Nitrogen in % of the total amount of atoms in the sample, acquired with the CHN analysis method from samples with silica-gel and β-CD modified silica-gel with and without FA. The results were kindly provided by René Holm at Lundbeck A/S.

Material	%C	%H	%N
Silica-gel	0.15	0.77	0.13
β-CD mod. Silica-gel	6.93	1.57	0.36
Silica-gel + FA	0.78	0.81	0.14
β-CD mod. Silica-gel + FA	8.02	1.72	0.31

Table 10.3: CHN data showing the atomic percentage of Carbon, Hydrogen, and Nitrogen before and after β-CD immobilization and with and without FA.

It can be seen that the amount of carbon on the matrix surface increases from negligible amounts to almost 7%p while the amount of hydrogen doubles upon surface modification with β-CDs. Upon FA inclusion the carbon levels with virgin silica-gel increase approximately 0.6%p relative to virgin silica-gel without FA, while the changes in hydrogen and nitrogen are negligible. Carbon levels with β-CD modified silica-gel matrix with FA increases with almost 1.1%p relative to the β-CD modified silica-gel matrix without FA, while hydrogen levels increase by 0.15%p. The increased amounts of carbon and hydrogen atoms upon matrix modification indicates that β-CDs and the 3-glycidyl oxypropyl trimethoxysilane spacer arms are grafted onto the surface of silica-gel. Furthermore, the increased amounts of carbon and hydrogen upon FA inclusion indicate that the affinity towards FA of the modified matrices has either increased or that more binding sites are available, relative to the virgin silica-gel with included FA.

XRPD The experiments were conducted to determine if β-CDs and FA molecules are adsorbed to the silica-gel surface in a crystalline ordering. The plot in figure 10.3 illustrates the acquired data from XRPD experiments with virgin and β-CD modified silica-gel with and without FA. The results were kindly provided by René Holm at Lundbeck A/S.
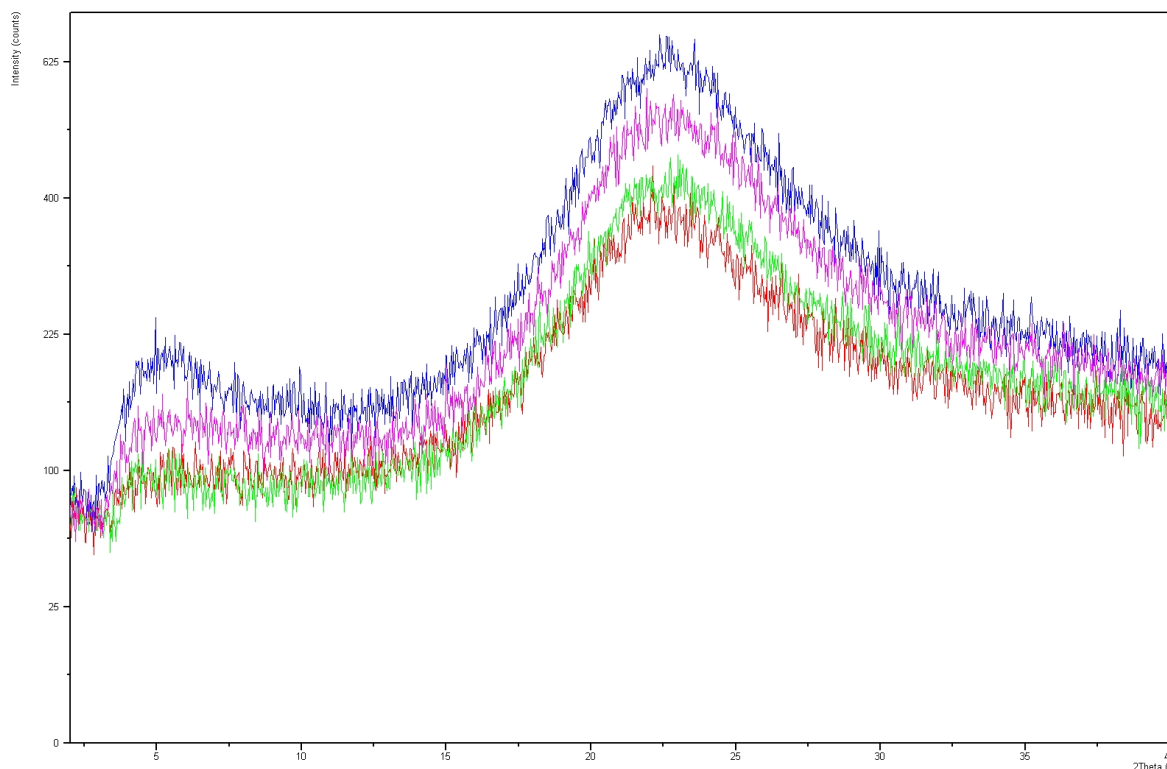

Figure 10.3: XRPD experiments conducted on virgin and β-CD modified silica-gel with and without FA. Blue: virgin silica-gel; Purple: virgin silica-gel + FA; Green: β-CD modified silica-gel; Red: β-CD modified silica-gel + FA.

No scattering signal is detected throughout any of the specimen, showing that the silica-gel is of amorphous structure and indicates that neither β-CDs or FA molecules are organised as crystalline structures in any of the samples.

10.3 Investigating Silica-gel with the FIB-SEM setup

The following figures and illustrations show the structural and elemental composition of virgin and β-CD modified silica-gel with and without FA, investigated with the FIB-SEM setup and EDX.

Virgin Silica-gel without FA

The figures 10.4 to 10.6 show a series of images taken with the SEM microscope throughout the stages of finding a suitable particle, placing the platinum layer on top of the site of interest, and the procedure of milling into the particle with the FIB system. The matrix type was virgin silica-gel without FA.
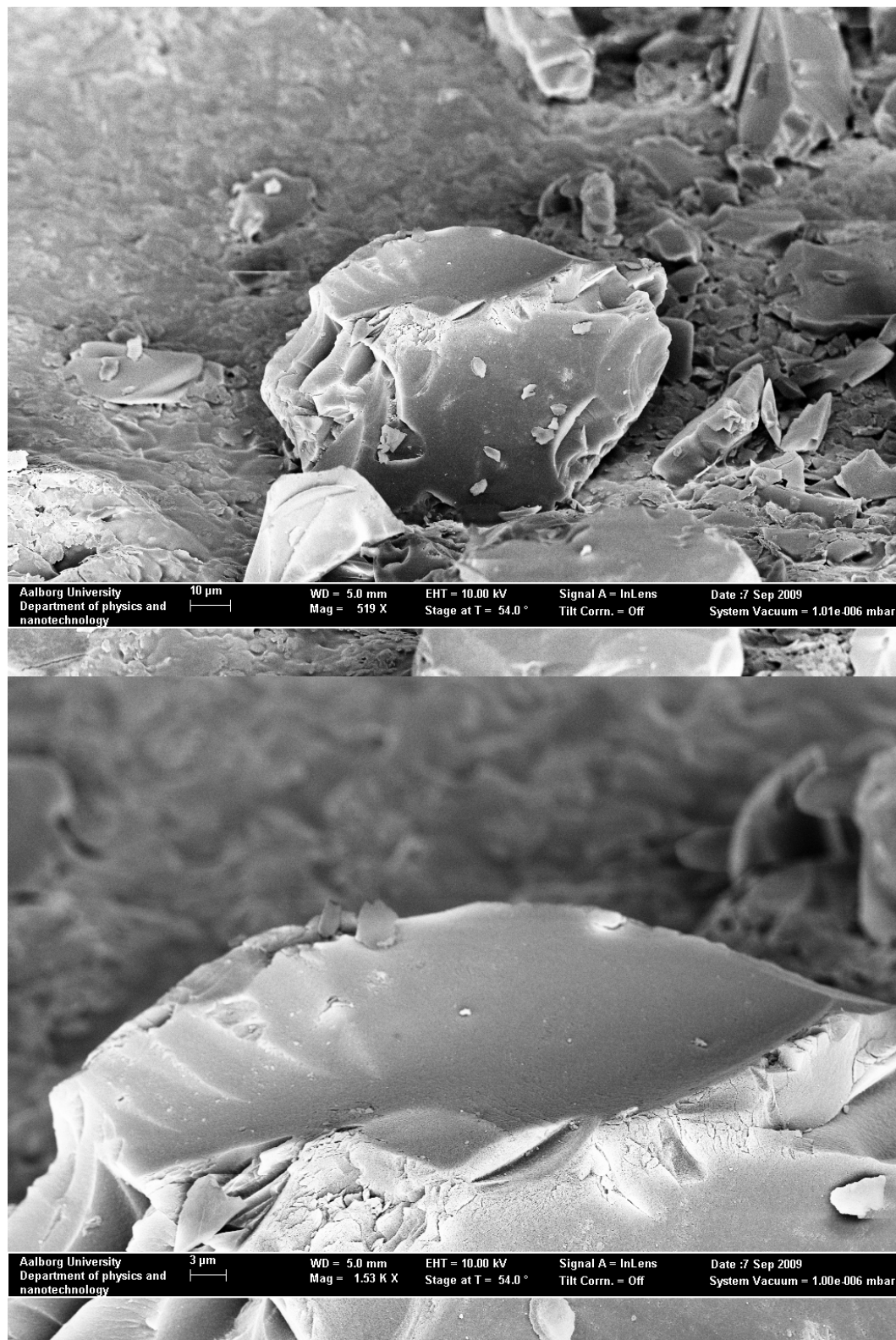
Figure 10.4: SEM images of virgin silica-gel without FA illustrating the chosen particle to investigate. Top image, the suitable planar region on the silica-gel particle is the milling target; Bottom image, zoom of the target region.
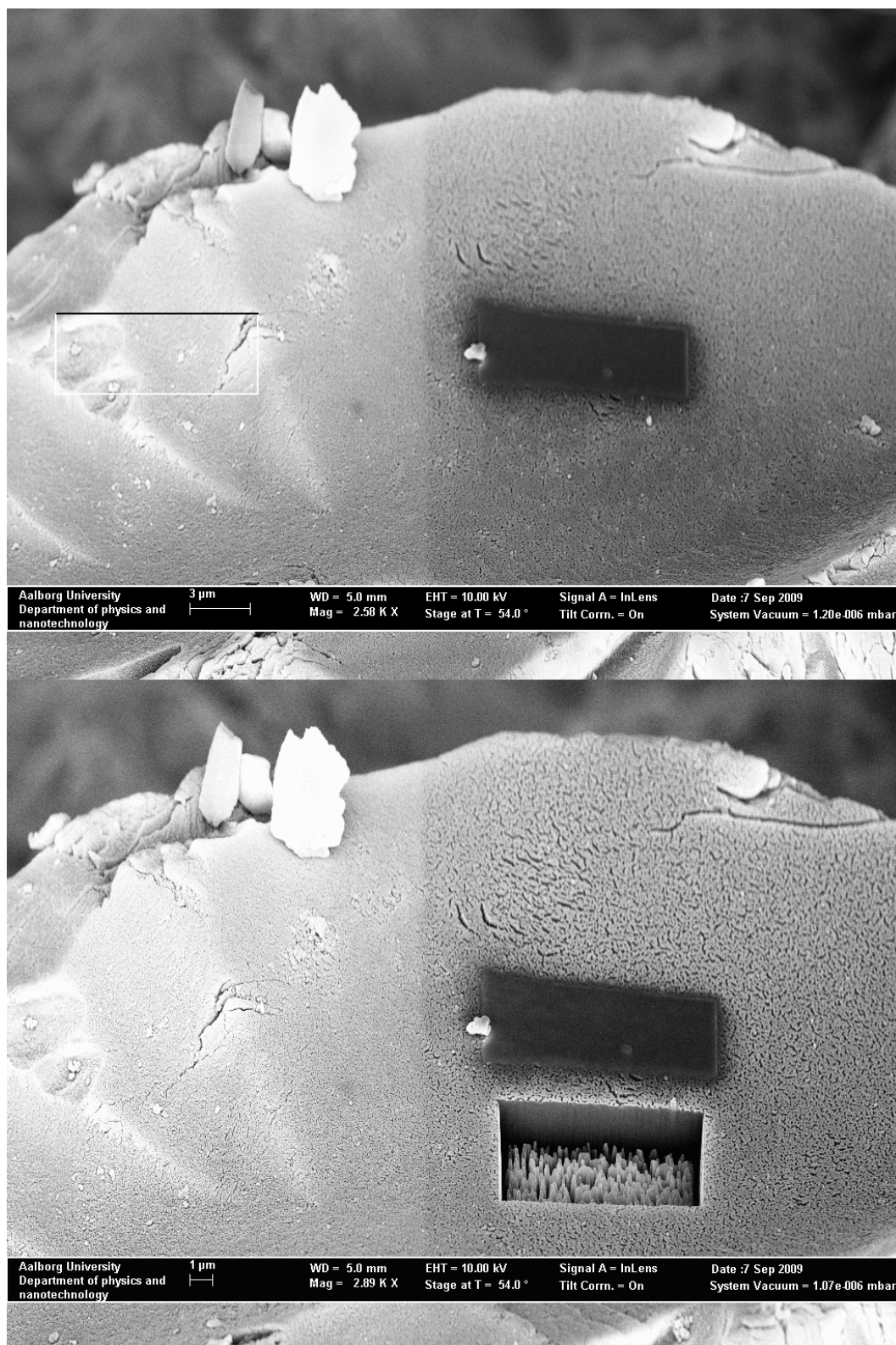
Figure 10.5: SEM images of virgin silica-gel without FA illustrating the placing and beginning of the milling procedure. Top image, illustrating a darker area on the surface which is the layer of platinum placed on top of the site of interest; Bottom image, milling procedure begins a few μm in front of the platinum layer.
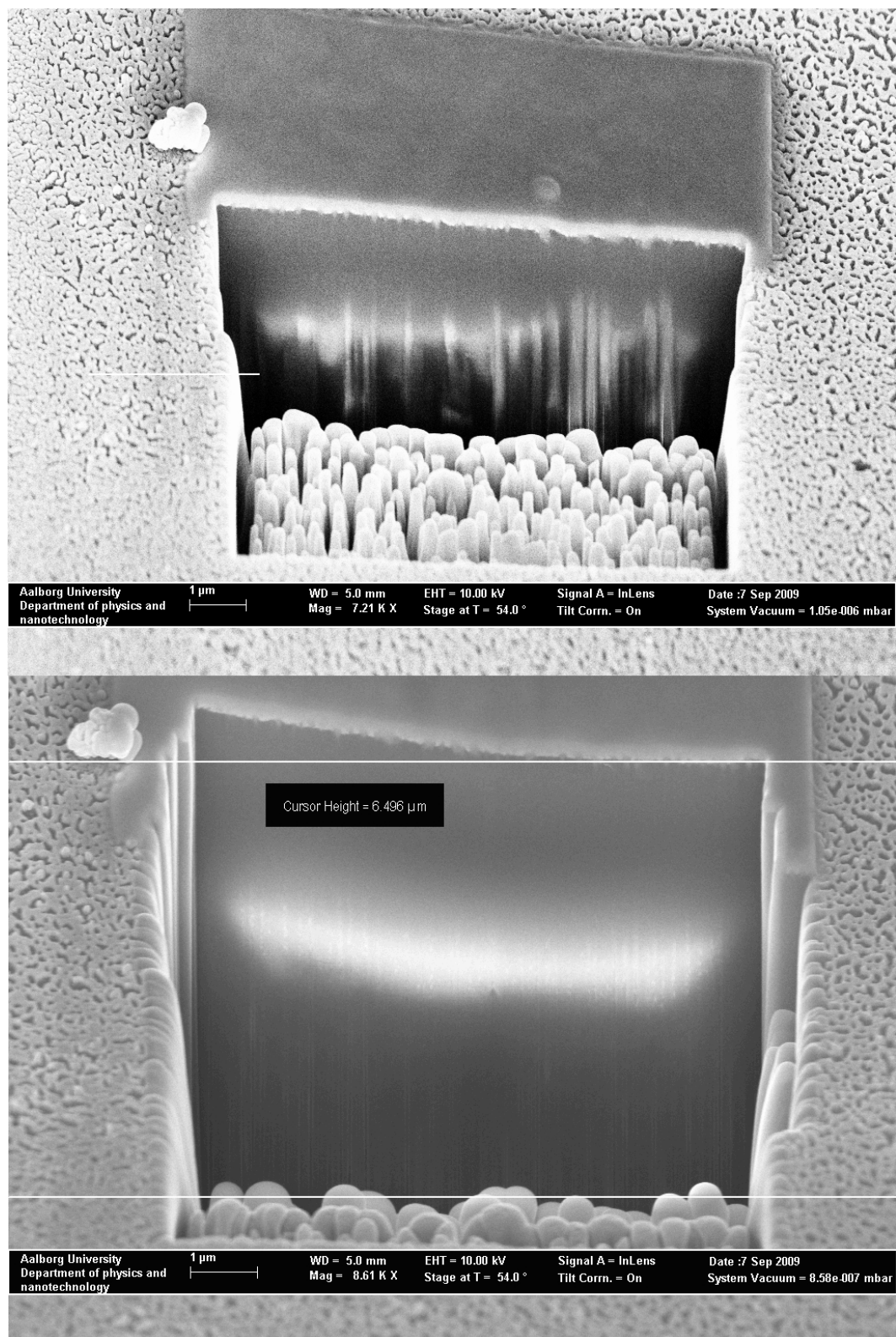
Figure 10.6: SEM images of virgin silica-gel without FA illustrating the final stages of the milling procedure. Top image, milling starts to cut into the platinum layer; Bottom image, specimen is ready for EDX analysis.

Figure 10.7 illustrates a vertical line EDX analysis of the processed site, measuring the concentration of the element carbon in terms of wt% relative to the detected concentrations of silicon, and oxygen.
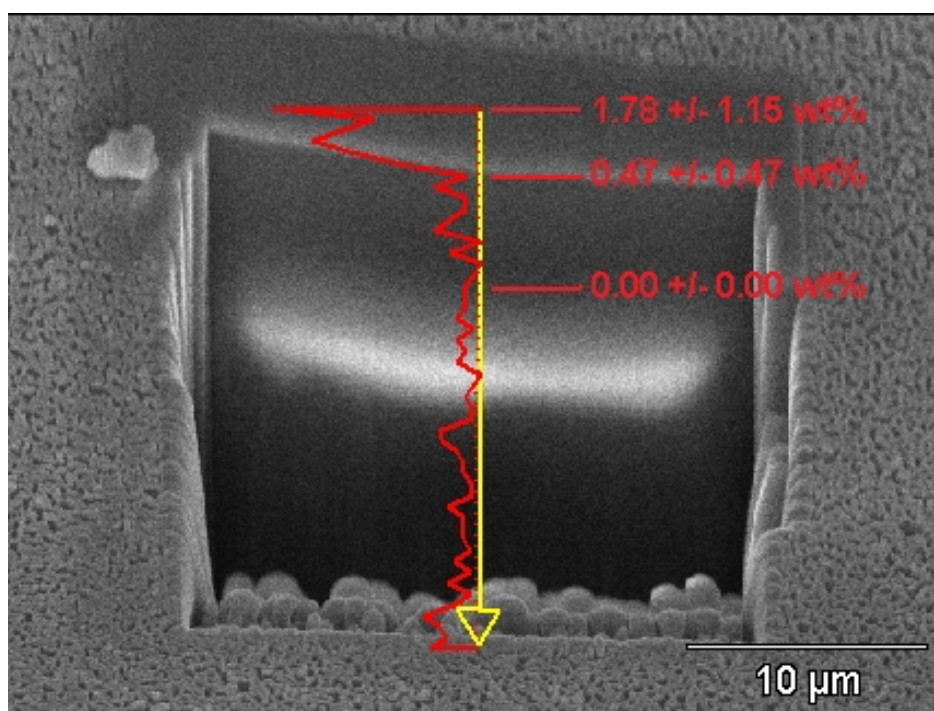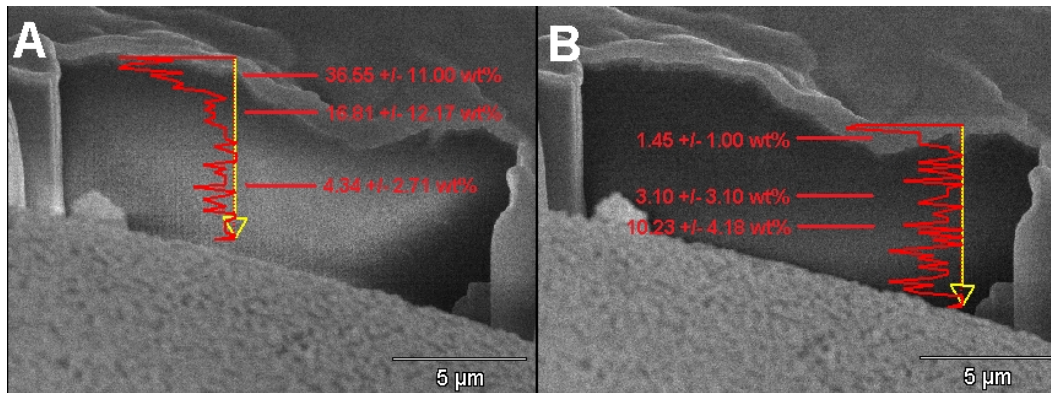

Figure 10.7: SEM image of virgin silica-gel without FA with vertical line EDX analysis illustrating the concentration of the element carbon throughout the processed site.

A small amount of 1.78 wt% carbon is detected at the very surface of the site. However, no carbon atoms are detected after approximately 1μm of sampling into the particle and since the matrix is unmodified silica-gel the observed carbon is most likely a surface impurity.
Figure 10.8 illustrates a point and shoot EDX analysis of various areas within the site. This analysis method examines the mean distribution of the elements carbon, oxygen, and silicon in the selected area. The data are given in table 10.4
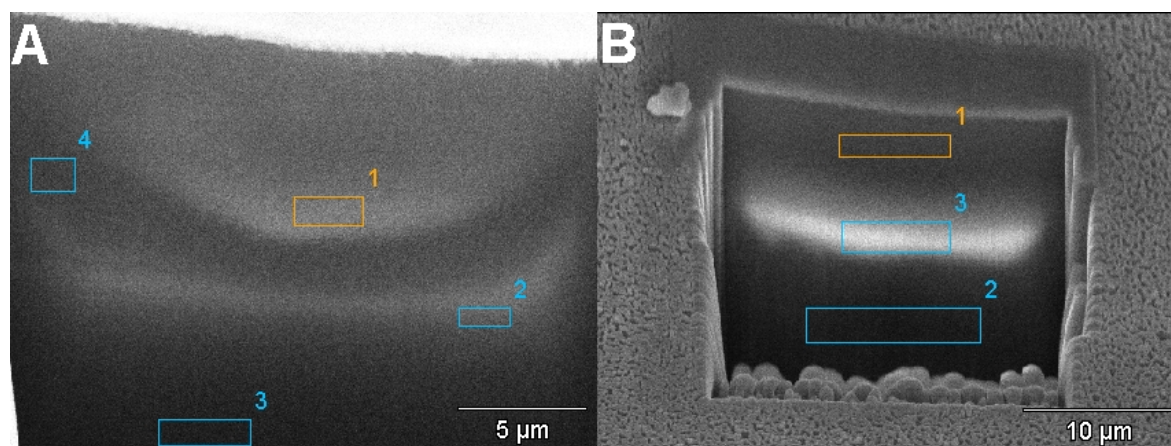
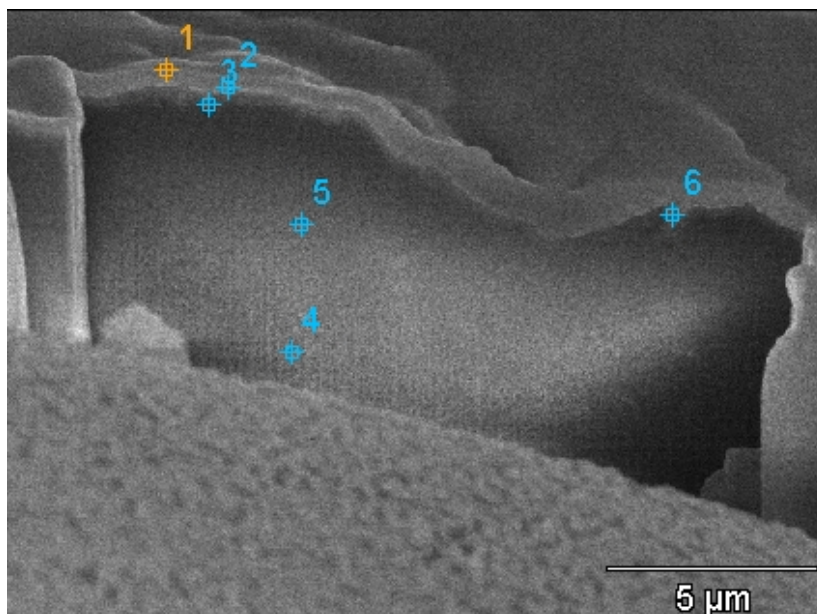Figure 10.8: SEM images of virgin silica-gel without FA with marked areas for a point and shoot EDX analysis. The data for the respective areas are illustrated in table 10.4

It is seen that only very slight amounts of carbon can be detected in the region B1, which

Area	wt%C	wt%O	wt%Si
A1	0.35 ±0.35	36.05 ±0.78	63.60 ±0.84
A2	0.00 ±0.00	42.58 ±0.75	57.43 ±0.72
A3	0.00 ±0.00	13.07 ±0.72	86.93 ±1.29
A4	0.00 ±0.00	13.50 ±0.84	86.50 ±1.21
B1	1.15 ±0.69	32.86 ±0.78	65.99 ±0.91
B2	0.00 ±0.00	36.09 ±0.80	63.91 ±0.86
B3	0.17 ±0.17	38.10 ±0.89	61.73 ±0.79

Table 10.4: Elemental concentrations from the marked areas in figure 10.8.

is almost at the very top of the analyzed site. It is furthermore interesting to notice the correlation between regions A1 + A2 and A3 + A4 in terms of oxygen and silica concentrations. A1 and A2 are placed in the lighter regions around the central structure, which could be a different type of crystal structure. A3 and A4 are located in the darker regions of the site and have far less oxygen atoms in terms of w% than silica. For the regions B1 to B3 it is observed that the silica concentrations tend to increase while scanning further into the particle. Thus, the overall observation is that the amount of oxygen decreases as we go deeper into the specimen.

β-CD modified Silica-gel without FA

The figures 10.9 and 10.10 show three images taken with the SEM microscope of a β-CD modified Silica-gel particle without FA. The site of interest has already been processed by FIB.
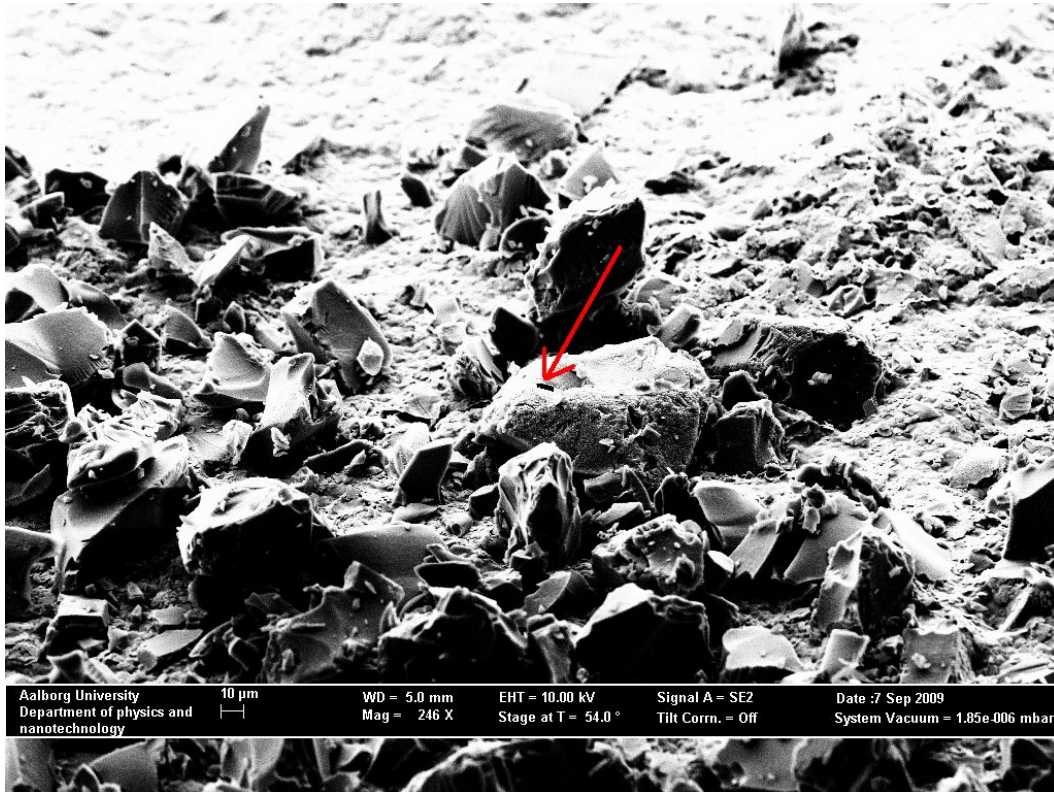
Figure 10.9: SEM image of β-CD modified silica-gel without FA illustrating the chosen particle to investigate. Note that the site of interest has already been processed by FIB and is ready for EDX analysis.
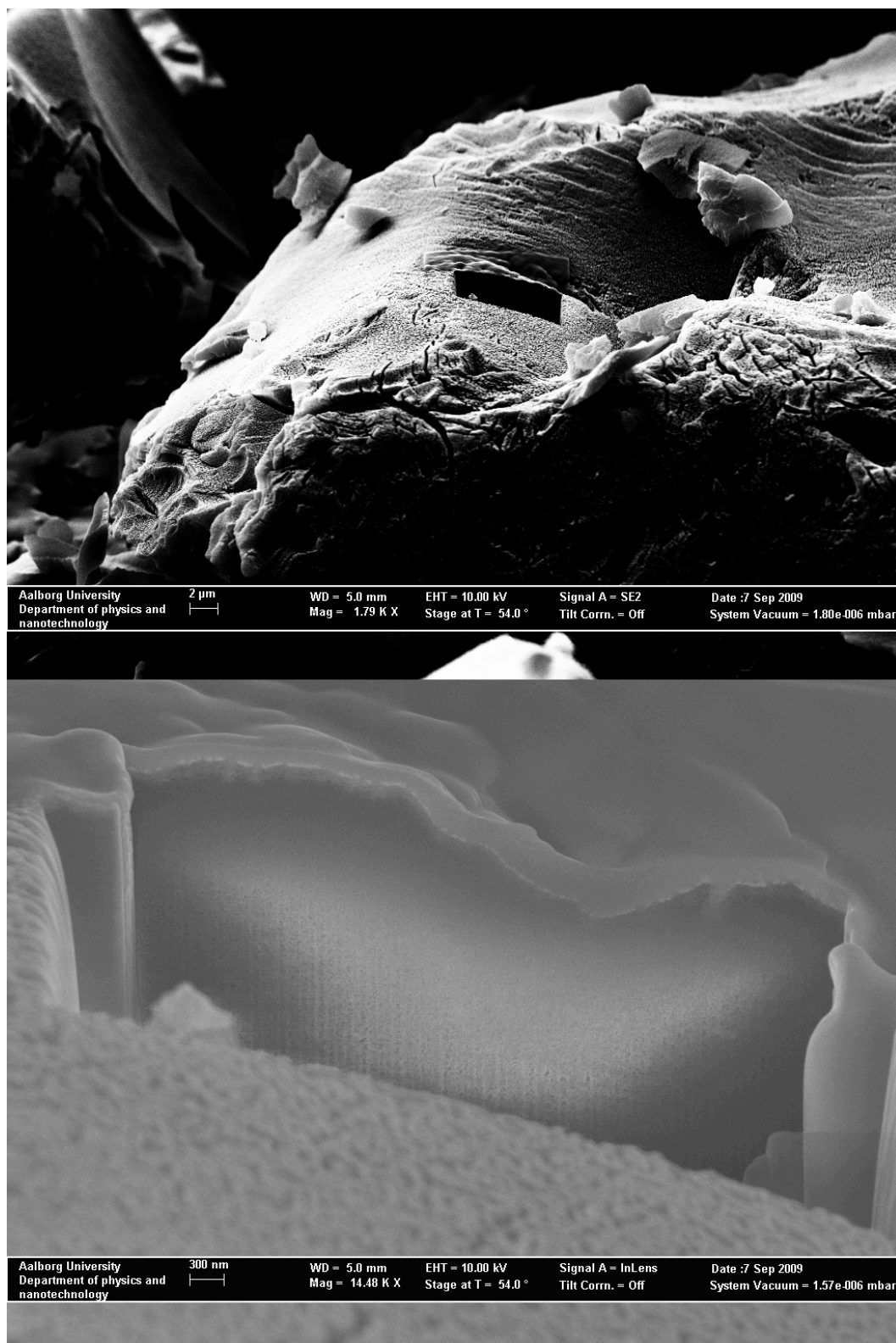
Figure 10.10: Top SEM image, a closer look of the processed particle; Bottom SEM image, a close picture of the site of interest.

Figure 10.11 illustrates two vertical line EDX analyses of the processed site, measuring the concentration of the element carbon in terms of wt% relative to the detected concentrations of silicon, and oxygen on a specimen of β-CD modified silica-gel without FA.
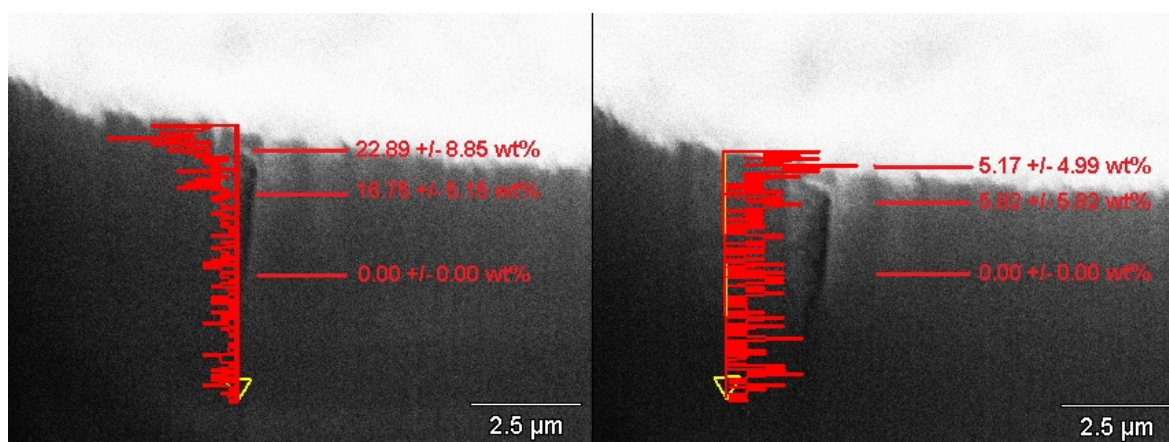

Figure 10.11: SEM images of β-CD modified silica-gel without FA with vertical line EDX analysis illustrating the concentration of the element carbon throughout the processed site.

It is seen that 36.55 wt% of the atoms present at the very surface in SEM image A are in fact carbon atoms. When proceeding further into the sample, however, the carbon concentrations are reduced. After only 1.4μm the carbon concentrations are less than half than at the surface with concentrations of 16.81 wt% and a large error relative to the measurement of 12.17 wt%. After roughly 4 μm the carbon concentrations are down at levels of 4.34 wt% and a error of 2.71 wt%. SEM image B illustrates far lower carbon concentrations on the surface than SEM image A. Only 1.45 wt% carbon is present at the surface at the edge of the site of interest. As the analysis proceeds into the sample, however, the carbon concentrations begin to increase, to 3.10 wt% at approximately 1.9μm and to 10.23 wt% at 2.8 μm. Figure 10.12 illustrates a point and shoot EDX analysis of various points within the site. This analysis method examines the mean distribution of the elements carbon, oxygen, and silicon of the selected point in the image. The data are given in table 10.5

Figure 10.12: SEM image of β-CD modified silica-gel without FA with marked points for a point and shoot EDX analysis. The data for the respective points are illustrated in table 10.5

Area	wt%C	wt%O	wt%Si
1	28.26 ±4.26	33.23 ±3.14	38.52 ±2.34
2	22.28 ±3.49	31.06 ±2.27	46.66 ±1.86
3	6.23 ±1.45	24.39 ±1.02	69.38 ±1.42
4	0.45 ±0.45	13.92 ±0.71	85.63 ±1.27
5	2.79 ±0.88	29.60 ±1.02	67.61 ±1.00
6	7.01 ±1.66	31.00 ±1.17	61.99 ±1.45

Table 10.5: Elemental concentrations from the marked points in figure 10.12.

It is seen in the point and shoot analysis that the carbon concentrations are diminishing when scanning deeper into the sample, again indicating that the carbon and hereby also the spacer arms and β-CDs may only be present at the surface and around the openings of the matrix pores. It is possible that the excess in carbon atoms is located in a pore of larger sizes, which means that more organic molecules can enter it and also go deeper into the matrix. The ratio between Oxygen and Silicon atoms is again observed to change in favor of silicon when going deeper into the particle.

Virgin Silica-gel with FA

The figures 10.13 and 10.14 show three images taken with the SEM microscope of a virgin Silica-gel particle with FA, from chosing the right particle with a planar surface to the processing with FIB and preparation for EDX analysis.
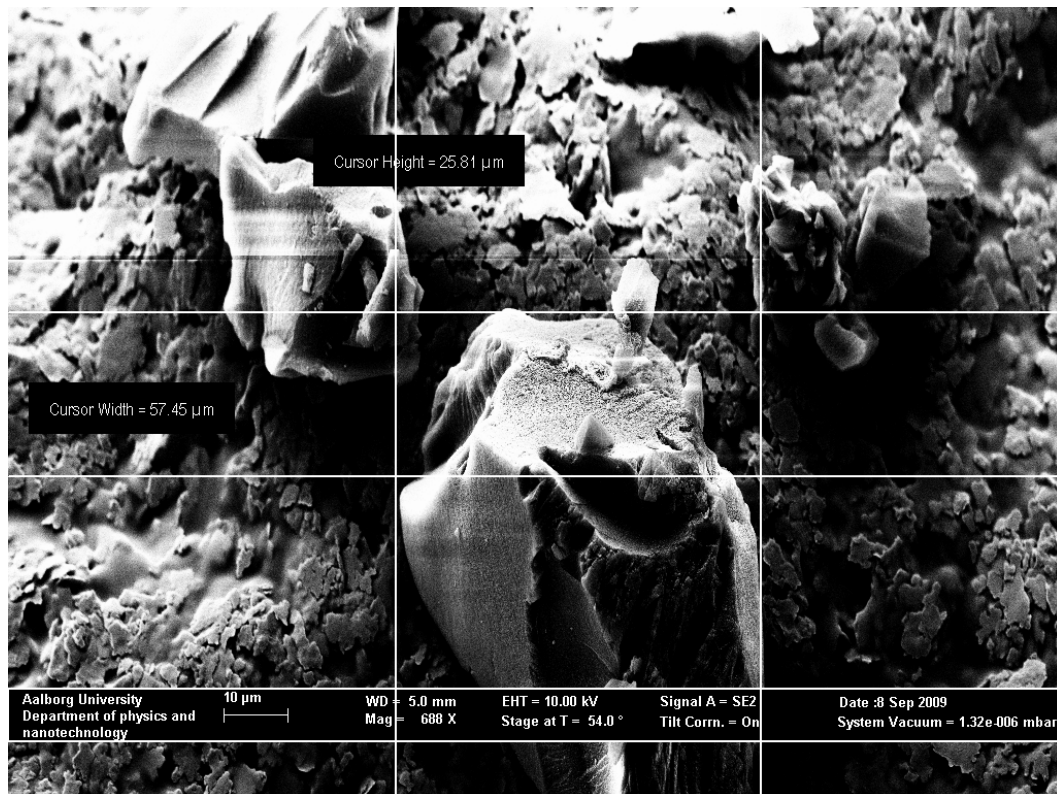
Figure 10.13: SEM image of virgin silica-gel with FA illustrating the chosen particle to investigate. The site of interest is the planar region within the cursor markings.

65

Figure 10.14: Top SEM image, a closer look of the particle that has now been processed by FIB; Bottom SEM image, a close picture of the site of interest, which is now ready for EDX analysis. Notice the large pore at the left top of the site and the smaller pore a little to the right from the middle.

Figure 10.15 illustrates two vertical line EDX analyses of the processed site, measuring the concentration of the element carbon in terms of wt% relative to the detected concentrations of silicon, and oxygen from a virgin silica-gel with FA specimen.

Figure 10.15: SEM images of virgin silica-gel with FA with vertical line EDX analysis illustrating the concentration of the element carbon throughout the processed site. Left SEM image, illustration of the elemental distribution from the inside of a pore; Right SEM image, illustration of the elemental distribution next to the same pore.

It can clearly be seen that the amount of carbon is higher within the pore than next to it, in the silica matrix. At the very top of the pore the carbon amount reaches 22.89 wt% whereas the carbon amount at the same particle depth but next to the pore only consists of 5.17 wt%, and with a very high error of 4.99 wt%. When scanning approximately 1μm into the particle the carbon amounts decrease to 16.75 wt% with an error of 5.15 wt% within the pore. Next to the pore the amounts seem to increase a little to 5.82 wt%, but since the error is also 5.82 wt% it can only be stated that there is still some amounts of carbon left. When scanning even deeper into the particle no more carbon is detected.

Figure 10.16 illustrates a point and shoot EDX analysis of various areas within the site. This analysis method examines the mean distribution of elements of the selected areas in the image. The data are given in table 10.6
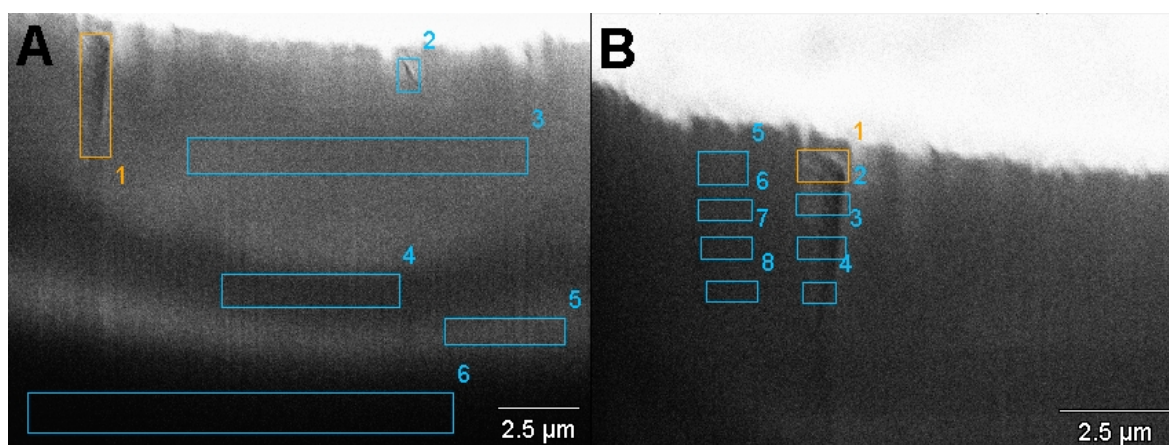
Figure 10.16: SEM images of virgin silica-gel with FA with marked areas for a point and shoot EDX analysis. The data for the respective areas are illustrated in table 10.6

67

Area	wt%C	wt%O	wt%Si
A1	1.27 ±0.80	30.53 ±0.97	68.21 ±0.97
A2	1.29 ±0.83	30.42 ±0.99	68.30 ±0.99
A3	1.43 ±0.65	35.03 ±0.77	63.54 ±0.86
A4	0.00 ±0.00	37.35 ±0.76	62.65 ±0.80
A5	0.00 ±0.00	39.06 ±0.74	60.94 ±0.77
A6	0.00 ±0.00	34.53 ±0.91	65.47 ±0.85
B1	3.02 ±0.95	27.57 ±0.83	69.40 ±1.07
B2	0.79 ±0.79	27.09 ±0.80	72.13 ±1.05
B3	1.95 ±0.76	28.16 ±0.81	69.89 ±1.00
B4	0.00 ±0.00	27.13 ±0.91	72.87 ±1.00
B5	0.13 ±0.13	28.04 ±1.03	71.82 ±1.08
B6	0.41 ±0.41	27.68 ±0.99	71.91 ±1.04
B7	0.00 ±0.00	27.19 ±0.80	72.81 ±1.02
B8	0.00 ±0.00	27.35 ±0.79	72.65 ±1.03

Table 10.6: Elemental concentrations from the marked points in figure 10.16.

Small traces of carbon are detected in the areas A1 to A3, while no carbon is found in the areas A4 to A6. The concentration ratio between Oxygen and Silicon is again changing in favor of silicon. The areas B1 to B3, which are located inside a pore, show a higher amount of carbon than the areas B5 to B7, which are located next to the pore. This indicates that FA is present inside the pore but is not incorporated into the matrix next to the pore. Furthermore, area B4 shows no traces of carbon, indicating that FA molecules are only present until a depth of around 3μm in the pore.

β-CD modified Silica-gel with FA

The figures 10.17 and 10.18 show three images taken with the SEM microscope of a β-CD modified Silica-gel particle with FA, from chosing the right particle with a planar surface to the processing with FIB and preparation for EDX analysis.
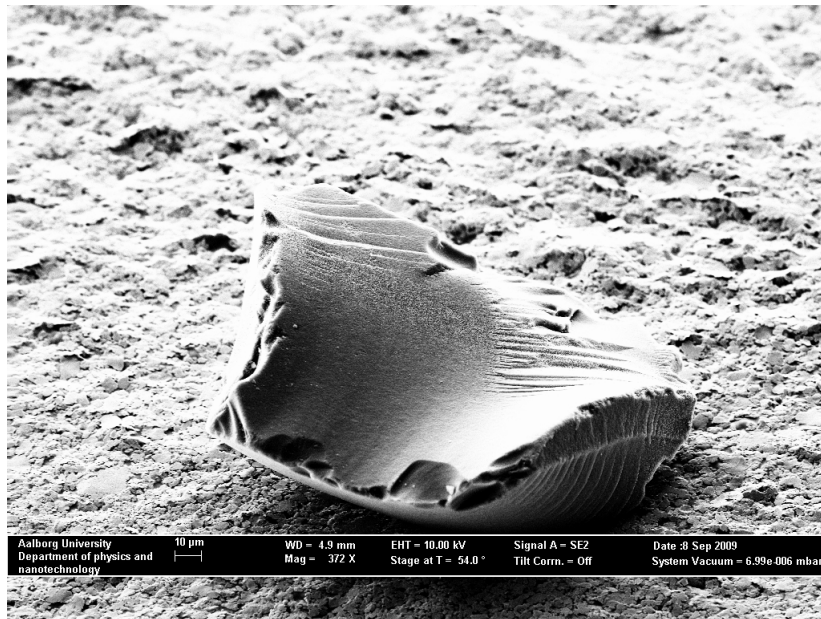
Figure 10.17: SEM image of β-CD modified Silica-gel with FA illustrating the chosen particle to investigate.

Figure 10.18: Top SEM image, a closer look of the particle that has now been processed by FIB; Bottom SEM image, a close picture of the site of interest, which is now ready for EDX analysis.

Figure 10.19 illustrates a vertical line EDX analysis of the processed site, measuring the concentration of the element carbon in terms of wt% relative to the detected concentrations of silicon, and oxygen from a β-CD modified Silica-gel with FA specimen.
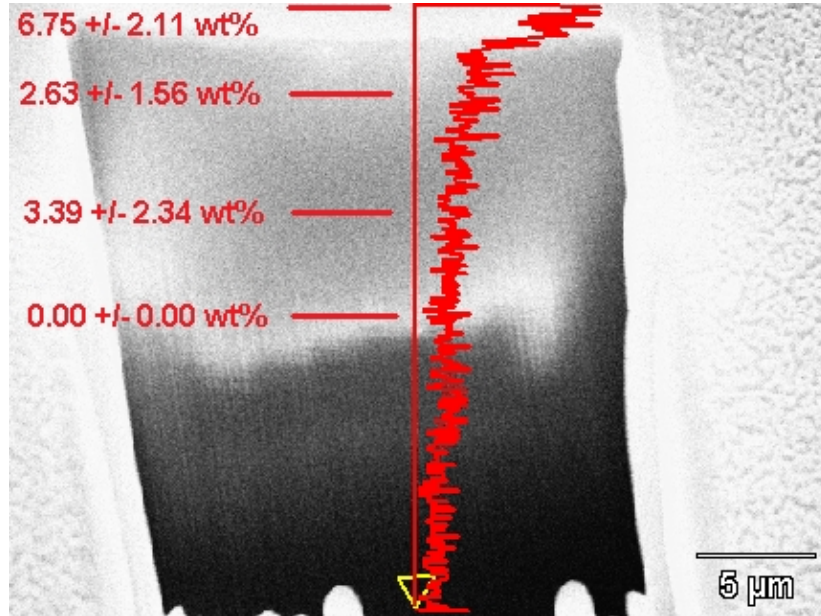

Figure 10.19: SEM image of β-CD modified Silica-gel with FA with vertical line EDX analysis illustrating the concentration of the element carbon throughout the processed site.

It is seen that the carbon concentrations diminish with increasing depht of analysis. At the very surface the carbon amounts are 6.75 wt%, but 4μm deeper the amounts are reduced to 2.63 wt%, and 6μm deeper the carbon levels are at 3.39 wt%. All three measurements have considerably high errors, being 2.11 wt%, 1.56 wt%, and 2.34 wt%, respectively. After approximately 8μm no more carbon could be detected.

Figure 10.20 illustrates a point and shoot EDX analysis of various areas within the site. The data are given in table 10.7

Area	wt%C	wt%O	wt%Si
1	1.94 ±1.14	35.37 ±0.92	62.69 ±0.50
2	1.95 ±0.99	36.64 ±0.73	61.42 ±0.48
3	1.74 ±0.92	34.41 ±0.90	63.86 ±0.49
4	1.45 ±0.99	35.15 ±0.92	63.40 ±0.51
5	0.62 ±0.62	28.70 ±0.82	70.68 ±0.58
6	0.00 ±0.00	22.72 ±1.06	77.28 ±0.67
7	0.00 ±0.00	20.35 ±1.10	79.65 ±0.70

Table 10.7: Elemental concentrations from the marked points in figure 10.20.

It is seen that carbon is present in approximately the same amounts throughout the areas 1 to 4, or from 0 to 7μm into the sample, whereafter it diminishes when analysing deeper into the particle. Oxygen concentrations are roughly the same through the areas 1 to 5 until approximately 10μm into the sample where the levels begin to decrease. Simultaneously, silicon concentrations begin to increase which indicates a change in crystal structure with a higher silica to oxygen ratio.
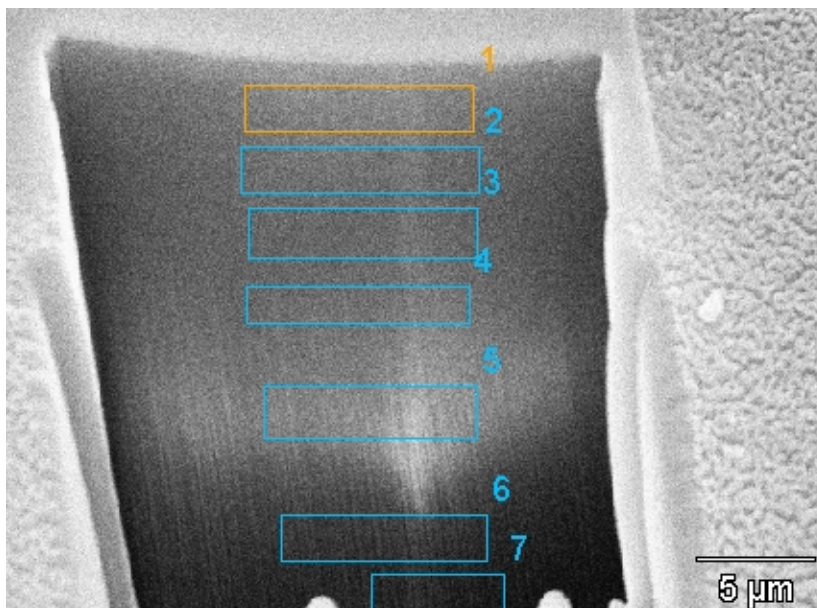
Figure 10.20: SEM image of β-CD modified Silica-gel with FA with marked areas for a point and shoot EDX analysis. The data for the respective areas are illustrated in table 10.7

10.4 Loading Isotherms of HA and Silica-gel with FA as Ligand

The results in this section describe the optimization steps of the UV-VIS method used to determine loading isotherms of FA when applied to virgin and β-CD modified HA and silica-gel as well as the final results.

Method 1

Figure 10.21 shows the standard series of FA prepared with method 1.
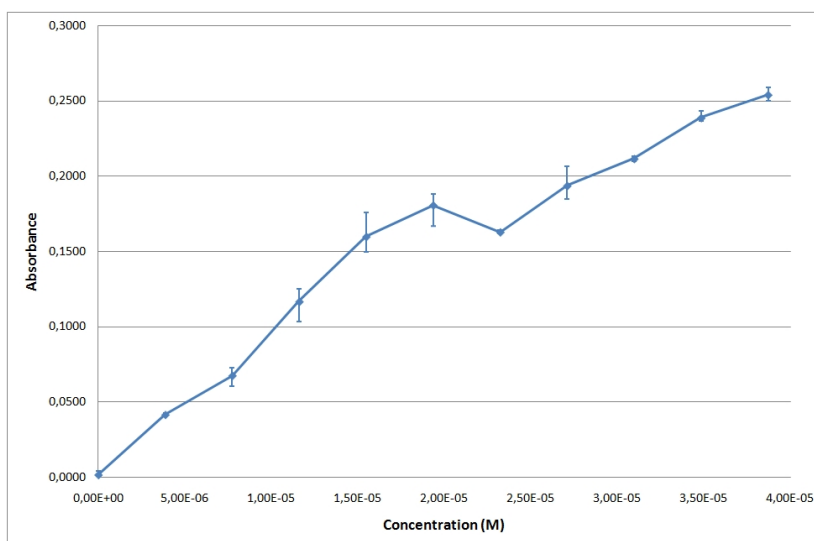
Figure 10.21: Standard series of 0.02g/L FA stock, using a single-use PVDF filter and measured at 215nm.

The series is randomly distributed but increasing in concentration. Variance differs between measurement points and it is not possible to correlate it with other fitting methods either.

For this reason the single-use filter was investigated further by scanning a PBS buffer solution before and after filtration. The resulting spectrum is illustrated in figure 10.22.
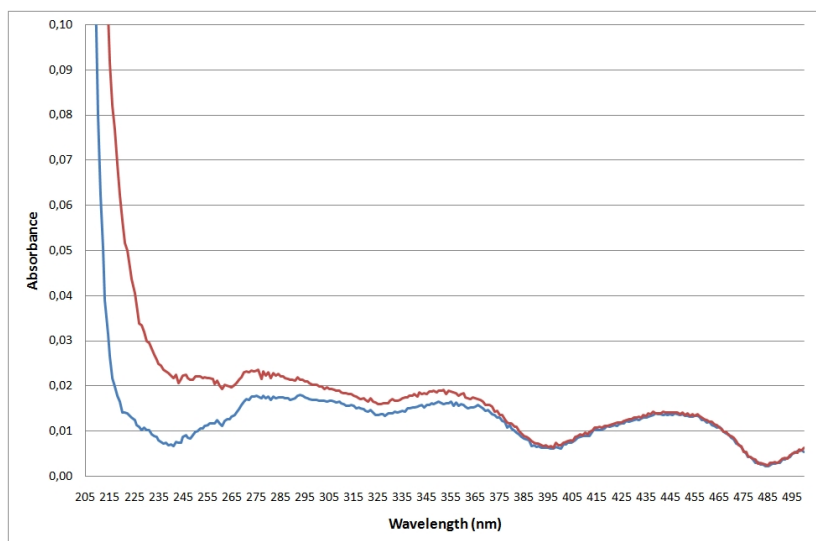
Figure 10.22: Absorbance spectrum of PBS-buffer. Blue line: Before filtration; Red line: After filtration.

The results clearly show that the light absorption from the sample after filtration increases in with the decreasing wavelength from around 375nm. Furthermore, there is no evidence of scattering since light absorption is approximately the same for both samples above 400nm. This leads to the conclusion that the single-use filter is releasing a compound into filtered solutions, which could describe the variations and non-linearity of the standard series. Figure 10.23 shows the standard series of FA where the samples were centrifuged at 3000 rcf for 5 minutes instead of filtrated.
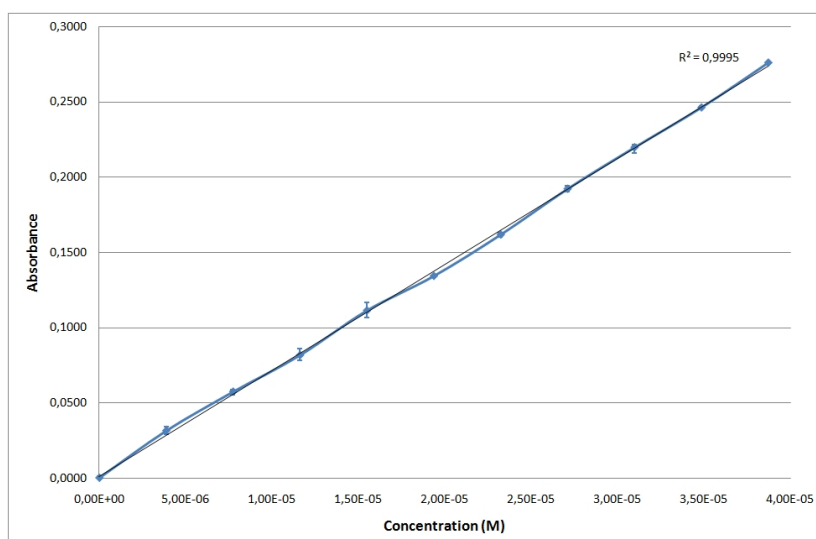
Figure 10.23: Standard series of 0.02g/L FA stock, where samples are centrifuged at 3000 rcf for 5 minutes instead of filtrated and measured at 215nm.

The standard series is clearly linear as can also be seen on the regression calculations made with Excel 2007.

Method 2

Figure 10.24 shows the standard series of FA prepared with method 2, in the attempt to create a stock solution with higher concentrations of FA.
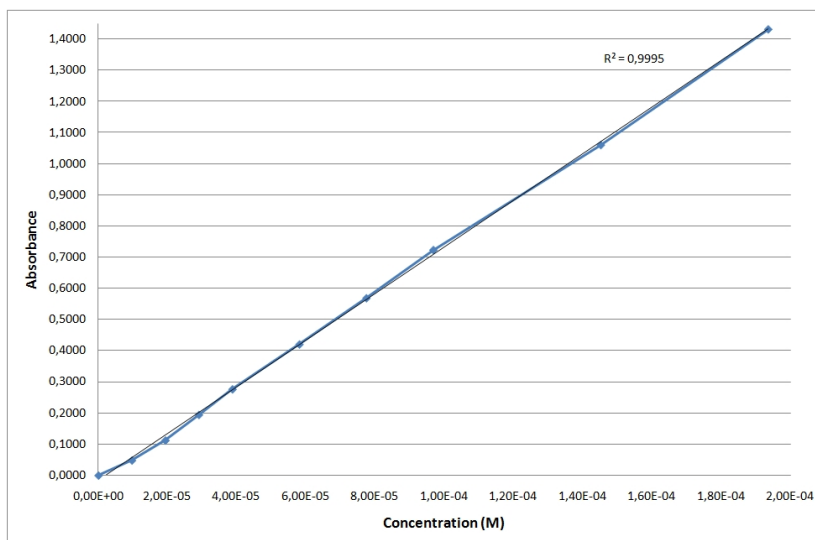
Figure 10.24: Standard series of 0.2g/L FA stock prepared with method 2 with centrifugation at 3000 rcf for 5 minutes and measurement at 215nm.

The standard series is clearly linear which can also be seen on the regression calculations. Figure 10.25 and 10.26 illustrate the specific isotherm data together with the mean average that were acquired when using method 2, using silica-gel and β-CD modified silica-gel as matrices, respectively.
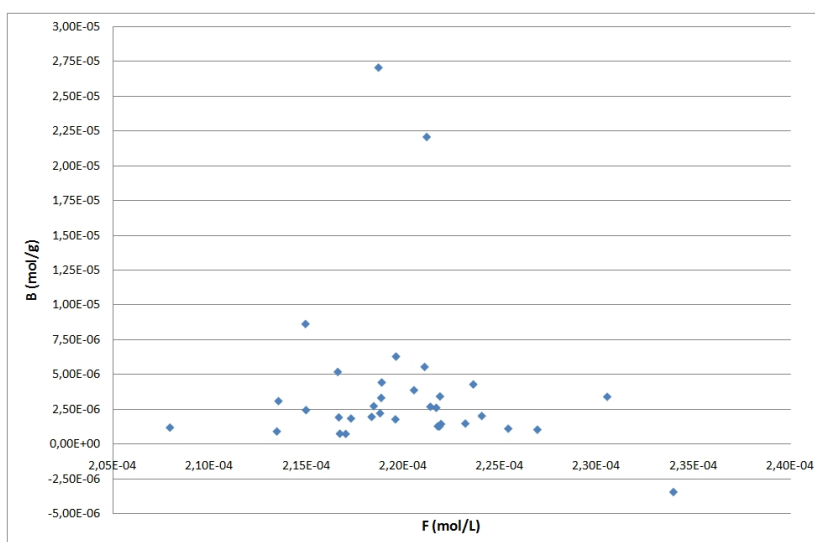
Figure 10.25: Isotherm plot of free drug, F, against matrix bound drug, B, showing acquired data using method 2 with virgin silica-gel as matrix.

It is obvious that the variance and standard error is far too high to be able to say much about these data. The FA stock solution became milky after a few days which leads to the conclusion that it was not stable in the PBS buffer at these concentrations. Furthermore, it proved to be very difficult to repeatedly weight and measure the exact amount when the sample matrix and the FA concentrations were mixed, which is likely to produce considerably
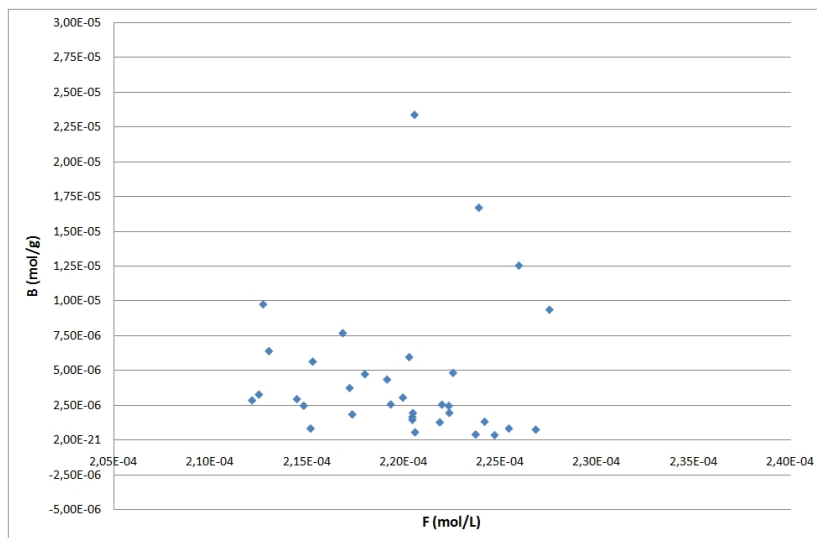
Figure 10.26: Isotherm plot of free drug, F, against matrix bound drug, B, showing acquired data using method 2 with β-CD modified silica-gel as matrix.

high errors since only a slight variation in volume, concentration, or mass is necessary for the absorbed concentrations to increase or decrease largely, especially since the working volume per sample is only 5ml and the matrices only absorb small amounts of FA.

Final Loading Isotherm Data

Figure 10.27 shows the standard series of FA prepared with the final examination method, where a phosphate buffer was used instead of the PBS buffer, the examination wavelength was 240nm instead of 215nm, and the volume and mass of all samples was doubled in order to minimize the sampling errors.
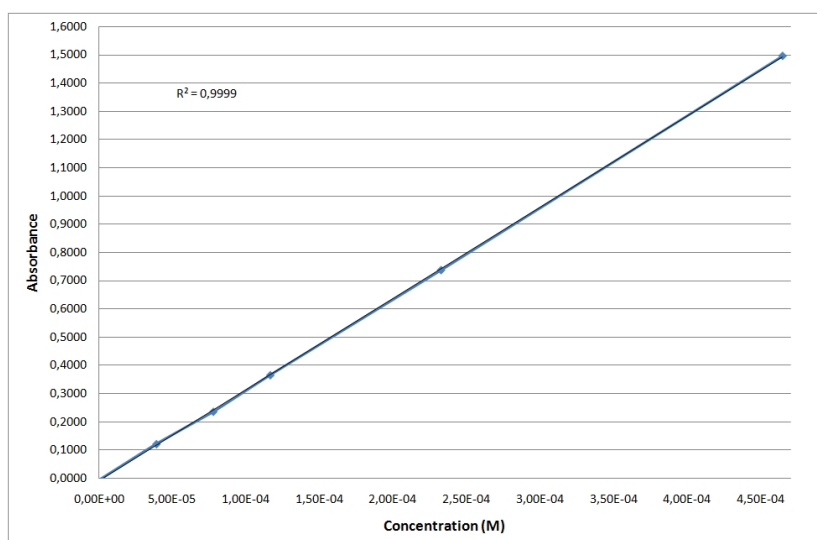
Figure 10.27: Standard series of 1.2g/L FA stock, where samples are centrifuged at 3000 rcf for 5 minutes and subsequently measured at 240nm.

The standard series is clearly linear at 240nm, which can also be seen on the regression calculations.

Loading Isotherm of virgin silica-gel

Figure 10.28 illustrates the specific isotherm data with the best fit of the langmuir isotherm for virgin silica-gel. The experiment was conducted to determine the adsorption pattern of FA onto the matrix.
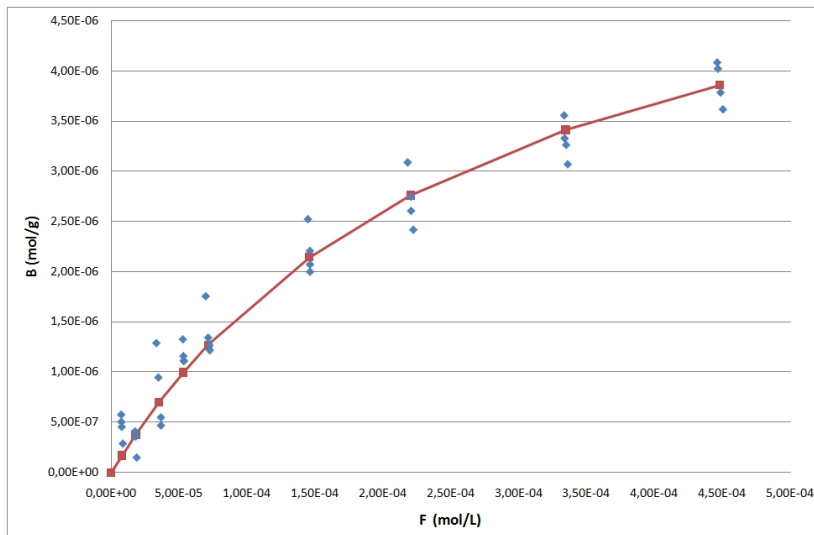

Figure 10.28: Isotherm plot of free drug, F, against bound drug, B, showing acquired data with best Langmuir Isotherm fit, using virgin silica-gel as matrix.

The best Langmuir Isotherm fit assumes a binding constant, K, of $3550\mathrm{M}^{-1}$ and a total amount of binding sites, N, of $6.28 \cdot 10^{-6}$. Figure 10.29 shows a Scatchard plot of the silica-gel experiment, which is used to examine the possible resemblance of the loading pattern to a bi-langmuir isotherm.
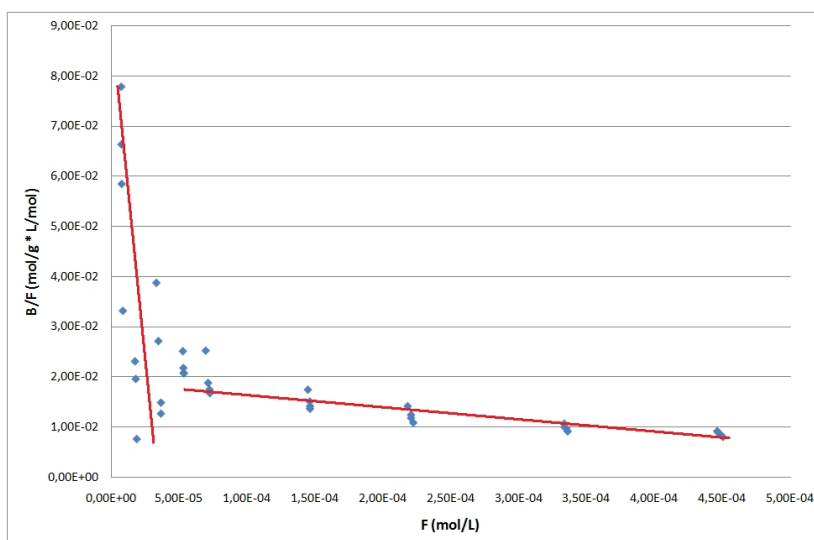
Figure 10.29: Scatchard plot of free drug, F, against bound drug divided by free drug, B/F, of the acquired data with virgin silica-gel as matrix. A possible correlation with the Bi-Langmuir Isotherm is a possibility.

The Scatchard plot illustrates that the binding of FA to the silica-gel matrix could be of the bi-langmuir type. Figure 10.30 shows a Double Logarithmic plot of the silica-gel experiment. The method is used to examine the possibility of the loading pattern to be of the freundlich or langmuir-freundlich type.
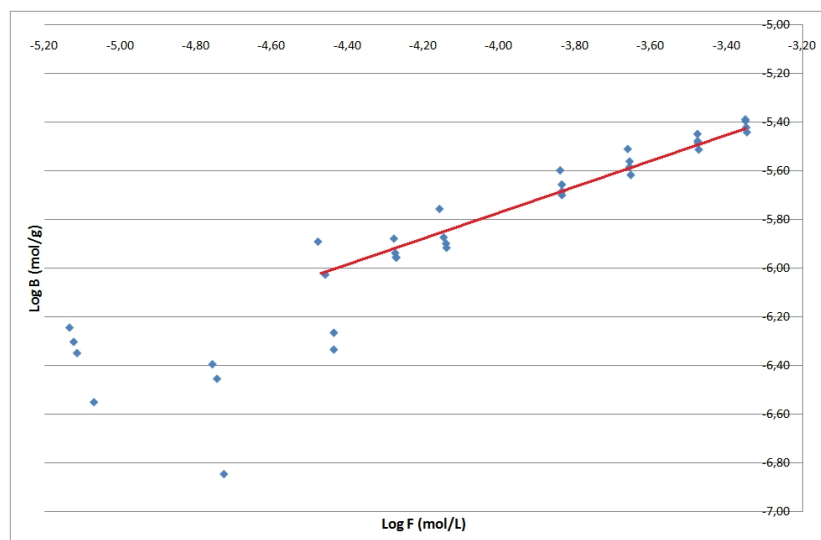
75

Figure 10.30: Double Logarithmic plot of LogF against LogB of the acquired data with virgin silica-gel as matrix. A possible correlation with the Freundlich Isotherm is a possibility.

The Double Logarithmic plot illustrates what appears to be a correlation with the Freundlich Isotherm. Considering the very porous structure of the silica-gel matrix with many hydroxy-groups on the surface and thus many similar adhesion sites for organic molecules, a binding model in which the drug affinity decreases with the addition of more drug seems reasonable. The Isotherm plot of free drug, F, against matrix bound drug, B, also has a similar shape to the Freundlich Isotherm. The silica-gel is therefore most likely following a binding model that is close to that of the Freundlich Isotherm model.

Loading Isotherm of b-CD modified silica-gel

Figure 10.31 illustrates the specific isotherm data with the best fit of the langmuir isotherm for β-CD modified silica-gel. The experiment was conducted to determine the adsorption pattern of FA onto the matrix.
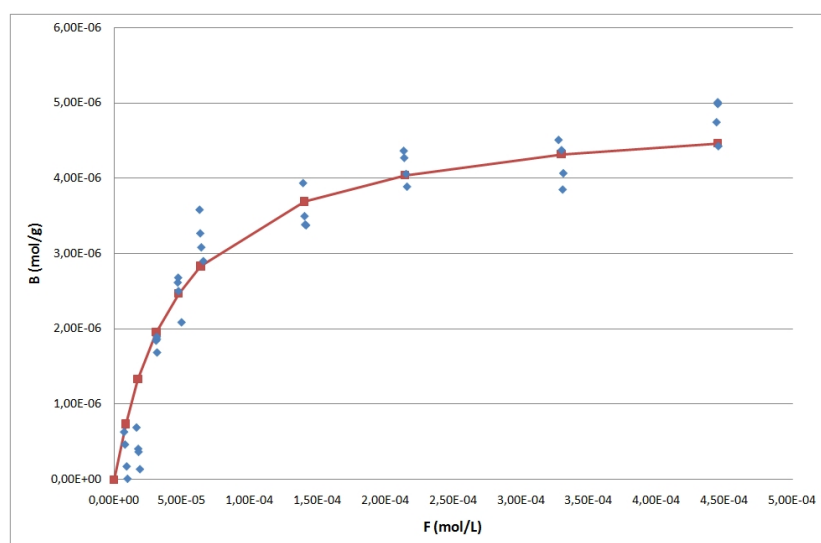

Figure 10.31: Isotherm plot of free drug, F, against matrix bound drug, B, showing acquired data with best Langmuir Isotherm fit, using β-CD modified silica-gel as matrix.

The best Langmuir Isotherm fit assumes a binding constant, K, of $21000M^{-1}$ and a total of $4.94 \cdot 10^{-6}$ binding sites, N. It can be seen that the binding strength in terms of K for FA has increased almost six times relative to pure silica-gel, while the amount of binding sites is reduced. Figure 10.32 shows a Scatchard plot of the β-CD modified silica-gel experiment, investigating the possibility of a resemblance with the bi-langmuir isotherm.
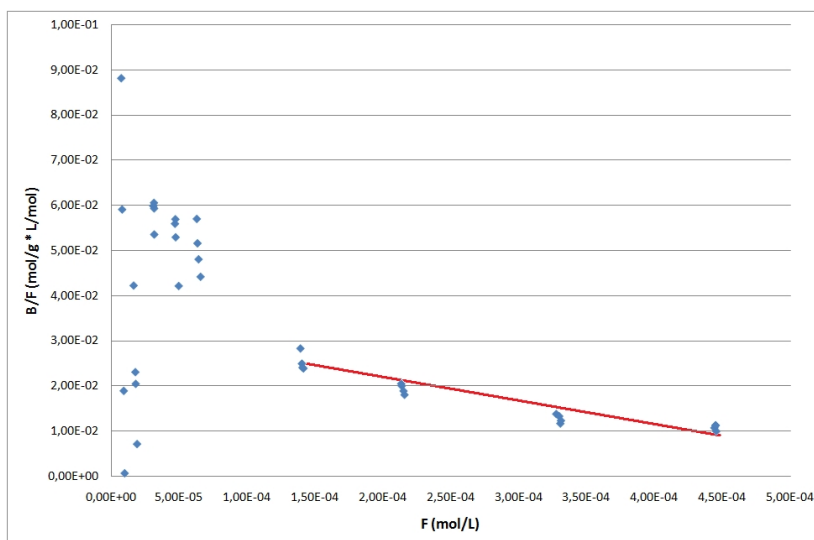

Figure 10.32: Scatchard plot of free drug, F, against bound drug divided by free drug, B/F, of the acquired data with β-CD modified silica-gel. A likely correlation with the Bi-Langmuir Isotherm is a possibility.

The Scatchard plot illustrates that the binding of FA to the β-CD modified silica-gel matrix could be of the bi-langmuir type, but it is difficult to plot a clear line for the high affinity binding sites due to a high experimental error at these concentrations. Thus, only a mean average line is plotted for the potential low affinity binding sites in the Bi-Langmuir Isotherm model. Figure 10.33 shows a Double Logarithmic plot of the β-CD modified silica-gel experiment.
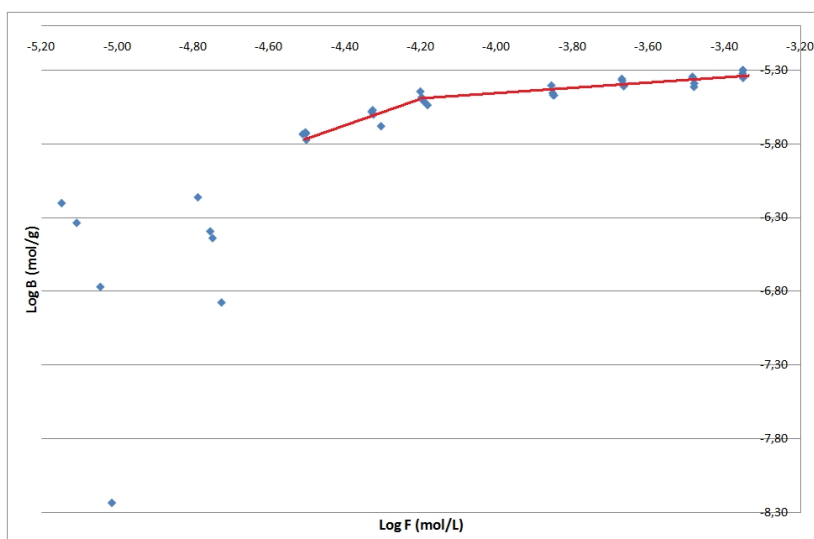

Figure 10.33: Double Logarithmic plot of LogF against LogB of the acquired data with β-CD modified silica-gel as matrix. A possible correlation with the Langmuir-Freundlich Isotherm is a possibility.

It is seen that the data assume what appears to be a correlation with the Langmuir-Freundlich Isotherm when the FA concentrations are approaching the saturation point of the matrix.

Considering the composition of the matrix with less hydroxy-groups on the surface and a w% between 1.5-5.17% β-CD the affinity of FA to the matrix could be of a more complex model structure, more specifically that of a primary Langmuir-Freundlich isotherm combined with sites of lower affinity expressed by the modified surface structure of the silica-gel matrix that now consists of a combination of hydroxy-groups with and without a silan-spacer arm with no attached β-CDs on the epoxy end.

Loading Isotherm of virgin HA

Figure 10.34 illustrates the isotherm for the loading profile of virgin HA. The experiment was conducted to determine the adsorption pattern of FA onto the matrix.
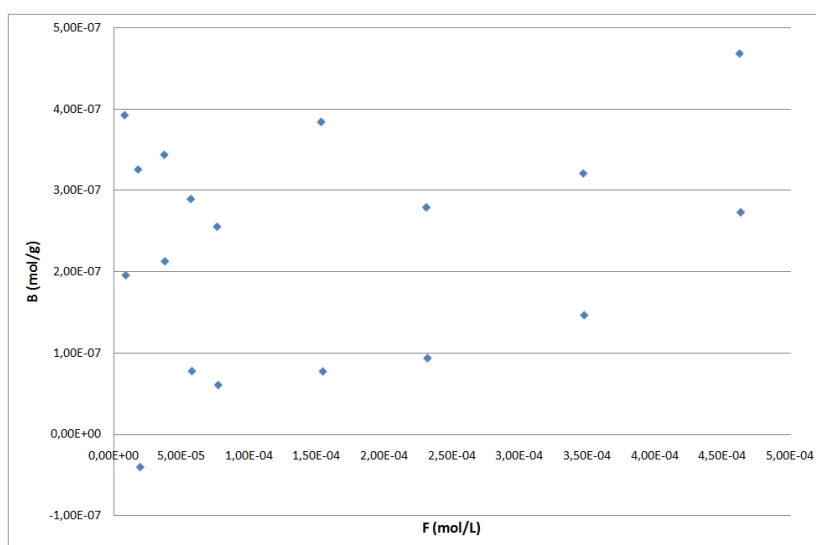

Figure 10.34: Isotherm plot of free drug, F, against bound drug, B, showing acquired data when using virgin HA as matrix.

Unfortunately the acquired data do not resemble any type of isotherm. No best fit for a Langmuir Isotherm could be calculated. The bound amounts of the drug FA are between 0.7 - 4.75·10^{-7} mol/g. No clear change in absorption strength can be seen throughout the various initial concentrations of FA. The precision of the examination method is considered too low in the range of absorbed FA within the HA experiment and as a result, no Scatchard or Logarithmic analysis is conducted.

Loading Isotherm of b-CD modified HA

Figure 10.35 illustrates the isotherm for the loading profile of β-CD modified HA. The experiment was conducted to determine the adsorption pattern of FA onto the matrix.
Unfortunately the acquired data do not resemble any type of isotherm. No best fit for a Langmuir Isotherm could be calculated. The bound amounts of the drug FA are between 0.02 - 7.4·10^{-7} mol/g. However, it seems that the concentration of bound FA increases linearly from 1.5·10^{-4} mol/L of free drug and with higher free drug concentrations. Similarly to the experiments of virgin HA, however, a scatchard or logarithmic analysis was not conducted as a result of the relatively low precision at the absorbed FA concentrations.
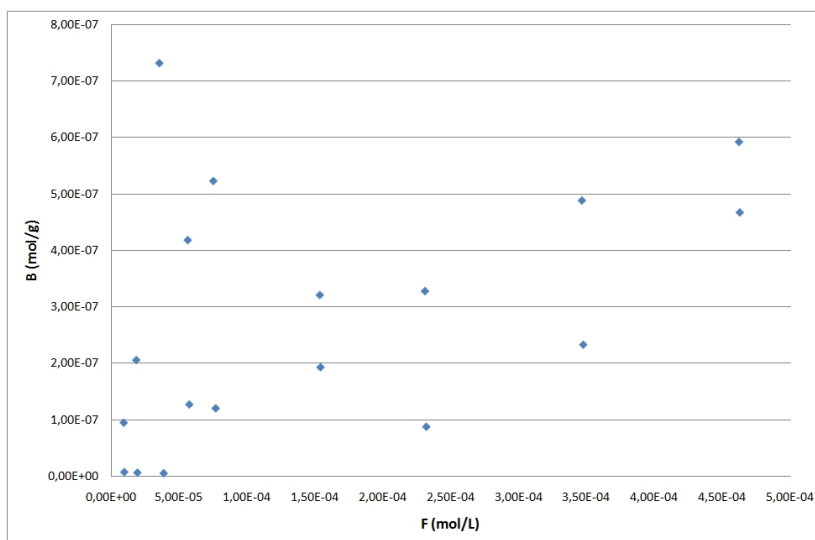
Figure 10.35: Isotherm plot of free drug, F, against bound drug, B, when using β-CD modified HA.

10.5   CLSM of HA and Silica-gel with 1,8-ANS as Ligand

All large fluorescence pictures are processed with the "z-axis stacking-function" of the image processing program ImageJ. Figure 10.36 illustrates the shape and fluorescence emission of some of the particles of a 0.04g virgin silica-gel sample prepared with 10ml $1 \cdot 10^{-3}$M 1,8-ANS. The experiment was conducted to show that 1,8-ANS does not fluorescend sufficiently unless it is present in a hydrophobic environment.
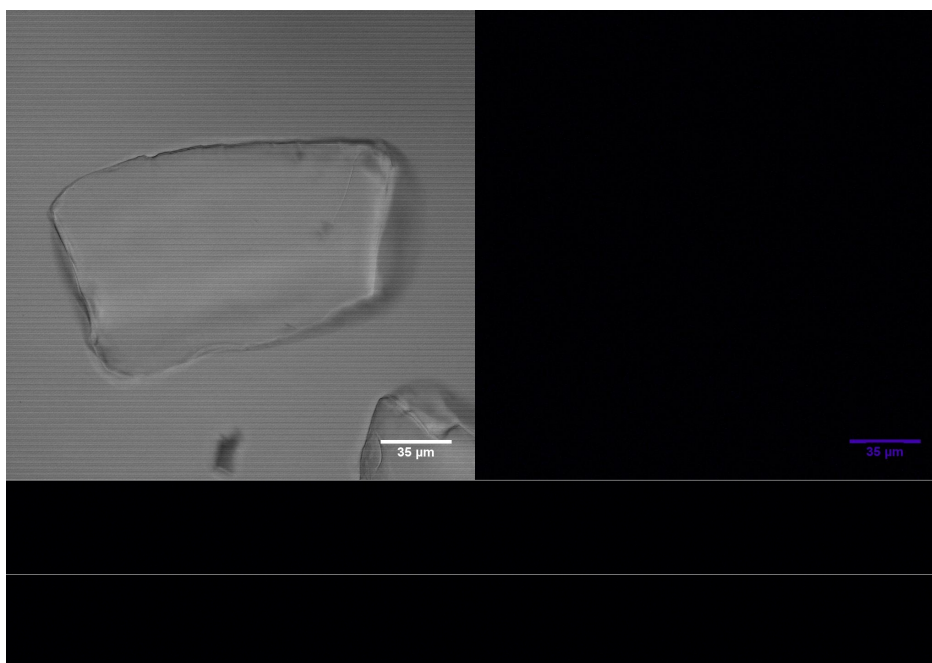

Figure 10.36: Illustration of shape and fluorescence emissions from virgin silica-gel prepared with $1 \cdot 10^{-3}$M 1,8-ANS. Left, a picture of the specimen with an optical microscope; The 20 images at the bottom, sampling of the specimen; Right, all 20 CLSM images combined with the stacking-function.

No fluorescence signals are observed, showing that no 1,8-ANS molecules are fluorescing sufficiently because of the lack of a hydrophobic environment in the virgin silica-gel matrix.

Figure 10.37 illustrates the shape and fluorescence emission of some of the particles of a 0.04g β-CD modified silica-gel sample prepared with 10ml $1 \cdot 10^{-3}$M 1,8-ANS. The experiment was conducted to investigate the presence of β-CDs in the silica-gel matrix.
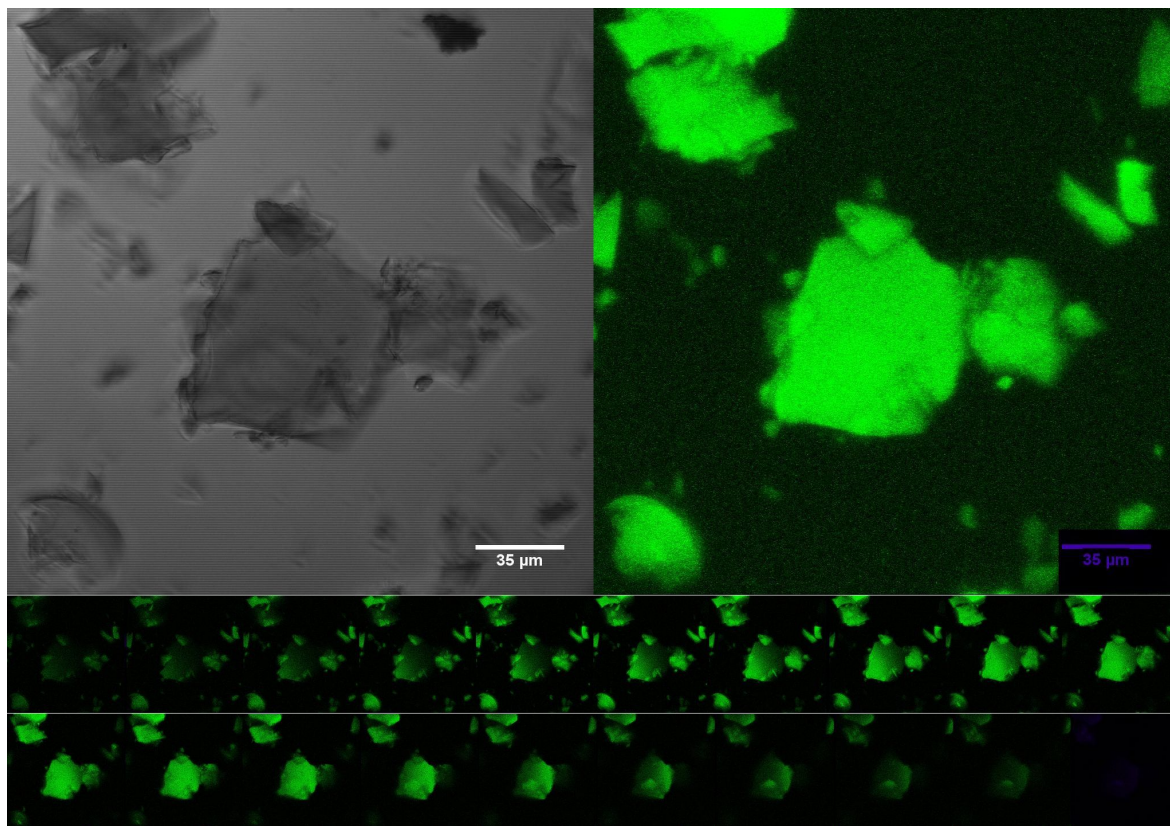

Figure 10.37: Illustration of shape and fluorescence emissions from β-CD modified silica-gel prepared with $1 \cdot 10^{-3}$M 1,8-ANS. Left, a picture of the specimen with an optical microscope; The 20 images at the bottom, sampling of the specimen with a confocal laser scanning microscope; Right, all 20 CLSM images combined with the stacking-function.

Fluorescence emission can clearly be observed in this specimen. Since 1,8-ANS is the only molecule present in this system that is able to fluorescend it is concluded that 1,8-ANS molecules must be present in the hydrophobic cavities of the β-CD modified silica-gel matrix prepared with $1 \cdot 10^{-3}$M 1,8-ANS, which in turn amplifies the fluorescence emissions from 1,8-ANS. Fluorescence is also detected within the particle, indicating that β-CDs are not only attached to the very surface of the respective particle but also in the deeper pore layers.

Figure 10.38 illustrates the shape and fluorescence emission of some of the particles of a 0.04g virgin HA sample prepared with 10ml $1 \cdot 10^{-3}$M 1,8-ANS. The experiment was conducted to show that 1,8-ANS does not fluorescend sufficiently as there are no hydrophobic environments or cavities to boost the fluorescence emission abilities of 1,8-ANS.
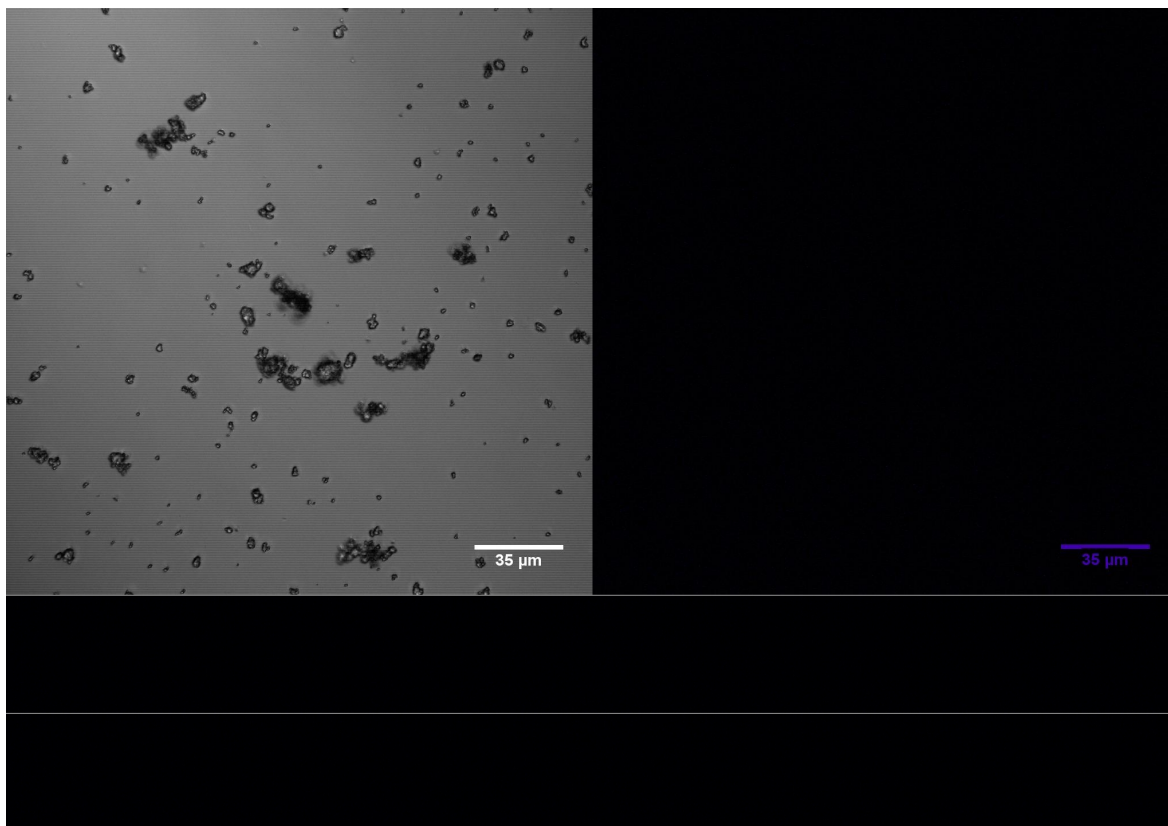

Figure 10.38: Illustration of shape and fluorescence emissions from virgin HA prepared with $1 \cdot 10^{-3}$M 1,8-ANS. Left, a picture of the specimen with an optical microscope; The 20 images at the bottom, sampling of the specimen with a confocal laser scanning microscope; Right, all 20 CLSM images combined with the stacking-function.

It is seen, that the specimen is not fluorescing at all suggesting that the 1,8-ANS molecules are not present in any hydrophobic environments within the matrix of the specimen.

Figure 10.39 illustrates the shape and fluorescence emission of some of the particles of a 0.04g β-CD modified HA sample prepared with 10ml $1 \cdot 10^{-3}$M 1,8-ANS. The experiment was conducted in order to investigate the presence of β-CDs in the HA matrix.
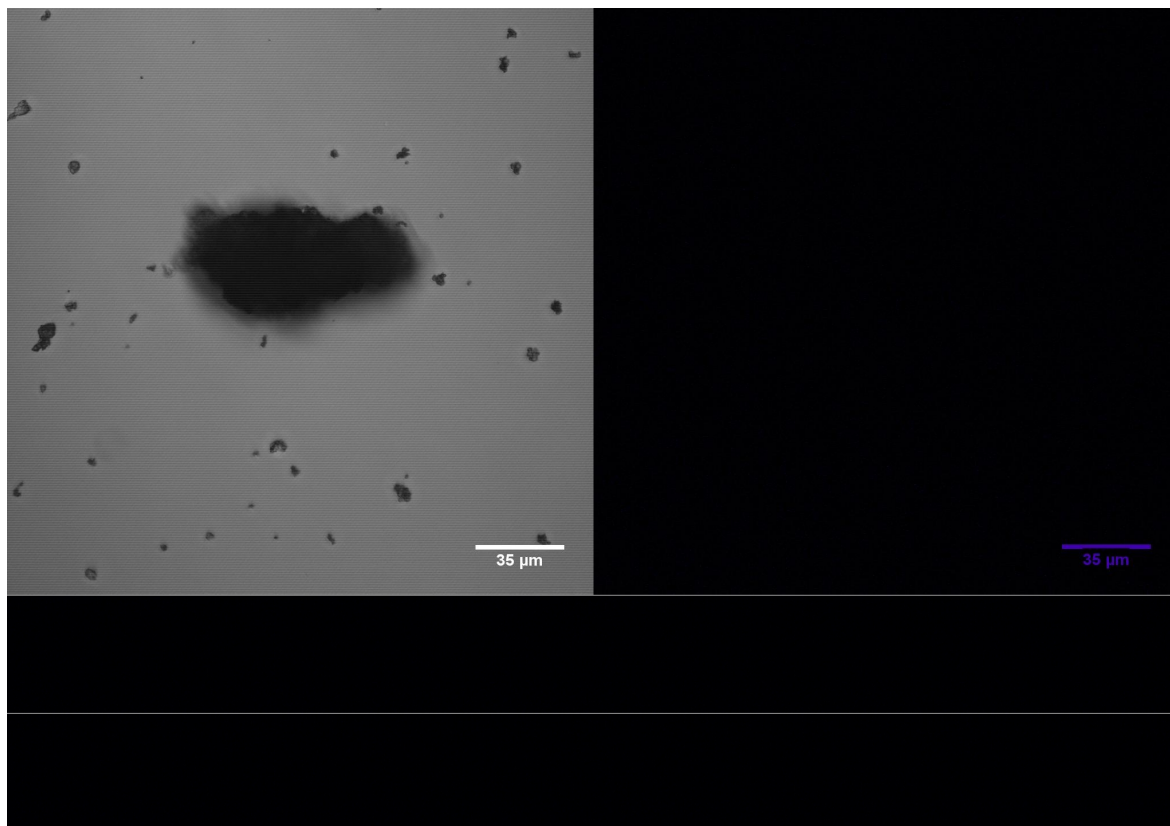

Figure 10.39: Illustration of shape and fluorescence emissions from β-CD modified HA prepared with $1 \cdot 10^{-3}$M 1,8-ANS. Left, a picture of the specimen with an optical microscope; The 20 images at the bottom, sampling of the specimen with a confocal laser scanning microscope; Right, all 20 CLSM images combined with the stacking-function.

No fluorescence signal is detected in this specimen as well. Thus, no presence of 1,8-ANS molecules in hydrophobic cavities of the matrix of the specimen can be concluded.

Figure 10.40 illustrates the shape and fluorescence emission of some of the particles of a 0.04g virgin silica-gel sample prepared with 10ml $1 \cdot 10^{-4}$M 1,8-ANS.

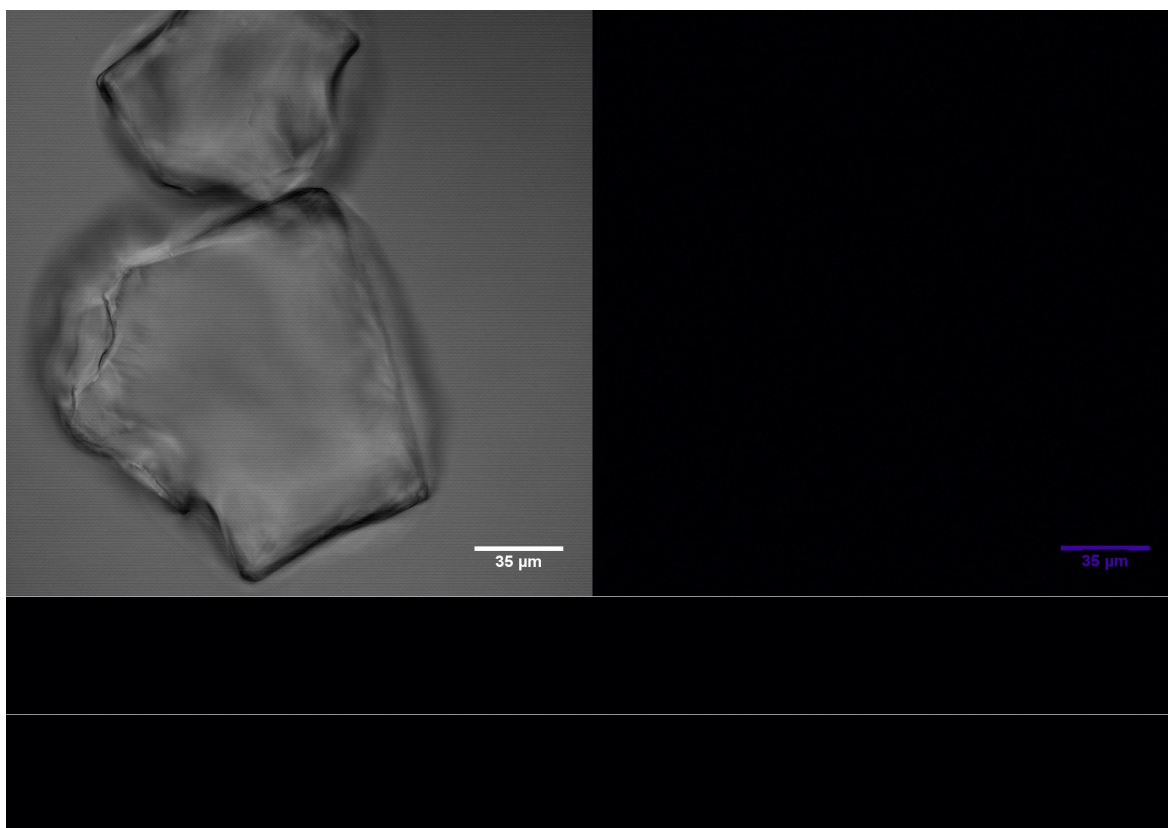
Figure 10.40: Illustration of shape and fluorescence emissions from virgin silica-gel prepared with $1 \cdot 10^{-4}$M 1,8-ANS. Left, a picture of the specimen with an optical microscope; The 20 images at the bottom, sampling of the specimen with a confocal laser scanning microscope; Right, all 20 CLSM images combined with the stacking-function.

No fluorescence is observed as expected, because of the lack of accessible hydrophobic cavities within the virgin silica-gel specimen with $1 \cdot 10^{-4}$M 1,8-ANS.

Figure 10.41 illustrates the shape and fluorescence emission of some of the particles of a 0.04g β-CD modified silica-gel sample prepared with 10ml $1 \cdot 10^{-4}$M 1,8-ANS. The experiment was conducted to investigate the presence of β-CDs with ten times lower concentrations of 1,8-ANS than the first CLSM experiment with $1 \cdot 10^{-3}$ M1,8-ANS and β-CD modified silica-gel.
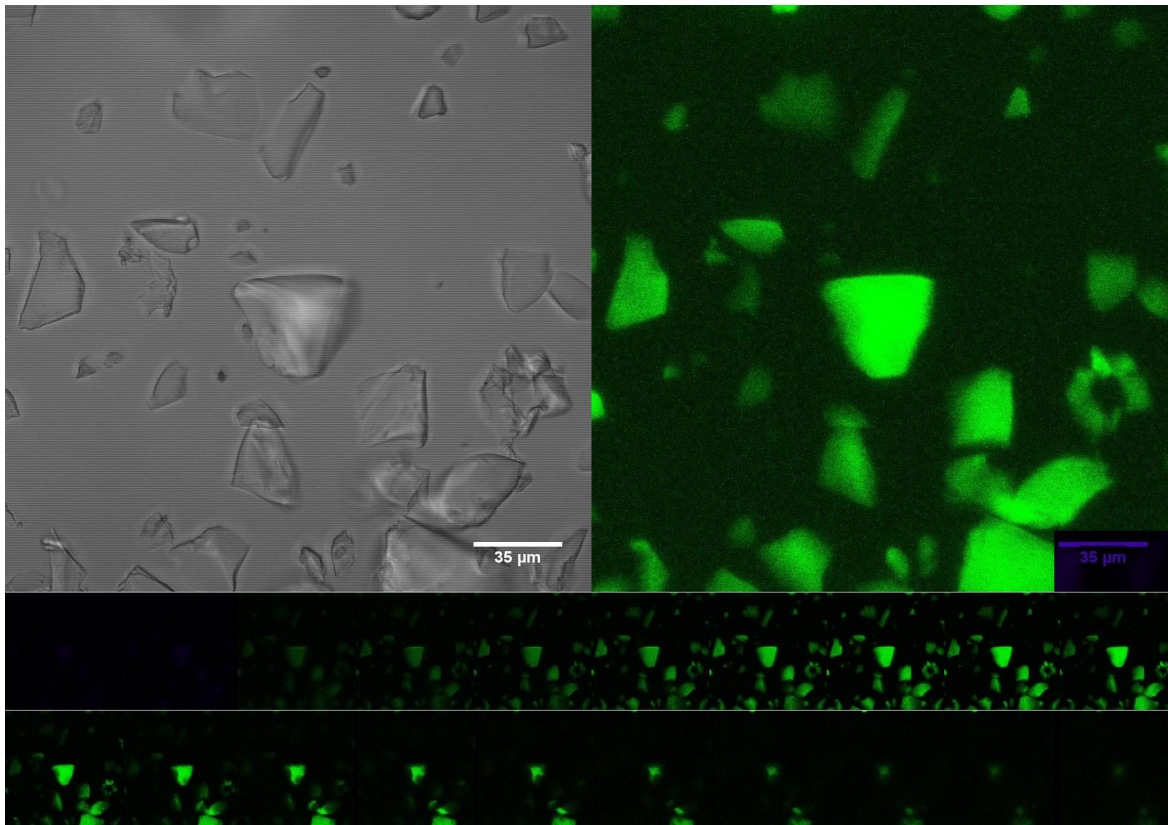

Figure 10.41: Illustration of shape and fluorescence emissions from β-CD modified silica-gel prepared with $1 \cdot 10^{-4}$M 1,8-ANS. Left, a picture of the specimen with an optical microscope; The 20 images at the bottom, sampling of the specimen with a confocal laser scanning microscope; Right, all 20 CLSM images combined with the stacking-function.

Fluorescence emission can clearly be observed in this specimen. Since 1,8-ANS is the only molecule present in this system that is able to fluorescend it is concluded that 1,8-ANS molecules must be present in the hydrophobic cativies of the β-CD modified silica-gel matrix prepared with $1 \cdot 10^{-4}$M 1,8-ANS. Also, fluorescence emissions are detected throughout all levels of the particles, indicating the presence of β-CDs inside the particle as well, and not only on the surface.

Figure 10.42 illustrates the shape and fluorescence emission of some of the particles of a 0.04g virgin silica-gel sample prepared with 10ml $2.32 \cdot 10^{-3}$M (1.2g/L) FA, whereafter it was filtered and dried at 50°C in a vacuum chamber. The experiment was conducted in order to show that FA does not fluorescend within the virgin silica-gel matrix.

Figure 10.42: Illustration of shape and fluorescence emissions from virgin silica-gel prepared with $2.32 \cdot 10^{-3}$M FA. Left, a picture of the specimen with an optical microscope; The 20 images at the bottom, sampling of the specimen with a confocal laser scanning microscope; Right, all 20 CLSM images combined with the stacking-function.

No fluorescence is observed, proving that FA does not fluorescend when added to a virgin silica-gel specimen.

Figure 10.43 illustrates the shape and fluorescence emission of some of the particles of a 0.04g β-CD modified silica-gel sample prepared with 10ml $2.32 \cdot 10^{-3}$M (1.2g/L) FA, whereafter it was filtered and dried at 50°C in a vacuum chamber. The experiment was conducted to show that FA does not fluorescend within the matrix of β-CD modified silica-gel.
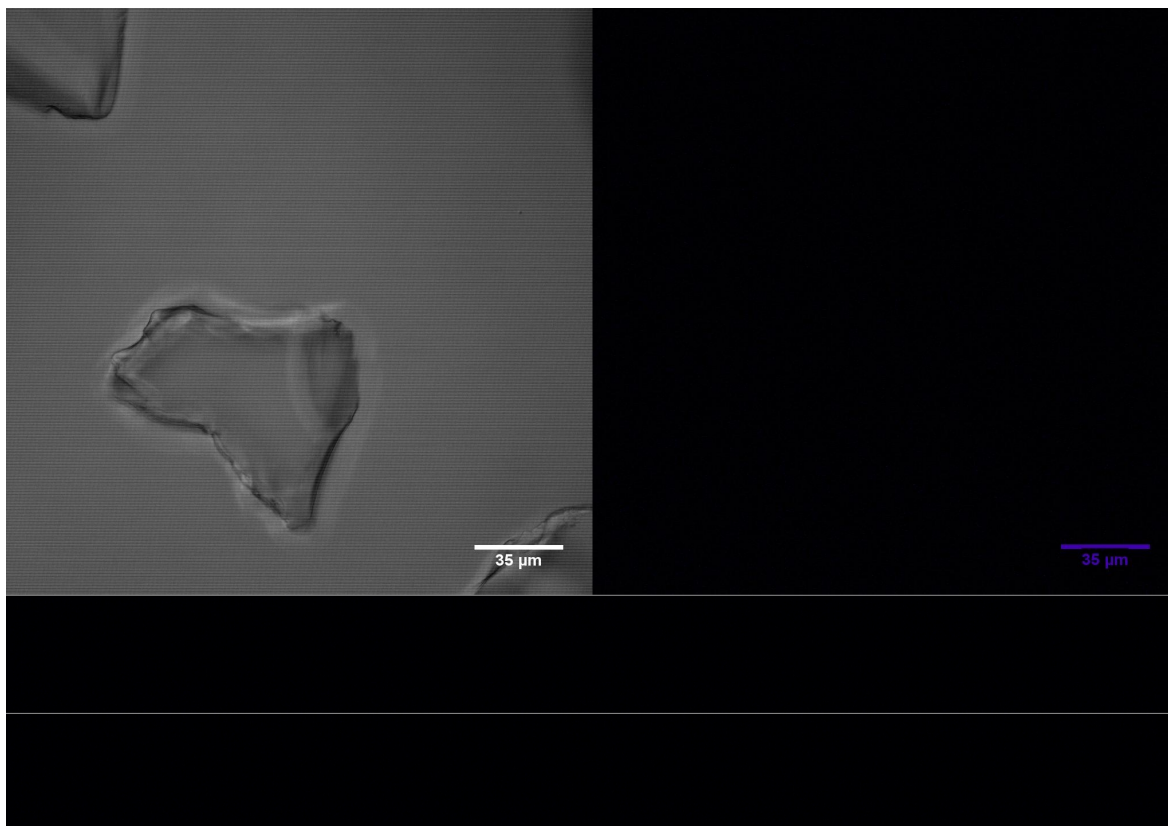

Figure 10.43: Illustration of shape and fluorescence emissions from β-CD modified silica-gel prepared with 10ml $2.32 \cdot 10^{-3}$M FA. Left, a picture of the specimen with an optical microscope; The 20 images at the bottom, sampling of the specimen with a confocal laser scanning microscope; Right, all 20 CLSM images combined with the stacking-function.

No fluorescence is observed, showing that FA molecules also do not fluorescend when hydrophobic cavities are present within a β-CD modified silica-gel specimen.

Figure 10.44 illustrates the shape and fluorescence emission of some of the particles of a 0.04g virgin silica-gel sample prepared with 10ml $2.32 \cdot 10^{-3}$M (1.2g/L) FA, whereafter it was filtered and dried at 50°C in a vacuum chamber. Subsequently, 10ml of $1 \cdot 10^{-4}$M 1,8-ANS was added and left for equilibration for 24 hours.
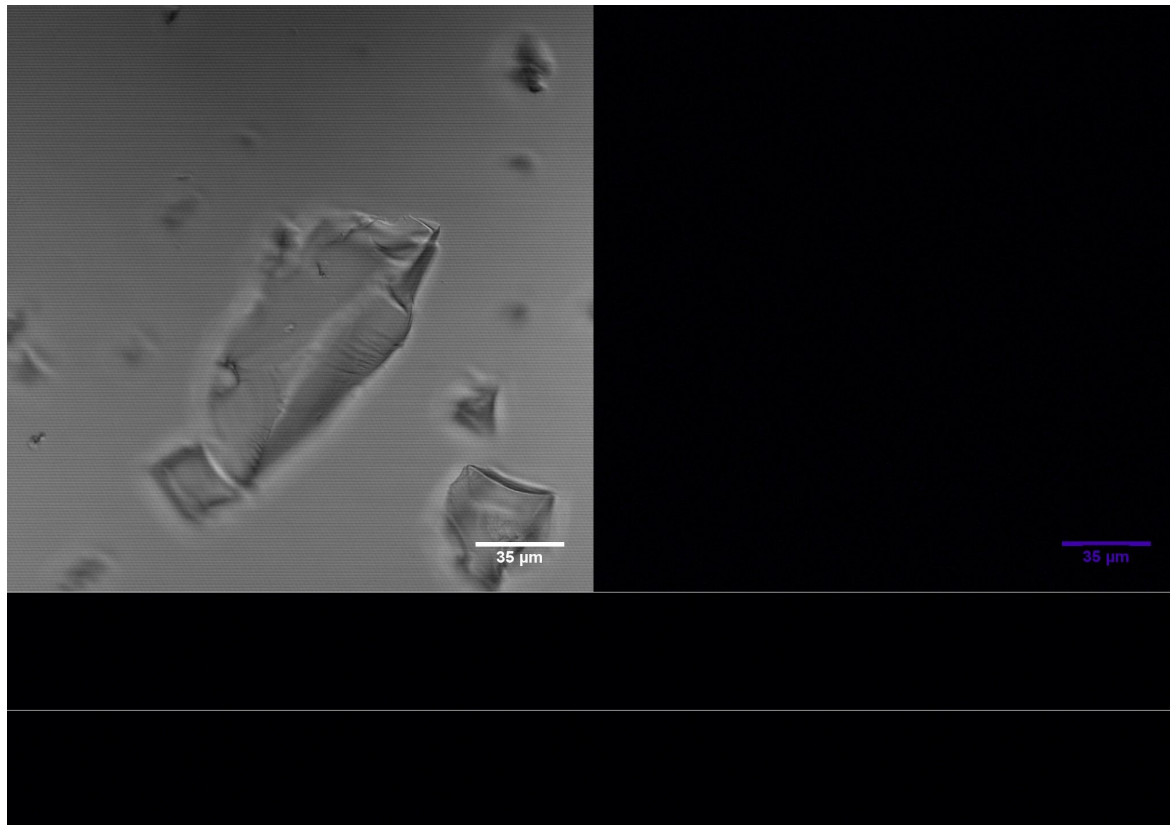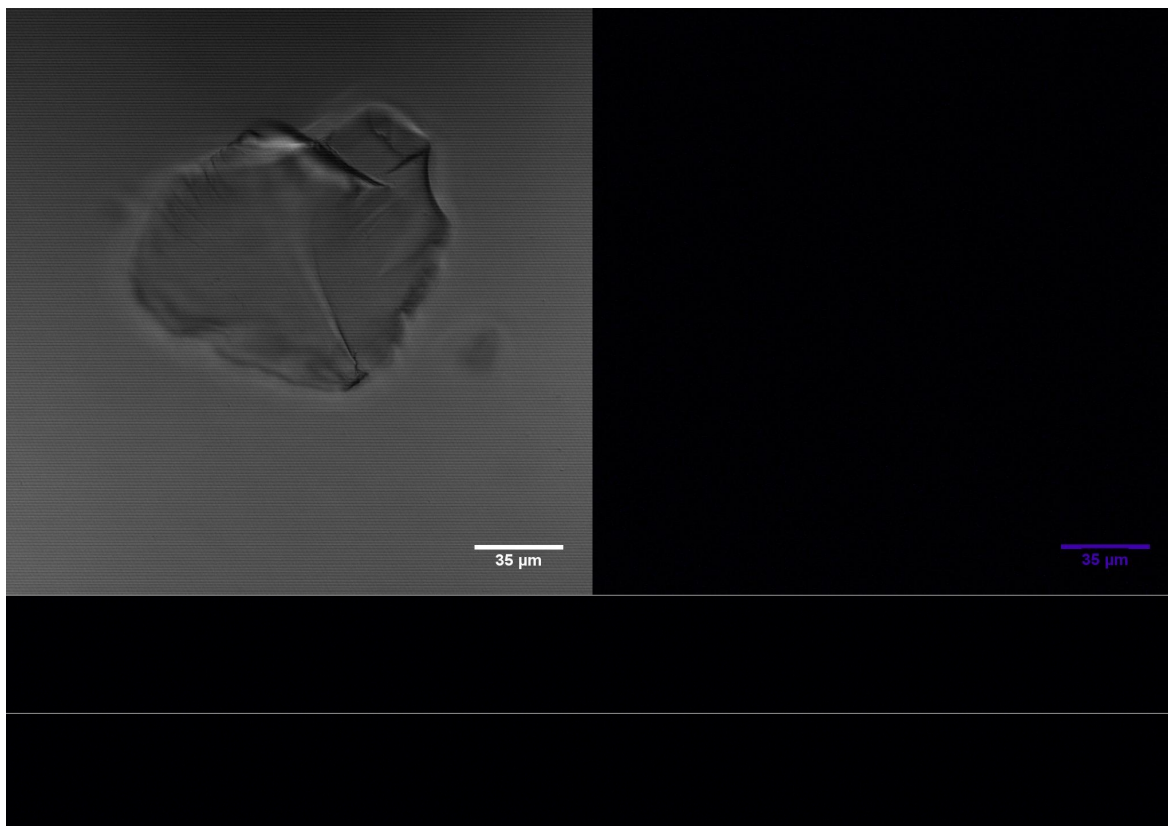

Figure 10.44: Illustration of shape and fluorescence emissions from virgin silica-gel prepared with $2.32 \cdot 10^{-3}$M FA and $1 \cdot 10^{-4}$M 1,8-ANS. Left, a picture of the specimen with an optical microscope; The 20 images at the bottom, sampling of the specimen with a confocal laser scanning microscope; Right, all 20 CLSM images combined with the stacking-function.

No fluorescence is observed suggesting that no hydrophobic environments are accessible by 1,8-ANS molecules in the virgin silica-gel specimen prepared with $2.32 \cdot 10^{-3}$M FA and, subsequently, $1 \cdot 10^{-4}$M 1,8-ANS.

Figure 10.45 illustrates the shape and fluorescence emission of some of the particles of a 0.04g β-CD modified silica-gel sample prepared with 10ml $2.32 \cdot 10^{-3}$M (1.2g/L) FA, whereafter it was filtered and dried at 50°C in a vacuum chamber. Subsequently, 10ml of $1 \cdot 10^{-4}$M 1,8-ANS was added and left for equilibration for 24 hours. The experiment was conducted to determine if 1,8-ANS can occupy the less hydrophilic β-CD cavities of β-CD modified silica-gel with FA.
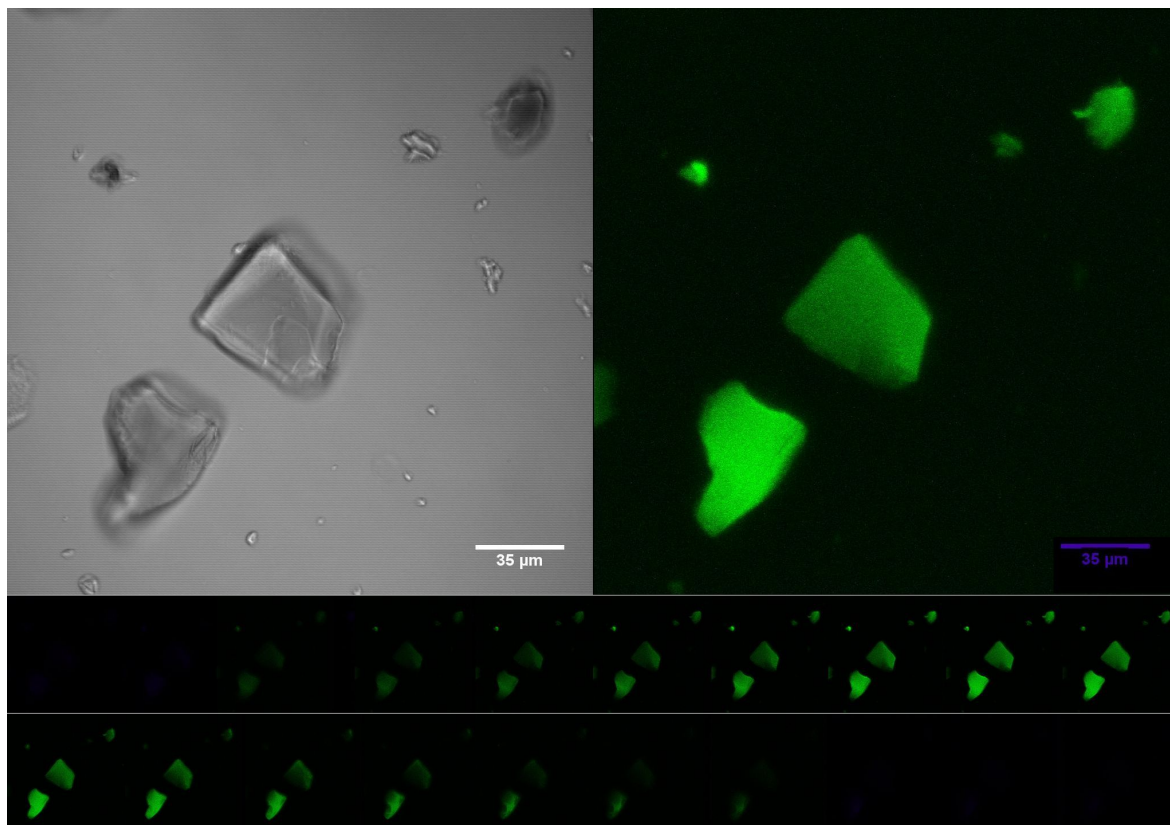

Figure 10.45: Illustration of shape and fluorescence emissions from β-CD modified silica-gel prepared with 10ml $2.32 \cdot 10^{-3}$M FA, and and $1 \cdot 10^{-4}$M 1,8-ANS. Left, a picture of the specimen with an optical microscope; The 20 images at the bottom, sampling of the specimen with a confocal laser scanning microscope; Right, all 20 CLSM images combined with the stacking-function.

Fluorescence emission can clearly be observed in this specimen. Since 1,8-ANS is the only molecule present in this system that is able to fluorescend it must be 1,8-ANS molecules that are observed in the hydrophobic cavities of the β-CD modified silica-gel matrix prepared with $1 \cdot 10^{-3}$M 1,8-ANS and $2.32 \cdot 10^{-3}$M FA. Furthermore, it is observed that a fluorescence signal can be observed throughout the whole particle, indicating the presence of β-CDs in all depth levels of the particles.

In summary, fluorescence is only observed from specimen with the β-CD modified silica-gel matrix. A fluorescence signal was observed when the matrix was prepared with both $1 \cdot 10^{-3}$M and $1 \cdot 10^{-4}$M 1,8-ANS. Subsequently, the results considering the β-CD modified silica-gel matrix which also was prepared with $2.32 \cdot 10^{-3}$M FA showed that 1,8-ANS can compete with FA for the less hydrophilic β-CD cavities attached to the modified matrix.

10.6   Loading Isotherms of Silica-gel with 1,8-ANS as Ligand

Figure 10.46 shows the standard series of 1,8-ANS, measured with fluorescence spectroscopy. The excitation wavelength was 311nm and the emission spectrum ranged between 450-600nm.
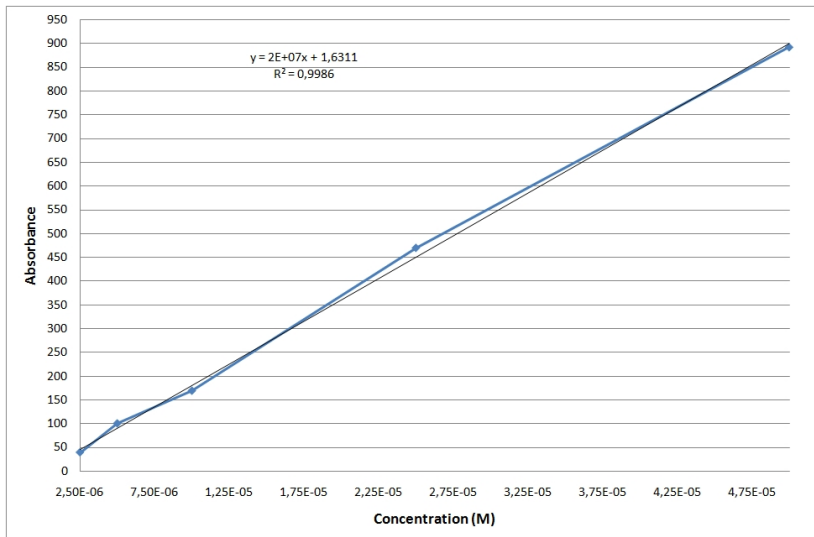

Figure 10.46: Standard series of 1,8-ANS with an excitation wavelength of 311nm and an emission spectrum between 450-600nm.

The standard series is considered to be linear, albeit there is an experimental error involved in the measurements. This error will be taken into account later in the discussion.

1,8-ANS Loading Isotherm of virgin silica-gel with and without FA

Figure 10.47 illustrates the isotherm for the loading profile of virgin silica-gel with various concentrations of 1,8-ANS with and without $2.32 \cdot 10^{-3}$M (1.2g/L) FA, in order to determine the competitor effects between 1,8-ANS and FA.
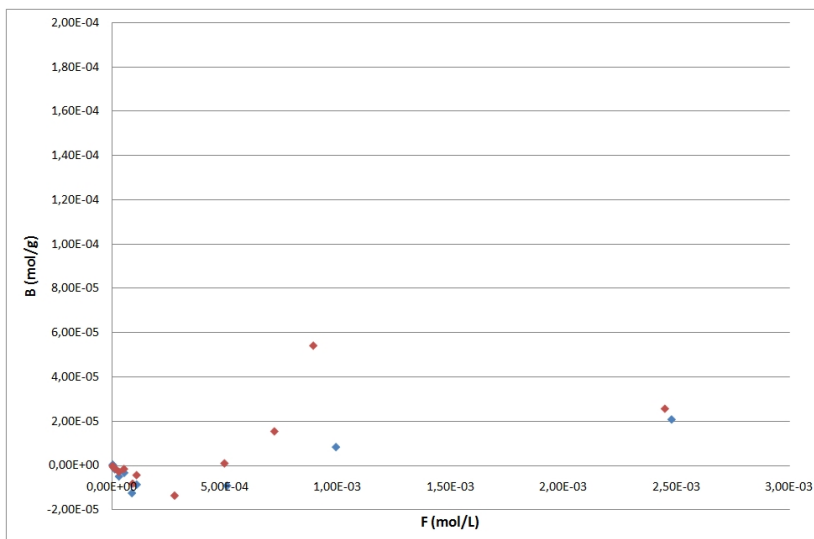

Figure 10.47: Isotherm plot of free drug, F, against bound drug, B, showing acquired data when using virgin silica-gel with 1,8-ANS with and without FA. Blue, with FA; Red, without FA.

Unfortunately the acquired data do not resemble any type of isotherm. No best fit for a

Langmuir Isotherm could be calculated. The highest amount of 1,8-ANS without FA that is bound is approximately $6 \cdot 10^{-5}$ mol/g, and for 1,8-ANS with FA approximately $2 \cdot 10^{-5}$ mol/g. However, except for the highest datapoint for 1,8-ANS without FA, both isotherm data are following each other in a similar pattern. Furthermore, some of the initial data actually illustrate a negative amount of bound 1,8-ANS, suggesting that 1,8-ANS amounts of $1 \cdot 10^{-5}$ mol/g or lower can give complications with an experimental error.

1,8-ANS Loading Isotherm of β-CD modified silica-gel with and without FA

Figure 10.48 illustrates the isotherm for the loading profile of β-CD modified silica-gel with 1,8-ANS with and without $2.32 \cdot 10^{-3}$M (1.2g/L) FA, in order to determine the competitor effects between 1,8-ANS and FA.

Figure 10.48: Isotherm plot of free drug, F, against bound drug, B, showing acquired data when using β-CD modified silica-gel with 1,8-ANS with and without FA. Blue, with FA; Red, without FA.

Both best fits suggest a somewhat relationship with the Freundlich or Langmuir-Freundlich isotherm. The highest amount of 1,8-ANS without FA that is bound is approximately $1.8 \cdot 10^{-4}$ mol/g, and for 1,8-ANS with FA approximately $8 \cdot 10^{-5}$ mol/g, which means that more 1,8-ANS is absorbed without the presence of FA.

Figure 10.49 shows a Scatchard plot of the experiment.
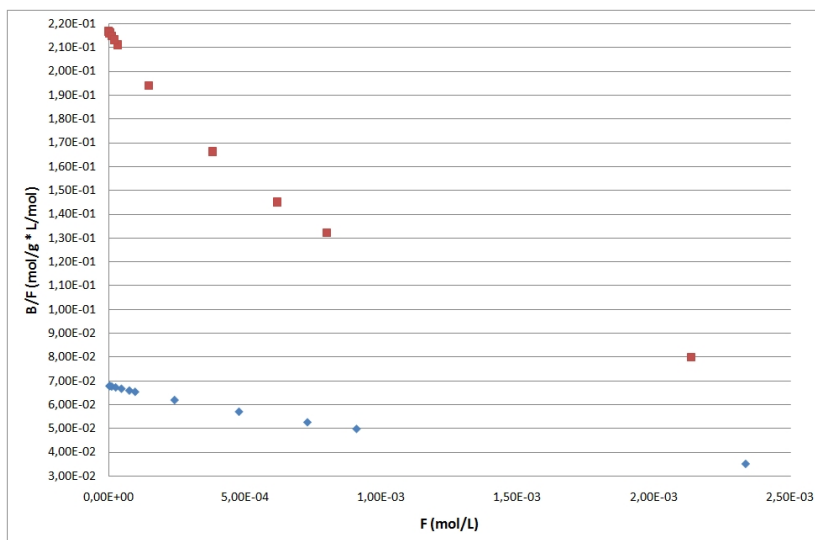
Figure 10.49: Scatchard plot of free drug, F, against bound drug divided by free drug, B/F, of the acquired data with β-CD modified silica-gel with 1,8-ANS with and without FA. Blue, with FA; Red, without FA.

The Scatchard plot illustrates no obvious correlation with a bi-langmuir isotherm for either of the data plots. Figure 10.50 shows a Double Logarithmic plot of the experiment.
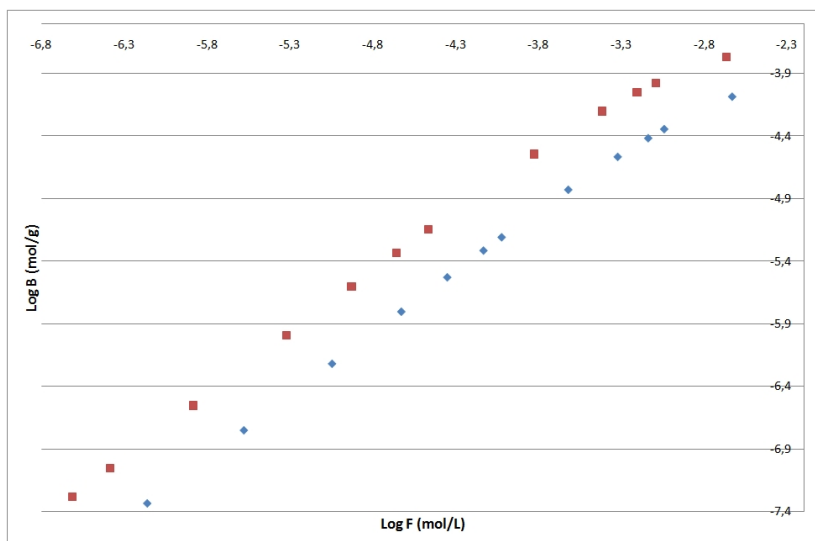
Figure 10.50: Double Logarithmic plot of LogF against LogB of the acquired data with β-CD modified silica-gel with 1,8-ANS with and without FA. Blue, with FA; Red, without FA.

The double logarithmic plot of both datasets suggests a resemblance with a Freundlich Isotherm.

Comparison of 1,8-ANS absorption with and without FA

The above loading isotherms have been rearranged in figure 10.51 and figure 10.52 in order to illustrate the effects on 1,8-ANS absorption with or without the β-CD modification of silica-gel.
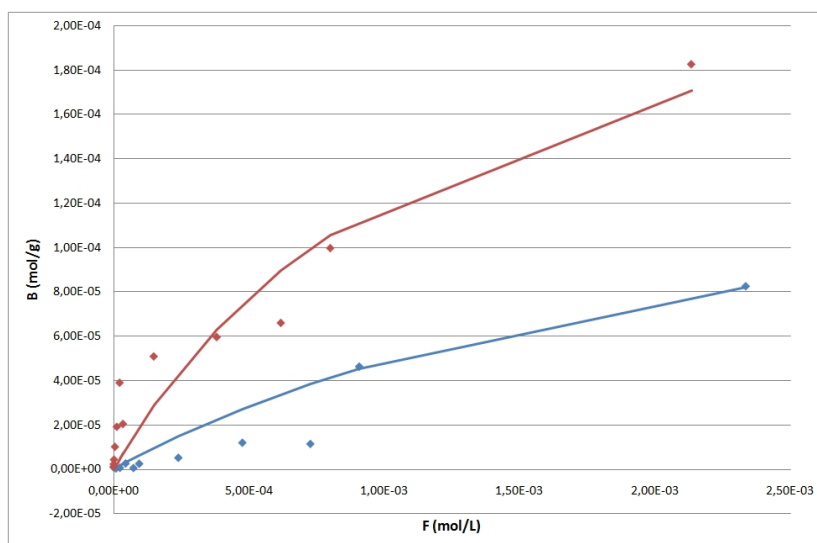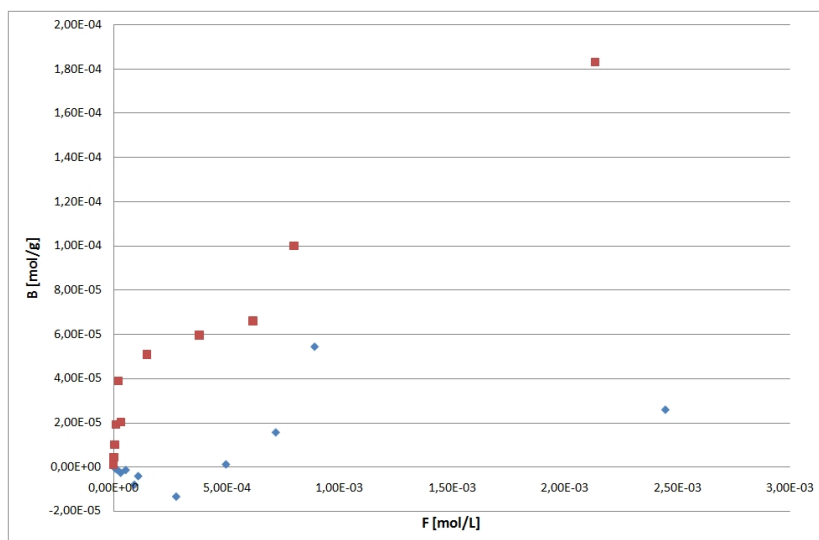
Figure 10.51: Isotherm plot of free drug, F, against bound drug, B, showing acquired data when using virgin and β-CD modified silica-gel with bound 1,8-ANS without FA. Blue, without β-CD modification; Red, with β-CD modification.
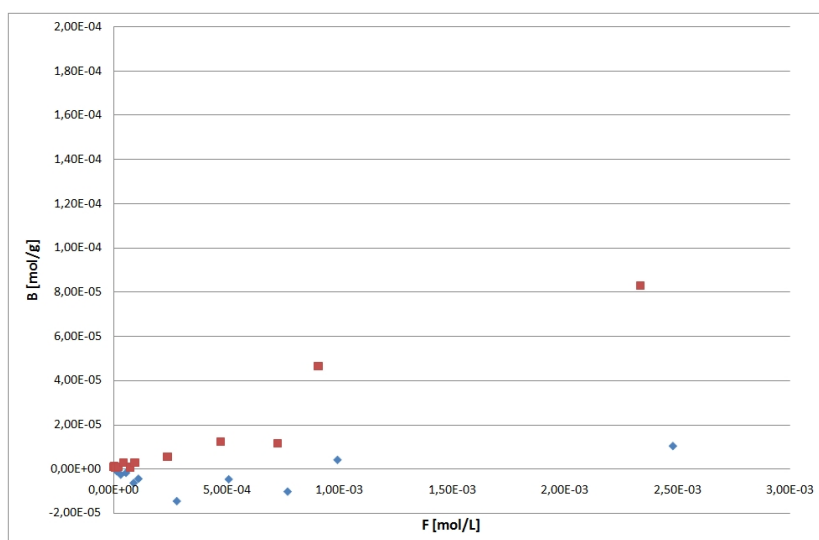
Figure 10.52: Isotherm plot of free drug, F, against bound drug, B, showing acquired data when using virgin and β-CD modified silica-gel with bound 1,8-ANS with FA. Blue, without β-CD modification; Red, with β-CD modification.

It can clearly be seen in both figures that more 1,8-ANS is absorbed when the silica-gel matrix has been modified with β-CDs. Without FA, the highest uptake of 1,8-ANS without β-CD modification is approximately $5.8 \cdot 10^{-5}$ mol/g whereas the uptake of 1,8-ANS with β-CD modification is approximately $1.8 \cdot 10^{-4}$ mol/g. With FA, the highest uptake of 1,8-ANS without β-CD modification is approximately $1.1 \cdot 10^{-5}$ mol/g whereas the uptake of 1,8-ANS with β-CD modification is approximately $8.1 \cdot 10^{-5}$ mol/g.

10.7 Examination of Drug Release

The following results represent the drug release data of FA when applied to both virgin and β-CD modified silica-gel and HA. The data in figure 10.53 and 10.54 show the continuous drug release per volume for silica-gel and β-CD modified silica-gel as well as HA and β-CD modified HA, respectively.
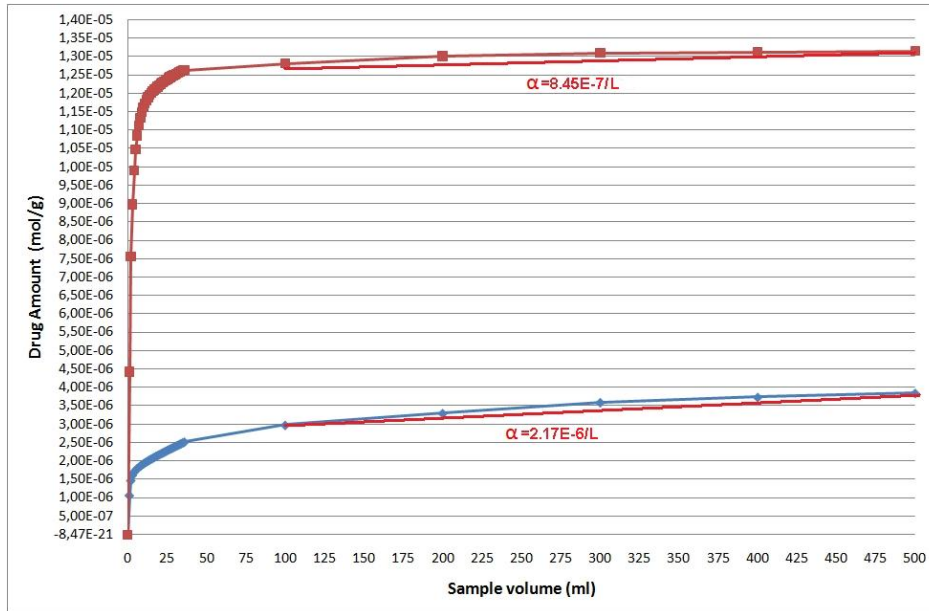
Figure 10.53: Illustration of the continuous total FA release per volume for 1g of virgin and β-CD modified silica-gel. Blue, unmodified; Red, modified.
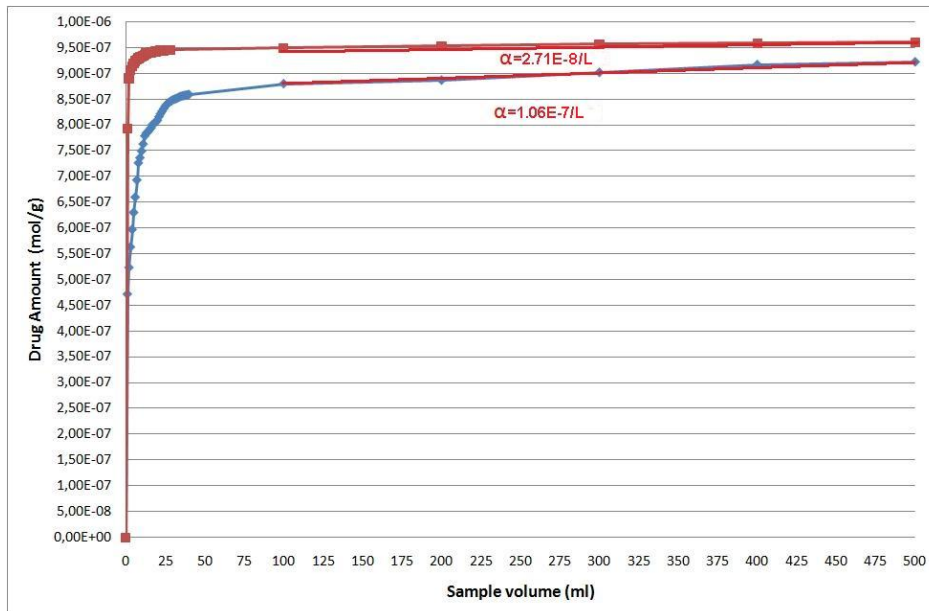
Figure 10.54: Illustration of the continuous total FA release per volume for 1g of virgin and β-CD modified HA. Blue, unmodified; Red, modified.

The burst effect of the β-CD modified and unmodified matrices are illustrated in figure 10.55 and 10.56.
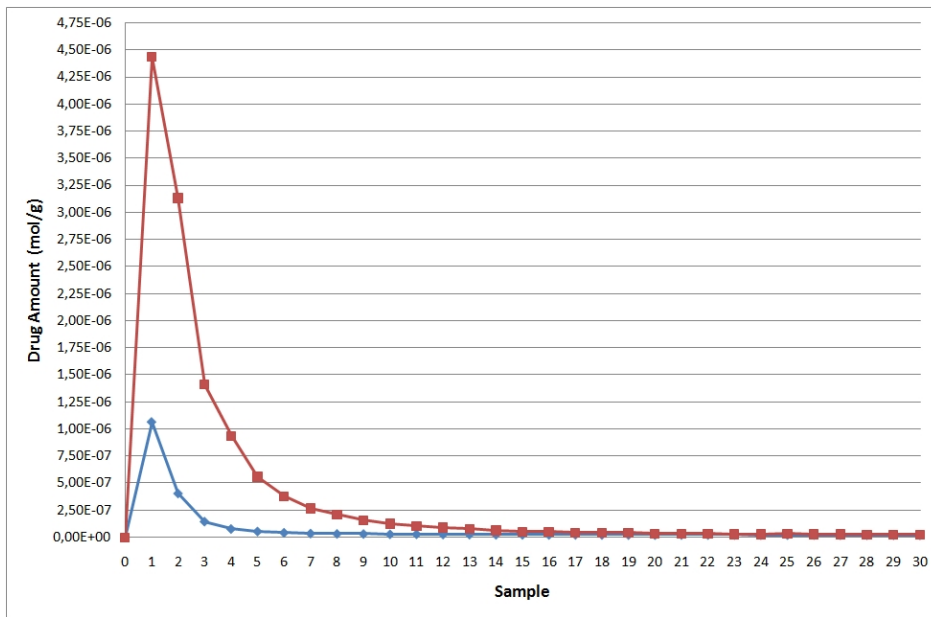
Figure 10.55: Illustration of the burst effect of the FA release per sample for 1g of virgin and β-CD modified silica-gel. Blue, unmodified; Red, modified.
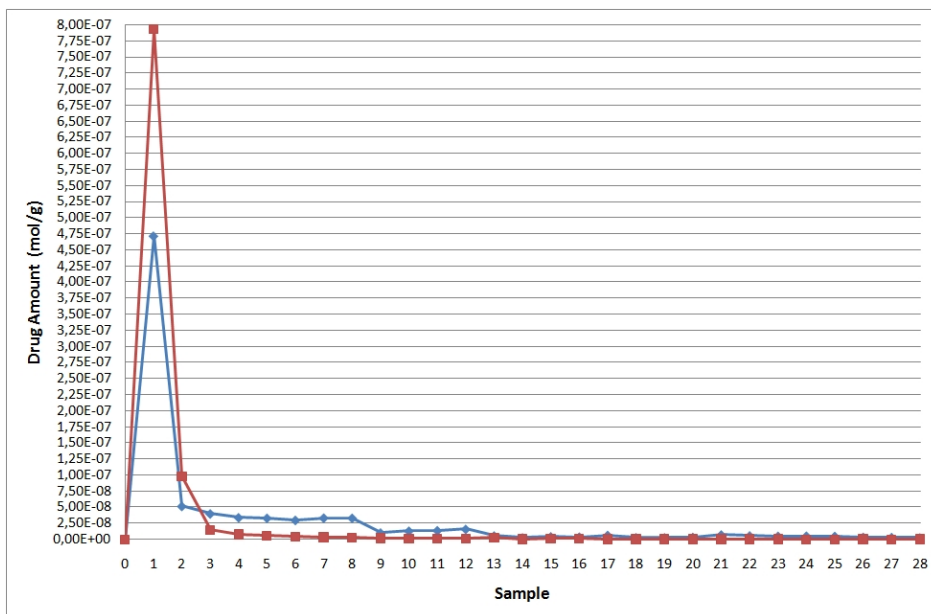
Figure 10.56: Illustration of the burst effect of the FA release per volume for 1g of virgin and β-CD modified HA. Blue, unmodified; Red, modified.

It can be observed that β-CD modified silica-gel has released far more FA during the first measurement than silica-gel has within terms of the whole experiment, indicating that the FA affinity for β-CD modified silica-gel is much stronger than that for virgin silica-gel. It can also be seen that the slope of β-CD modified silica-gel is lower than that of virgin silica-gel. The FA release pattern from virgin and β-CD modified HA is considered to be almost identical. However, the initial burst effect of β-CD modified HA is a bit higher than that of virgin HA. As with the silica-gel experiments the slope of β-CD modified HA is observed to be lower than that of virgin HA as well.

Discussion

<div style="text-align: right; font-size: 3em;">11</div>

The experimental work conducted in the current project is here discussed in relation to the literature studies and to the usability of the results for further work concerning CDs on bioceramic-based materials for controlled drug release. The quantification of attached β-CD on the matrix surfaces as well as the features of silica-gel and HA before and after β-CD modification are reviewed at first, followed by a discussion of the FIB-SEM studies of virgin and β-CD modified silica-gel. Hereafter, the loading isotherms for FA acquired with absorption spectroscopy are discussed followed by a walkthrough of the CLSM results. Subsequently, the loading isotherms for 1,8-ANS that were acquired with FS will be covered. Finally, the HPLC experiments on drug release from virgin and β-CD modified HA and silica-gel will be evaluated.

11.1   CD Quantification

TGA experiments indicate that there are at least 1.6wt% β-CDs attached to the silica-gel surface, while the amount of β-CDs attached to the HA surface can be no higher than 0.21w% since β-CDs are made entirely of glucose molecules which will completely pyrolyse at temperatures above 300°C. Furthermore, there are almost negligible variations in the TGA results for HA which concludes that only very slight amounts of silane spacer arm and β-CDs, if any, are attached to the HA matrix. Hydroxy-groups undergo a hydration reaction and form water at high temperatures which is prevented by modifying the hydroxy-groups with the silane spacer arm. The now modified oxygens closest to the matrix will not pyrolyse before the spacer arm does resulting in a postponed loss of mass by the specimen. The observation of virgin HA losing more mass in terms of wt% than silane-modified and β-CD modified HA could thus be caused by a slightly increased thermal stability of hydroxy-groups upon each step of modification, which can not be observed in the experiment with silica-gel.

The Phenol Sugar Assay method revealed a β-CD attachment of 38.1 ±7.4 μmol or roughly 4.3 ±0.8 wt% β-CD/g silica-gel matrix, and 2.7 ±0.9 μmol or 0.3 ±0.1 wt% β-CD/g HA matrix. During the experiments it was observed, that the samples with phenol added to pure HA formed chemical compounds capable of absorbing light at 487nm. Since pure bioceramic was used as references for the β-CD modified samples for both HA and silica-gel a change in interaction between HA and phenol caused by the β-CD modification itself, or more complex interactions that also involve the silane-spacers, would become a likely cause for the variations. Absorbance was also slightly observed with pure silica-gel but not nearly as high as for HA. The absorption by pure silica-gel is most likely caused by backscattering from smaller silica-gel particles that were sufficiently light to be carried into the cuvette together with the collected amount of sample, just before UV-VIS measurements were conducted. In conclusion, the combined Thermogravimetric Analysis and Phenol Assay data show that 14.2-45.5 μmol β-CD was immobilized on silica-gel while no more than 1.9μmol β-CD was immobilized on HA. Ponchel and colleagues stated that they successfully immobilized up to 67μmol β-CD per g silica-gel [Ponchel *et al.*, 2004] and it is known by the author that Ponchels results for β-CD attachment have been reproduced by colleagues from the institute. The lower yield in β-CD attachment in this work is therefore most likely a result of statistical reasons, or otherwise, a cause of natural variance.

11.2   Investigating Matrix Changes Upon CD Modification

BET results conducted on silica-gel before modification showed a surface area of 470.40 m^2/g gel, which is considered a large surface area and is in agreement with the theory from section 5, albeit somewhat below the surface areas measured by previous works. After β-CD immmobilization the surface area decreased to 322.27m^2/g gel which is a drop to 68.5% of the initial surface area. The total pore volume decreases accordingly from 0.709 cm^3/g gel to 0.484 cm^3/g gel, a 32% drop from the initial pore volume.

At first it would seem as if a substantial amount of β-CDs have been immobilized on the silica-gel, which hereby reduces its surface area due to steric hindrance and surface alteration. Physical stress from the grinding by the stirring during the synthesis is also most likely decreasing the surface area. Another plausible explanation for the smaller surface area could be that the covering of adsorption sites on the silica-gel surface by silane spacer arms is restricting the adsorption site availability for the N_2 molecules during BET sessions. Furthermore, the change in total pore volume is most likely caused by the filling of smaller pores by β-CDs. The smallest pores that are inaccessible by a molecule of the size of β-CD would still be accessible for the smaller spacer arms to some degree. Ponchel and colleagues [Ponchel *et al.*, 2004] have made similar observations when considering β-CD attachment to silica-gel. Furthermore, this explanation correlates with the CHN results, which confirm the attachment of β-CDs to the surface of silica-gel, and also the subsequent adsorption of FA. It is also seen, that more FA is adsorbed onto the specimen after β-CD modification, indicating that the modification has a beneficial effect towards FA matrix inclusion. In this project the silanol groups have been chemically attached to a silane compound, of which some of them are covalently connected to the primary hydroxyl of a β-CD molecule. It is therefore assumed that the decrease in surface area and total pore volume is a combined result of the silanol group modification, adsorption site restriction by the silane compound, and the partial filling of some of the smaller pores by β-CDs and silane spacer. The slight increase in nitrogen levels of the CHN data could have occured from the attachment synthesis of β-CDs to the matrices which is partially conducted in a nitrogen atmosphere.

The XRPD experiments illustrated a clear crystal structure with a diffraction angle of 23° in all specimen, indicating the crystal structure of silica-gel. Upon β-CD modification and FA adsorption the intensity decreases in accordance with the theoretical expectations as the modification occurs randomly. The smaller signal that is measured at a diffraction angle of around 6° is most likely an impurity that is washed away during the β-CD attachment synthesis, and is therefore only observed on virgin silica-gel specimen. Another explanation of the second diffraction angle could be a change in the ratio of silicon and oxygen in the crystal lattice throughout the particle. If this occurs it is very likely that the crystal structure changes as well, and hereby also the scattering of electrons and X-rays.

11.3   Investigating Silica-gel with the FIB-SEM setup

FIB-SEM investigations of virgin silica-gel without FA showed that only slight amounts of carbon, if any, were present and only at the very surface. Most likely the carbon is an impurity from the virgin silica-gel batch. After β-CD modification higher amounts of carbon could be detected at the surface concluding that the β-CD attachment was successful. The depth of carbon detection was roughly 6-10 μm meaning that all types of modification are only occuring close to the surface and will not be found in the deeper parts of the particle. Furthermore, the carbon measurements on figure 10.11B suggests that an inclined pore with either silane spacer arms or even β-CDs might have been discovered since carbon concentrations were low at the surface but suddenly increased at a particle depth of 3.8 μm. It is highly likely that the

detected carbon comes from either the silane spacer arms, the β-CDs or both since the high amounts of carbon are detected within a pore, whereas the carbon amounts outside of the pore are relatively lower. The specimen containing virgin silica-gel with FA also represents carbon at the surfaces. However, after approximately 3 μm of analysis into the particle crust no more carbon could be detected. Thus, by comparison with virgin silica-gel without FA it is suggested that organic molecules such as FA will adsorb to the inner walls of the matrix pores of silica-gel as well.

The increase in silicon amounts and decrease in oxygen amounts that can be observed in all specimen while the analysis goes deeper into the particle suggests that the conformation of the crystal structure is changing throughout the particle, or, that the particle simply becomes more solid and less porous with increasing depth. This is nicely illustrated in figure 10.12 and table 10.5 where points 4 and 5 have distinct ratios of the elements silicon, carbon and oxygen. Another example is given in figure 10.20 and table 10.7. The observations are very interesting and could be a subject for further studies in the future in order to be able to conclude any further on the phenomenon.

11.4 Loading Isotherms of HA and Silica-gel with FA as Ligand

After a period with various optimizations of the loading procedure, where different buffers, pH values, ligand concentrations, and measurement approaches were tried a final working procedure was the result. The author quickly moved onto the use of a centrifuge instead of silica-gel filtration with PVDF filters as it became evident that the filter membrane could only be used for organic solvents. When used with aqueous solvents it dissolved into the supposedly filtered solution. Initially the PBS buffer was used to completely simulate the conditions of the human body. However, this buffer proved that no concentrations of FA that were sufficiently high enough were stable with this system. Instead, a phosphate buffer was used and decreased to a pH of 7.4 after the maximum amounts of 1.2g/L FA were dissolved. Experiments considering the FA loading of virgin silica-gel indicate a relationship with the bi-Langmuir and the Freundlich isotherm. This means that the silica-gel matrix consists of either two high/low affinity binding sites, or a theoretically infinite amount of binding sites with the binding energy decreasing logarithmically as a function of FA concentration, according to the theory of section 7. Remembering that silica-gel surface modifications will result in a noticeable change in adsorption characteristics, the Freundlich isotherm is believed to be the most reliable model to describe FA loading of silica-gel. As it is unlikely that the highly porous silica-gel matrix only consists of one high and one low affinity type of binding site, the approximation of the bi-Langmuir isotherm is considered too simple. Furthermore, the considerations regarding silica-gel adsorption kinetics made by Vallet-Regi and colleagues is in agreement with this explanation [Vallet-Regi *et al.*, 2007].

Investigating the FA loading of β-CD modified silica-gel reveals a relatively close relationship to the Langmuir-Freundlich isotherm. Since the total pore volume and surface area of the gel both decrease sufficiently as a result of β-CD and silane spacer arm modification, the saturation point of the gel is expected to be reached at lower concentrations of FA than for silica-gel without any compounds grafted to the surface. At this point, this is seen to be the case. However, the modification of the silica-gel surface has seemingly resulted in stronger drug binding to the gel, which is seen in the form of the higher binding constant for β-CD modified silica-gel, in agreemeent with Martel and colleagues [Martel *et al.*, 2007]. One possible explanation is that an inclusion compound between β-CD and FA is formed to some degree, which is in agreement with the related work by Ponchel and colleagues albeit considering a different guest molecule [Ponchel *et al.*, 2004]. Another possibility is the conformational change of the silica-gel surface by the various modifications, rendering

the surface more non-polar and thus with a higher affinity towards a relatively hydrophobic molecule such as FA.

When considering the FA loading of virgin HA the only clear correlation is with the Bi-Langmuir Isotherm. However, due to the the size of the experimental error because the adsorbed FA concentrations are very low it is difficult to rule out the Freundlich or even the Langmuir-Freundlich Isotherms. The reason herefore is the matrix structure of HA which is porous and has many hydroxy-groups, albeit not as many as silica-gel. With a matrix structure it seems most obvious to have many binding sites where the drug affinity decreases with the addition of more FA seems more reasonable. In terms of measuring FA absorption with Absorption Spectroscopy HA has proven itself to be very difficult to work with. The high experimental error and relatively low adsorption leaves the analysis of the adsorption pattern inconclusive.

The adsorption pattern of β-CD modified HA when loaded with FA is almost similar to that of virgin HA, although β-CD modified HA adsorbs a little more FA. A slight correlation exists with the low affinity region in the scatchard plot but no clear correlation with a Bi-langmuir Isotherm can be concluded. However, with a little imagination, one can observe a slight correlation with the Freundlich Isotherm in the double logarithmic plot. Since no obvious change is observed between the loading patterns of virgin and β-CD modified HA it is concluded that HA must either be the wrong bioceramic matrix for a FA drug delivery application, or, a more effective β-CD attachment synthesis is necessary as a maximum of 0.21wt% β-CDs on the HA surface is close to being negligible.

In summary, virgin silica-gel is believed to have a high amount of adsorption sites, with decreasing binding affinity when the drug concentration increases. The drug is considered to be loosely bound to the binding sites. β-CD modified silica-gel has less binding sites than virgin silica-gel as a result of the β-CD and silane spacer arm attachment onto the surfaces. However, they are facing a stronger binding affinity towards the drug which is also reflected in the values of the calculated binding constants. At this point the stronger binding affinity is thus believed to cause a slower drug release over time than virgin silica-gel. The drawn conclusions are in agreement with the related work conducted by the research groups of Ginebra and Zhang [Ginebra *et al.*, 2006], [Zhang *et al.*, 1999]. Although it is believed that HA possesses similar adsorption abilities, no clear correlation with any of the known isotherms could be found. Furthermore, no obvious difference in loading pattern between virgin and β-CD modified HA can be observed.

11.5 CLSM of HA and Silica-gel with 1,8-ANS as Ligand

Neither virgin or β-CD modified HA fluorescend indicating that no 1,8-ANS is bound to hydrophobic cativies or other environments in the matrices. Ultimately, this concludes the fact that there are no noticeable amounts of β-CDs attached to the HA surface. Thus, it makes no sense to continue the work with HA when considering loading isotherm experiments with the current method for β-CD grafting. Virgin silica-gel with both low and high 1,8-ANS concentrations does also not fluorescend as was expected. A strong emission of fluorescence is, however, present with β-CD modified silica-gel with both low and high concentrations of 1,8-ANS. Furthermore, the CLSM data show that β-CDs are likely present and attached throughout the whole particle in any depths which contradicts with the FIB-SEM experiments where β-CDs are only observed within depths of approximately 10μm. This increases the demand of further investigations of the β-CD attachment and experiments with both the FIB-SEM setup and the CLSM method. Though, for now, it can be concluded that β-CDs have been succesfully attached to the silica-gel matrix by means of the synthesis method used, which was ineffective on HA. Finally, the presence of FA together with 1,8-ANS in the silica-

gel sample does not affect the fluorescending ability of 1,8-ANS, which is shown to be able to compete with FA for the β-CD cavities. It is possible that less 1,8-ANS is bound per gram of silica-gel when FA is present since FA will occupy some of the adsorption sites on the surface. The following quantitative fluorescence analysis will determine the experimental outcome of this hypothesis.

11.6   Loading Isotherms of Silica-gel with 1,8-ANS as Ligand

It can be seen from the FS experiments with 1,8-ANS that the β-CD modification increases the matrices affinity for 1,8-ANS in any case, with and without FA. The experiment showed though, that FA adsorbs to the surface of both virgin and β-CD modified silica-gel, since the amount of adsorbed 1,8-ANS was reduced when the sample was treated with FA prior to the FS experiments.

All experiments seem to correlate with the Freundlich Isotherm when looking at the double logarithmic plot. The Isotherm plots of the β-CD modified matrices also resembled that of a Freundlich Isotherm. None of the experiments could however give a clear indication of a binding constant. The causes herefore are most likely a question of experimental design. The FS apparatus could only detect 1,8-ANS concentrations linearly in the region ranging from $2.5 \cdot 10^{-6}$M to $5.0 \cdot 10^{-5}$M, whereas the concentrations reached as high as $2.5 \cdot 10^{-3}$M. Thus, dilutions of up to 1:100 had to be prepared in order to examine the samples properly leaving the samples of higher concentrations more prone to measurement errors since the slightest variation of the diluted sample gives a large variation of the original sample when calculating backwards.

11.7   Examination of Drug Release

The release experiment proves that β-CD modified silica-gel and HA follows the same kinetic model as virgin silica-gel and HA and other bioactive ceramics, since the pattern called Higuchi's Law in which the drug release decreases exponentially is observed, which is in agreement with the theory in section 7, and also stated by Higuchi and Ginebra and colleagues [Higuchi, 1963], [Ginebra *et al.*, 2006]. The binding affinity for the drug is entirely left out of the theoretical approach of Higuchis law, most likely because the law was initially used for bioactive cements [Ginebra *et al.*, 2006], [Higuchi, 1963]. A higher binding affinity towards a certain drug would result in a decreased release rate and vice versa. Thus, a new parameter defining the binding affinity and hereby also the effect of the inclusion compound between CD and the guest molecule should be included into the law. This is however beyond the scope of this project.

When looking at the slope calculations, it is seen that both virgin and β-CD modified silica-gel are able to release enough FA to maintain the levels of the average MIC_{50} for *S. aureus* of $1.28 \cdot 10^{-7}$mol/L, and as described in section 8.2. It is however observed that silica-gel has not released the theoretical $6.28 \cdot 10^{-6}$mol maximum amount of FA from the matrix calculated with the Langmuir Isotherm fit, while β-CD modified silica-gel has released approximately 2.6 times as much as its theoretical maximum of $4.94 \cdot 10^{-6}$. This indicates, that β-CD modified silica-gel has more binding sites than originally calculated by the Langmuir Isotherm fit. Considering that the loading experiments were not saturated with FA and that it has been previously concluded that virgin and β-CD modified silica-gel are most likely resembling the Freundlich and Langmuir-Freundlich Isotherms, respectively, it is very plausible that higher concentrations of FA can adsorb to both matrices if the free amounts of FA were increased. Furthermore, the virgin silica-gel release data indicate that there is more FA present in the

matrix that has not been released yet, which is undesirable. Recalling that the surface area, A, is proportional to the amount of drug released over time, a sufficiently smaller amount of drug release was expected as a result of the observed reduction in silica-gel surface area after β-CD grafting by BET experiments. Additionally, the decrease in total pore volume is also expected to decrease the porosity of the gel. The grafting of β-CD and silane spacer to the surface will in return increase the gel tortuosity and as a result, the rate defining parameter $\frac{D'\epsilon}{\tau}$ will decrease. Vallet-regi and colleagues mention that modifications on the silanol groups on the silica-gel surface will result in a noticeable change in adsorption characteristics of the silica surface as well as in its polarity [Vallet-Regi *et al.*, 2007]. As FA is not a very hydrophilic molecule the modification of silica-gel with both the 3-glycidyloxypropyl trimethoxsilane spacer arm and the β-CDs would effectively reduce the polarity of the many hydroxy-groups that are represented on the surface, making the silica-gel particle readily more hydrophobic. This, in combination with the presence of the β-CD cavities, could result in more binding sites for FA on β-CD modified silica-gel.

The molar release of FA from both virgin and β-CD modified HA is considered to be in the same region as with the loading isotherm data if one assumes that FA loading increases in a linear way with increasing initial FA concentrations as has been concluded with silica-gel. Thus, the loading and release data of virgin and β-CD modified HA correlate with each other. The calculated slopes of either virgin or β-CD modified HA do not suggest that sufficient levels of FA are released per sample in order to fight an *S. aureus* infection. Since it has been concluded that close to none β-CDs are attached to the modified HA, it is likely that only very few 3-glycidyloxypropyl trimethoxsilane spacer arms are attached as well. Thus the surface of the modified HA is still very similar to that of virgin HA, consisting of many polar groups which will most likely rather prefer interactions with water or other hydrophilic substances instead of FA.

Conclusion

<div style="text-align: right">**12**</div>

β-CDs have been successfully attached to silica-gel surfaces, whereas the modification synthesis failed to work sufficiently on HA surfaces. A β-CD coverage between 1.6-5.1wt% was obtained for silica-gel whereas the attached β-CD amounts on HA where less than 0.21wt%. After β-CD modification both the surface area and the total pore volume decreased as expected.

Virgin silica-gel and β-CD modified silica-gel was investigated with a FIB-SEM system with EDX, which further concluded that the β-CD attachment was successful. When scanning further into the particle crust it was discovered that the silicon concentrations begin to increase while the oxygen amounts slowly begin to decrease. Two possibilities were suggested as cause of this phenomena; either the crystal structure changes throughout the particle as a result of the varying component ratio, or the amount of pores decreases with increasing depth and the particle is becoming more solid. However, more experiments are needed in order to conclude anything further.

The loading isotherms of FA when applied to virgin and β-CD modified HA and silica-gel was investigated as well. The HA experiments turned out inconclusive and β-CD modified HA and virgin HA patterns were very closely related. The conclusion was that the β-CD grafting was not effective enough for any clear loading effect to be observed. Finally, it was shown that virgin silica-gel with FA resembled a loading profile similar to a Freundlich Isotherm whereas β-CD modified silica-gel resembled that of the Langmuir-Freundlich Isotherm.

CLSM experiments concluded that the fluorescence of 1,8-ANS molecules could only be detected on β-CD modified silica-gel samples, which is in agreement with the theory in which the less hydrophilic cavity of CDs are able to boost the fluorescence emission. FS experiments with 1,8-ANS and the virgin and β-CD modified silica-gel showed that all matrix and ligand combinations resembled the loading profile of the Freundlich Isotherm. When applying FA before 1,8-ANS to the samples it was furhtermore observed that less 1,8-ANS could be adsorbed, indicating that some of the previously available 1,8-ANS binding sites were now occupied by FA.

All release experiments were seen to follow Higuchi's Law. It was furthermore observed that the release patterns of virgin and β-CD modified HA were very similar. β-CD modified silica-gel released far more FA than virgin silica-gel suggesting that more binding sites for FA were created with the modification. It is suggested that this is a combination of the presence of β-CDs but also caused by a change in the polarity of the particle surface as a result of the substitution of hydroxy-groups with the silane spacer arm and the β-CDs, rendering the surface less polar and thus with a higher affinity for the relatively hydrophobic FA molecules.

Future Perspectives

An effective synthesis procedure for the modification of HA should be investigated. Suggestions for the changes for the procedure are the modification of 3-glycidyloxypropyl trimethoxsilane and β-CD concentrations and no reflux, which will push the reaction towards forming ether bonds with the surface hydroxy-groups as the methanol is now removed from the reaction. More FIB-SEM experiments with different acceleration currents should be conducted. Loading procedures on other devices for both FA and 1,8-ANS should be conducted. For instance, it would be interesting to see the outcome and precision of a HPLC procedure for both loading systems. Finally, a bacterial assay should be prepared in order to test the antibiotic effect of the silica-gel application.

Bibliography

[1] Ugeskrift for Læger - Hospitalsinfektioner - en samfundsøkonomisk udfordring
http://www.ugeskriftet.dk/portal/page/portal/laegerdk/
ugeskrift_for_laeger/tidligere_numre/2007/
ufl_ekcma_2007_48/ufl_ekcma_2007_48_51040 (Access date: 30/05-08)

[2] Herlev Hospital - Infektioner Generelt
http://www.herlevhospital.dk/menu/Afdelinger/Gastroenheden/
Antibiotika+og+infektioner/Infektioner+generelt.htm (Access date: 16/05-08)

[3] WIPO Patents - Artificial Blood Vessel
http://www.wipo.int/pctdb/en/wo.jsp?IA=WO1993023090&DISPLAY=DESC (Access date: 12/11-08)

[4] Netdoktor.dk
http://www.netdoktor.dk/sygdomme/fakta/
tuberkulose.htm (Access date: 10/09-08)
leddegigt.htm (Access date: 10/09-08)
kroniskpancreatit.htm (Access date: 10/09-08)

[5] Osteomyelitis - Wikipedia, the free encyclopedia
http://en.wikipedia.org/wiki/osteomyelitis (Access date: 15/06-09)

[6] Nosocomial infection - Wikipedia, the free encyclopedia
http://en.wikipedia.org/wiki/nosocomial_infection (Access date: 10/06-09)

[7] BBC - GCSE Bitesize - The skeleton, bones and joints
http://www.bbc.co.uk/schools/gcsebitesize/pe/appliedanatomy/
2_anatomy_skeleton_rev4.shtml (Access date: 12/04-09)

[8] Duke Orthopaedics - Wheeless' Textbook of Orthopaedics
http://www.wheelessonline.com/ortho/bone_remodeling (Access date: 13/04-09)

[9] University of Wisconsin
http://www.waukesha.uwc.edu/lib/reserves/pdf/zillgitt/zoo170/
diagrams2/diagrams2.html (Access date: 01/07-09)

[10] Silica Gel - Wikipedia, the free encyclopedia
http://en.wikipedia.org/wiki/silica_gel (Access date: 17/05-09)

[11] Cyclodextrin Technologies Development, Inc.
http://www.cyclodex.com/index.html (Access date: 10/04-08)

[12] Tortuosity - Wikipedia, the free encyclopedia
http://en.wikipedia.org/wiki/Tortuosity (Access date: 07/08-09)

BIBLIOGRAPHY

[13] Routes of Administration - Wikipedia, the free encyclopedia
http://en.wikipedia.org/wiki/route_of_administration (Access date: 08/01-09)

[14] Online Pharmacy Catalog
http://www.onlinepharmacycatalog.com/category/common-drugs-and-medications/
antibiotics/fusidic-acid-fucidin-fucicort-fucithalmic-fusidin/ (Access date: 8/11-08)

[15] Newcastle University - Isotherms and Adsorption Theory
http://www.staff.ncl.ac.uk/a.j.fletcher/isotherms.htm (Access date: 22/08-09)

[16] Powder Diffraction - Wikipedia, the free encyclopedia
http://en.wikipedia.org/wiki/Powder_Diffraction (Access date: 16/08-09)

[17] Purdue University - Scanning Electron Microscope
http://www.purdue.edu/REM/rs/sem.htm (Access date: 10/09-09)

[18] HAMM - Energy Dispersive X-ray Spectroscopy
http://mee-inc.com/eds.html (Access date: 10/09-09)

[19] FluoView Resource Center - Confocal Laser Scanning Microscopy
http://www.olympusconfocal.com/theory/confocalintro.html (Access date: 20/08-09)

[20] High Performance Liquid Chromatography - Wikipedia, the free encyclopedia
http://en.wikipedia.org/wiki/HPLC (Access date: 22/08-09)

[Andersen, 2001] S. B. Andersen; Masters Thesis: Analysis and Production of Fusidic Acid
using Cyclodextrin Technology, Institute of Life Sciences, Department of Biotechnology
at Aalborg University, 2000−2001.

[Aoki, 1994] H. Aoki; Medical Applications of Hydroxyapatite, Ishiyaku EuroAmerica, Inc.,
ISBN: 1-56386-023-6, 1994.

[Aoki et al., 1973] H. Aoki, K. Kato, and T. Sokawa; Development of a Handy Hot Press
Apparatus and Its Application; Reports of Institute for Medical and Dental engineering,
1973, vol. 7, pp. 113−118.

[Besier et al., 2003] S. Besier, A. Ludwig, V. Brade, T. Wichelhaus; Molecular analysis of
fusidic acid resistance in Staphylococcus aureus; Molecular Microbiology, 2003, vol. 47,
issue 2, pp. 463−469.

[Best et al., 2008] S. Best, A. Porter, E. Thian, and J. Huang; Bioceramics: Past, present and
for the future; Journal of the European Ceramic Society, 2008, vol. 28, pp. 1319−1327.

[Brendel et al., 1992] T. Brendel, A. Engel, and C. Rüssel; Hydroxyapatite coatings by a
polymeric route; Journal of Materials Science: Materials in Medicine, 1992, vol. 3, pp.
175−179.

[Brown et al., 1997] N. M. Brown, D. S. Reeves, and C. M. McMullin; The pharmakokinetics
and protein-binding of fusidic acid in patients with severe renal failure requiring either
haemodialysis or continuous ambulatory peritoneal dialysis; Journal of Antimicrobial
Chemotherapy, 1997, vol. 39, pp. 803−809.

[Brunauer et al., 1938] S. Brunauer, P. H. Emmett, and E. Teller; Adsorption of Gases in
Multimolecular Layers; Journal of the American Chemistry Society, 1938, vol. 60, issue
2, pp. 309−319.

[Chai *et al.*, 2009] F. Chai, S. Leprêtre, J.-C. Hornez, N. Blanchemain, M. Descamps, B. Martel, and H. F. Hildebrand; Antibiotics Loading on Cyclodextrin Polymer (Poly-CDs) Functionalized Hydroxyapatite for Prolonged Delivery; Research presented at the International Bone-Tissue-Engineering Congress from the 7-9th of November 2008 in Hannover Germany, Abstract published at Mary Ann Liebert Publishers in May 2009, Tissue Engineering Part A, vol. 15, issue 5, pp. O5−O6.

[Connors, 1987] K. Connors; Binding Constants: The Measurement of Molecular Complex Stability, John Wiley & Sons Incorporated, ISBN: 0-471-83083-6, 1987.

[Correia *et al.*, 1996] R. Correia, M. Magalhães, P. Marques, and A. Senos; Wet synthesis and characterization of modified hydroxyapatite powders; Journal of Materials Science, 1996, vol. 7, pp. 501−505.

[Dewick, 2006] P. M. Dewick; Essentials of Organic Chemistry, John Wiley & Sons Incorporated, ISBN: 0-470-01666-3, 2006.

[Drevon, 2002] Géraldine Drevon, PhD: Enzyme immobilization into polymers and coatings, University of Pittsburgh, 2002.

[Ehrenstein *et al.*, 2004] G.W. Ehrenstein, G. Riedel, and P. Trawiel; Thermal analysis of plastics, Carl Hanser Verlag, Munich, Germany, 2004.

[Fantin *et al.*, 1993] B. Fantin, R. Leclercq, J. Duval, and C. Carbon; Fusidic Acid Alone or in Combination with Vancomycin forTherapy of Experimental Endocarditis Due to Methicillin-Resistant Staphylococcus aureus; Antimicrobial Agents and Chemotherapy, 1993, vol. 37, issue 11, pp. 2466−2469.

[Ginebra *et al.*, 2006] M. P. Ginebra, T. Traykova, and J. A. Planell; Calcium phosphate cements as bone drug delivery systems: A review; Journal of Controlled Release, 2006, vol. 113, pp. 102−110.

[Godtfredsen, 1967] W. O. Godtfredsen; Doctoral Thesis: Fusidic Acid and some related antibiotics, Copenhagen 1967.

[Greenwood *et al.*, 1984] N. N. Greenwood and A. Earnshaw; Chemistry of the Elements, first edition, Pergamon Press, ISBN: 0-08-022056-8, 1984.

[Guldager, 2002] S. Guldager; Basal Sygdomslære, second edition, Munksgaard, ISBN: 87-628-0297-6, 2002.

[Gupta *et al.*, 2008] R. Gupta, and A. Kumar; Bioactive materials for biomedical applications using sol-gel technology; Biomedical Materials, 2008, vol. 3.

[Harris, 2007] D. C. Harris; Quantitative Chemical Analysis, Seventh Edition, W. H. Freeman and Company, ISBN: 0-7167-7041-5, 2007.

[Higuchi, 1963] T. Higuchi; Mechanism of sustained-action medication. Theoretical analysis of release of solid drugs dispersed in solid matrices; Journal of Pharmaceutical Sciences, 1963, vol. 52, issue 12, pp. 1143−1149.

[Holmes, *et al.*, 2005] R. Holmes, R. Bucholz, and V. Mooney; Porous Hydroxyapatite as a Bone Graft Substitute in Diaphyseal Defects: A Histometric Study; Journal of Orthopaedic Research, 2005, vol. 5, pp. 114−121.

[Holst *et al.*, 2002] G. Seltmann and O. Holst; The Bacterial Cell Wall, second edition, Springer, ISBN: 3-540-42608-6, 2002.

[Howden, *et al.*, 2006] B. Howden and M. Grayson; Dumb and Dumber-The Potential Waste of a Useful Antistaphylococcal Agent: Emerging Fusidic Acid Resistance in Staphylococcus aureus; Antimicrobial Resistance, 2006, vol. 42, pp. 394−400.

[Horcajada, *et al.*, 2004] P. Horcajada, A. Rámila, K. Boulahya, J. González-Calbet, and M. Vallet-Regi; Bioactivity in ordered mesoporous materials; Solid State Sciences, 2004, vol. 6, issue 11, pp. 1295−1300.

[Jicsinszky *et al.*, 1996] L. Jicsinszky, É. Fenyvesi, H. Hashimoto, and A. Ueno; Cyclodextrin derivatives; Comprehensive Supramolecular Chemistry, vol. 3, Cyclodextrins, first edition, Elsevier Science Ltd., ISBN: 0-08-042715-4, 1996.

[Junqueira *et al.*, 2005] L. C. Junqueira and J. Carneiro; Basic Histology, eleventh edition, Mcgraw-Hill Medical, ISBN: 0-07-144091-7, 2005.

[Kittel, 2005] C. Kittel; Introduction to Solid State Physics, John Wiley & Sons Incorporated, ISBN: 0-471-68057-5, 2005.

[Kobayashi *et al.*, 1994] H. Kobayashi, H. Aoki, M. Sakatsume and H. Namiki; Respiration Rates of Cell Cultured with Hydroxyapatite Microcrystals By MTT-test; from H. Aoki - Medical Applications of Hydroxyapatite, Ishiyaku EuroAmerica, Inc., ISBN: 1-56386-023-6, 1994, pp 20−21.

[Lakowitz, 1999] J. R. Lakowitz; Principles of Fluorescence Spectroscopy, Kluwer Academic Publishers Group, ISBN: 0-306-46093-9, 1999.

[Larsen, 2006] Lea L. Larsen; Master Thesis: Aqueous Rebinding of Rhodamine B in Molecularly Imprinted Silica, Poly(methacrylate) Networks, and Organic/Inorganic Poly(methacrylate)/Silica hybrids; Department of Biotechnology, Chemistry and Environmental Engineering, Section for Chemistry, Aalborg University, 2006.

[Larsen, 2002] Kim Lambertsen Larsen; Large Cyclodextrins; Journal of Inclusion Phenomena and Macrocyclic Chemistry, 2002, vol. 43, issue 1-2, pp. 1−13.

[Li *et al.*, 1994] P. Li, C. Ohtsuki, T. Kokubo, K. Nakanishi, N. Soga, K. Groot; The role of hydrated silica, titania, and alumina in inducing apatite on implants; Journal of Biomedical Materials Research, 1994, vol. 28, pp. 7−15.

[Li *et al.*, 2005] X. Li, and, B. R. Jasti; Design of Controlled Release Drug Delivery Systems, Mcgraw-Hill Professional Publishing, ISBN: 0-07-141759-1, 2005.

[Lipinski, 2000] C. A. Lipinski; Drug-like properties and the causes of poor solubility and poor permeability; Journal of Pharmacological and Toxicological Methods, 2000, vol. 44, pp. 235−249.

[Loftsson *et al.*, 1996] T. Loftsson, and M. Brewster; Pharmaceutical applications of cyclodextrins. 1. Drug solubilization and stabilization; Journal of Pharmaceutical Sciences, 1996, vol. 85, Issue 10, pp. 1017−1025.

[Loftsson *et al.*, 2002] T. Loftsson, A. Magnúsdóttir, M. Másson, and J. Sigurjónsdóttir; Self-Association and Cyclodextrin Solubilization of Drugs; Journal of Pharmaceutical Sciences, 2002, vol. 91, issue 11, pp. 2307−2316.

[Loftsson *et al.*, 2007] T. Loftsson, and D. Duchêne; Cyclodextrins and their pharmaceutical applications; International Journal of Pharmaceutics, 2007, vol. 329, pp. 1−11.

[Loftsson *et al.*, 2007] T. Loftsson, P. Jarho, M. Másson, and T. Järvinen; Cyclodextrins in drug delivery; Expert Opinion on Drug Delivery, 2005, vol. 2, issue 2, pp. 335−351.

[Marquis *et al.*, 2009] M. Marquis, E. Lord, E. Bergeron, O. Drevelle, H. Park, F. Cabana, H. Senta, and N. Faucheux; Bone cells-biomaterials interactions; Frontiers in Bioscience, 2009, vol. 14, pp. 1023−1067.

[Martel *et al.*, 2007] N. Blanchemain, T. Laurent, S. Haulon, M. Traisnel, C. Neut, J. Kirkpatrick, M. Morcellet, H. F. Hildebrand, and B. Martel; In vitro study of a HPγ-cyclodextrin grafted PET vascular prosthesis for application as anti-infectious drug delivery system; Journal of Inclusion Phenomena and Macrocyclic Chemistry, 2007, vol. 57, pp. 675−681.

[Martini, 2006] F. Martini; Fundamentals of Anatomy and Physiology, seventh edition, Pearson Education Benjamin Cummings, ISBN: 0-321-31198-1, 2006.

[Murugan *et al.*, 2005] R. Murugan, and S. Ramakrishna; Aqueous mediated synthesis of bioresorbable nanocrystalline hydroxyapatite; Journal of Crystal Growth, 2005, vol. 274, pp. 209−213.

[Pawley, 2006] J. B. Pawley; Handbook of Biological Confocal Microscopy, Springer Verlag, ISBN: 978-0-387-25921-5, 2006.

[Perry *et al.*, 2002] J. Perry, J. Staley, and S. Lory; Microbial Life, Sinauer Associates, ISBN: 0-87893-675-0, 2002.

[Ponchel *et al.*, 2004] A. Ponchel, S. Abramson, J. Quartararo, D. Bormann, Y. Barbaux, and E. Monflier; Cyclodextrin silica-based materials: advanced characterizations and study of their complexing behavior by diffuse reflectance UV-Vis spectroscopy; Elsevier - Microporous and Mesoporous Materials, 2004, vol. 75, pp. 261−272.

[Ratledge *et al.*, 2001] C. Ratledge and B. Kristiansen; Basic Biotechnology, second edition, Cambridge University Press, ISBN: 0-521-77917-0, 2001.

[Robyt, 1999] J.F. Robyt; Essentials of Carbohydrate Chemistry, Springer Verlag New York Inc., ISBN: 0-387-94951-8, 1999.

[Sakatsume *et al.*, 1992] H. Aoki, M. Akao, S. Kano, K. Matsumoto, Y. Ogawa and M. Sakatsume; Effects of Hydroxyapatite-sol on Cell Growth; Reports of Institute for Medical and Dental Engineering, 1992, vol. 26, pp. 15−21.

[Soga *et al.*, 1992] P. Li, C. Ohtsuki, T. Kokubo, K. Nakanishi, and N. Soga; Apatite Formation Induced by Silica Gel in a Simulated Body Fluid; Journal of the American Ceramic Society, 1992, vol. 75, issue 8, pp. 2094−2097.

[Stevie et al., 2005] F. A. Stevie and L. A. Giannuzzi; Introduction to Focused Ion Beams - Instrumentation, Theory, Techniques, and Practice; Springer Verlag New York Inc., ISBN: 978-0-387-23116-7, 2005.

[Stryer *et al.*, 2002] L. Stryer, J. M. Berg, and J. L. Tymoczko; Biochemistry, fifth edition, W.H. Freeman and Company, ISBN: 0-7167-4684-0, 2002.

[Szejtli, 1996] J. Szejtli; Chemistry, Physical and Biological Properties of Cyclodextrins; Comprehensive Supramolecular Chemistry, vol. 3, Cyclodextrins, first edition, Elsevier Science Ltd., ISBN: 0-08-042715-4, 1996.

[Szente, 1996] L. Szente; Preparation of Cyclodextrin Complexes; Comprehensive Supramolecular Chemistry, vol. 3, Cyclodextrins, first edition, Elsevier Science Ltd., ISBN: 0-08-042715-4, 1996.

[Talaro, 2006] A. and K. P. Talaro; Foundations in Microbiology, sixth Edition, Mcgraw-Hill Higher Education, ISBN: 978-0-07-110229-2, 2006.

[Vallet-Regi *et al.*, 2007] M. Vallet-Regi, F. Balas, M. Colilla, and M. Manzano; Bioceramics and pharmaceuticals: A remarkable synergy; Solid State Sciences, 2007, vol. 9, pp. 768−776.

[Wang *et al.*, 2005] B. Wang, T. Siahaan, and R. Soltero; Drug Delivery: Principles and Applications, John Wiley & Sons Incorporated, ISBN: 0-471-47489-4, 2005.

[Waser, 2003] R. Waser; Nanoelectronics and Information Technology - Advanced Electronic Materials and Novel Devices, Wiley-VCH GmbH & Co. KGaA, ISBN: 3-527-40363-9, 2003.

[Yoshizawa *et al.*, 1992] K. Yoshizawa, H. Aoki, M. Akao, Y. Shin, and S. Kano; Reaction of Hydroxyapatite-Gel to Blood as Application to DDS; from H. Aoki - Medical Applications of Hydroxyapatite, Ishiyaku EuroAmerica, Inc., ISBN: 1-56386-023-6, 1994, pp 38−45.

[Zhang *et al.*, 1999] L. Zhang, Y. Wong, L. Chen, C. Ching, and S Ng; A Facile Immobilization Approach for Perfunctionalised Cyclodextrin onto Silica via the Staudinger Reaction; Tetrahedron Letters, 1999, vol. 40, issue 9, pp. 1815−1818.